

AFRL-VA-WP-TR-2005-3130

**CONTROL OF AERODYNAMIC
FLOWS**

**Delivery Order 0051: Transition Prediction
Method Review Summary for the Rapid
Assessment Tool for Transition Prediction
(RATTraP)**



**Dr. Myron B. Davis, Dr. Helen Reed, Harold Youngren, Dr. Brian Smith,
and Dr. Erich Bender**

**Lockheed Martin Corporation
Lockheed Martin Aeronautics Company
P.O. Box 748
Fort Worth, TX 76101**

JUNE 2005

Interim Report for 20 September 2004 – 15 June 2005

Approved for public release; distribution is unlimited.

STINFO FINAL REPORT

© 2005 Lockheed Martin Corporation.

This work is copyrighted. The U.S. Government has for itself and others acting on its behalf an unlimited, paid-up, nonexclusive, irrevocable worldwide license to use, modify, reproduce, release, perform, display, or disclose the work by or on behalf of the Government. Any other form of use is subject to copyright restrictions.

**AIR VEHICLES DIRECTORATE
AIR FORCE RESEARCH LABORATORY
AIR FORCE MATERIEL COMMAND
WRIGHT-PATTERSON AIR FORCE BASE, OH 45433-7542**

NOTICE

Using Government drawings, specifications, or other data included in this document for any purpose other than Government procurement does not in any way obligate the U.S. Government. The fact that the Government formulated or supplied the drawings, specifications, or other data does not license the holder or any other person or corporation; or convey any rights or permission to manufacture, use, or sell any patented invention that may relate to them.

This report was cleared for public release by the Air Force Research Laboratory Wright Site Public Affairs Office (AFRL/WS) and is releasable to the National Technical Information Service (NTIS). It will be available to the general public, including foreign nationals.

PAO Case Number: AFRL/WS 05-2280, 03 Oct 2005.

THIS TECHNICAL REPORT IS APPROVED FOR PUBLICATION.

/s/

Jeffrey R. Komives, 2d Lt, USAF
Aerospace Engineer
Aerodynamic Configuration Branch

/s/

Christopher P. Remillard
Chief
Aerodynamic Configuration Branch

/s/

Tim J. Schumacher
Chief
Aeronautical Sciences Division

This report is published in the interest of scientific and technical information exchange and its publication does not constitute the Government's approval or disapproval of its ideas or findings.

REPORT DOCUMENTATION PAGE				Form Approved OMB No. 0704-0188	
<p>The public reporting burden for this collection of information is estimated to average 1 hour per response, including the time for reviewing instructions, searching existing data sources, gathering and maintaining the data needed, and completing and reviewing the collection of information. Send comments regarding this burden estimate or any other aspect of this collection of information, including suggestions for reducing this burden, to Department of Defense, Washington Headquarters Services, Directorate for Information Operations and Reports (0704-0188), 1215 Jefferson Davis Highway, Suite 1204, Arlington, VA 22202-4302. Respondents should be aware that notwithstanding any other provision of law, no person shall be subject to any penalty for failing to comply with a collection of information if it does not display a currently valid OMB control number. PLEASE DO NOT RETURN YOUR FORM TO THE ABOVE ADDRESS.</p>					
1. REPORT DATE (DD-MM-YY) June 2005		2. REPORT TYPE Interim		3. DATES COVERED (From - To) 09/20/2004 – 06/15/2005	
4. TITLE AND SUBTITLE CONTROL OF AERODYNAMIC FLOWS Delivery Order 0051: Transition Prediction Method Review Summary for the Rapid Assessment Tool for Transition Prediction (RATTraP)				5a. CONTRACT NUMBER F33615-00-D-3053-0051	
				5b. GRANT NUMBER	
				5c. PROGRAM ELEMENT NUMBER 0602201	
6. AUTHOR(S) Dr. Myron B. Davis, Dr. Helen Reed, Harold Youngren, Dr. Brian Smith, and Dr. Erich Bender				5d. PROJECT NUMBER A00B	
				5e. TASK NUMBER	
				5f. WORK UNIT NUMBER 0D	
7. PERFORMING ORGANIZATION NAME(S) AND ADDRESS(ES) Lockheed Martin Corporation Lockheed Martin Aeronautics Company P.O. Box 748 Fort Worth, TX 76101				8. PERFORMING ORGANIZATION REPORT NUMBER FZM-9113	
9. SPONSORING/MONITORING AGENCY NAME(S) AND ADDRESS(ES) Air Vehicles Directorate Air Force Research Laboratory Air Force Materiel Command Wright-Patterson AFB, OH 45433-7542				10. SPONSORING/MONITORING AGENCY ACRONYM(S) AFRL/VAAA	
				11. SPONSORING/MONITORING AGENCY REPORT NUMBER(S) AFRL-VA-WP-TR-2005-3130	
12. DISTRIBUTION/AVAILABILITY STATEMENT Approved for public release; distribution is unlimited.					
13. SUPPLEMENTARY NOTES Report contains color. © 2005 Lockheed Martin Corporation. This work is copyrighted. The U.S. Government has for itself and others acting on its behalf an unlimited, paid-up, nonexclusive, irrevocable worldwide license to use, modify, reproduce, release, perform, display, or disclose the work by or on behalf of the Government. Any other form of use is subject to copyright restrictions.					
14. ABSTRACT The purpose of this report is to review available methods for predicting the transition of boundary layers. The emphasis will be on methods for transition mechanisms which are relevant to the flight conditions and geometric configurations of high altitude, long endurance aircraft, although the methods themselves may be much more general than this specific case. Each method will be evaluated according to certain criteria which are appropriate to the development of a computationally efficient, accurate and robust transition prediction module which is fully integrated into a general purpose CFD code. For each particular transition mechanism, a method will be selected which best satisfies all of the criteria.					
15. SUBJECT TERMS Laminar Flow, Laminar, Transition, Transition Prediction					
16. SECURITY CLASSIFICATION OF:			17. LIMITATION OF ABSTRACT: SAR	18. NUMBER OF PAGES 98	19a. NAME OF RESPONSIBLE PERSON (Monitor) 2Lt Jeffrey Komives 19b. TELEPHONE NUMBER (Include Area Code) (937) 255-1190
a. REPORT Unclassified	b. ABSTRACT Unclassified	c. THIS PAGE Unclassified			

TABLE OF CONTENTS

1	INTRODUCTION	1
2	GENERAL METHODS	3
2.1	Linear Stability Theory	3
2.1.1	e^N Method	5
2.1.2	Numerical Methods	6
2.2	Parabolized Stability Equations	8
2.3	Direct Numerical Simulation	11
2.3.1	Numerical Methods	12
2.3.2	Disturbance Input	14
2.3.3	Downstream Boundary Conditions	14
2.3.4	Validation and Verification	15
3	TOLLMIEEN-SCHLICHTING INSTABILITIES	17
3.1	Empirical correlations	17
3.2	e^N Methods	17
3.2.1	Nonparallel Effects	19
3.2.2	Envelope methods/Mode tracking methods	20
3.3	Other methods	20
4	CROSSFLOW INSTABILITIES	21
4.1	Empirical correlations	22
4.2	e^N Methods	22
4.2.1	Envelope methods/Mode tracking methods	23
4.3	Other methods	25
4.4	Control with Distributed Roughness	27
4.5	Secondary Instabilities	28
5	APPROXIMATE E^N METHODS	34
5.1	Envelope methods vs mode tracking methods	34
5.2	Approximate TS Methods	35
5.2.1	Drela's Envelope e^N TS Method	35
5.2.2	Drela's Full e^N TS Method	36
5.2.3	Sturdza's Compressible Envelope e^N TS Method	39
5.2.4	Crouch, Crouch and Ng Neural Net e^N TS Method	40
5.3	Approximate Crossflow Methods	42
5.3.1	Dagenhart's e^N Crossflow Method (MARIA)	42
5.3.2	Sturdza's Compressible Envelope e^N Crossflow Method	44

5.3.3	Crouch, Crouch and Ng Neural Net e^N Crossflow Method	45
6	ATTACHMENT LINE INSTABILITIES	46
6.1	Empirical correlations	46
6.2	Other Methods	49
7	LAMINAR-TURBULENT INTERACTION	50
7.1	Empirical correlations	50
7.2	Other Methods (turbulent diffusion)	50
8	COMPRESSIBILITY EFFECTS	51
8.1	Compressibility corrections	51
8.2	Other methods	51
8.3	Generalized Inflection-Point Criterion	51
8.4	Multiple Acoustic Modes: Mack Modes	52
8.5	3-D Viscous Disturbances	53
9	INTERMITTENCY	54
9.1	Overview	54
9.2	Transition region experiments and theory	55
9.2.1	Turbulent Spots	55
9.2.2	Mean Boundary Layer Characteristics in the Transitional Region	55
9.2.3	The Intermittency Function	56
9.2.4	Spot Formation and Propagation	57
9.2.5	Pressure Gradient Effects	58
9.2.6	Freestream Turbulent Intensity Effects	61
9.2.7	Reynolds Number Effects	62
9.2.8	Crossflow Instability Induced Transition Regions	62
9.3	Transitional Region Modeling	63
9.3.1	Zero Pressure Gradient Based Model – Narasimha	63
9.3.2	Pressure Gradient Based Model – Dey and Narasimha	64
9.3.3	Solomon – Gostelow model	64
9.3.4	Transport Equation Intermittency Models	68
10	SURFACE ROUGHNESS	71
10.1	Isolated and Distributed Roughness	71
10.1.1	Tollmien-Schlichting (T-S)	71
10.1.2	Stationary Crossflow	71
10.2	Steps	72
10.3	Gaps	72
10.4	Surface Waves	72
11	RECOMMENDATIONS	74

1 Introduction

The purpose of this report is to review available methods for predicting the transition of boundary layers. The emphasis will be on methods for transition mechanisms which are relevant to the flight conditions and geometric configurations of high altitude, long endurance aircraft, although the methods themselves may be much more general than this specific case. Each method will be evaluated according to certain criteria which are appropriate to the development of a computationally efficient, accurate and robust transition prediction module which is fully integrated into a general purpose CFD code. For each particular transition mechanism, a method will be selected which best satisfies all of these criteria.

In low-disturbance environments such as flight, boundary layer transition to turbulence generally occurs through the uninterrupted growth of linear instabilities. The initial conditions for these instabilities are introduced through the receptivity process, which depends on a variety of factors (Saric et al. 2002). There is no shortage of publications in the field of boundary layer stability and transition. Comprehensive reviews for both 2-D and 3-D flows are given by Arnal (1994), Mack (1984), Reed & Saric (1989), Reshotko (1994), Saric (1994), and Saric et al. (2003). Reed et al. (1996) give an up-to-date discussion of the effectiveness and limitations of linear theory in describing boundary layer instabilities. The reader is referred to these reports for overviews of much of the early work in stability and transition, and much of the work referenced below in this report. Schrauf et al. (1995), Crouch (1997), Crouch & Ng (2000), Crouch et al. (2001), and Herbert (1997) have presented analyses of transition with specific applications to flight.

Four basic instability mechanisms can contribute to transition on a swept wing. Concave curvature can give rise to Görtler instabilities (Saric 1994) but this can be controlled by the appropriate profile design. Leading-edge radius and sweep give rise to attachment-line contamination and instability (Pfenninger 1977, Poll 1985) but this can be controlled by keeping the leading-edge radius below a critical value. Streamwise instabilities related to the Tollmien-Schlichting mechanism typically occur in the mid-chord region and transition can be reasonably correlated (Reed et al. 1996). It is now well known that using a favorable pressure gradient and minimizing the extent of the pressure-recovery region both contribute to the control of these instabilities. The crossflow instability has been the primary Chimera holding back laminar flow control (LFC). Favorable pressure gradients used to stabilize streamwise instabilities destabilize crossflow. For years, it seemed as though the only solution to crossflow control was surface suction. The perceived complications with moving parts and additional maintenance were always discouraging factors toward laminarizing swept wings. This final hurdle may have been overcome with passive nonlinear biasing of stationary crossflow wave growth (Saric et al. 1998).

There are additional factors which affect swept-wing transition. Intersection of a laminar boundary layer with a turbulent boundary layer (at the wing root for instance) causes contamination of the laminar boundary layer and transition to turbulence in a wedge-shaped region. The effect of compressibility in the high subsonic/low supersonic range is

normally stabilizing, but at higher Mach numbers the nature of the instabilities changes. Transition to fully turbulent flow is rarely instantaneous, and so the length of the transition region must be determined so that accurate skin friction or heat transfer calculations can be made. The roughness of the surface, which includes such things as bumps, steps, gaps, and surface waviness, obviously affects transition and so this must be investigated as well.

Recommendations for transition prediction methods to be used in the Rapid Assessment Tool for Transition Prediction (RATTraP) program are summarized at the end of each section and a more complete description is given as a separate section at the end of the report. A classic e^N method will be used for both Tollmien-Schlichting and crossflow instabilities. In both cases an envelope method as well as individual mode tracking will be used. For attachment line instabilities, an empirical formula relating the momentum thickness Reynolds number to transition location for both disturbed and undisturbed flow is recommended. Laminar-turbulent interaction will be predicted using an influence angle approach. Corrections to the critical N factor will be used to account for compressibility. Transition in the presence of roughness elements is predicted using empirical rules and N factor corrections.

2 General Methods

2.1 Linear Stability Theory

Mack (1984) should be considered required reading for those interested in all aspects of boundary layer stability theory, including all the basic details for deriving, analyzing, and solving the stability equations for 2-D flows, compressible flows, and 3-D flows. His report updates the 3-D material in Mack (1969), which covers in large part his own pioneering contributions to the area. Aspects on secondary instability theory are reviewed in Herbert (1988), Cowley & Wu (1994), and Healy (1995), and are not covered here.

The basic idea behind linear stability theory is to superpose small disturbances onto the local, undisturbed boundary layer state (termed the "basic state") and determine whether these perturbations grow or decay. If all decay, then the flow is termed "stable". Control schemes creating a more stable basic state delay transition. The analysis is performed locally by linearizing the complete unsteady Navier-Stokes equations about the basic state. With (x,y,z) being the chordwise, normal-to-the-wall, and spanwise coordinates, the Navier-Stokes equations are made dimensionless by introducing the length scale

$$\delta_r = (vx/U_\infty)^{1/2}$$

The quantity δ_r is called the local reference boundary layer thickness. The quantities U_∞ and ν are the freestream velocity and kinematic viscosity, respectively. The quantity R , the square root of the x -Reynolds number, is used to represent distance along the surface. The basic-state flow is assumed to be locally parallel; thus the basic-state quantities Q satisfy

$$U=U(y), V=0, W=W(y), T=T(y)$$

where (U, V, W) are the chordwise, normal-to-the wall, and spanwise velocity components, and T is the temperature. It is, of course, an incongruity to speak of a parallel boundary layer flow since no such thing can exist except under very special circumstances. However, the parallel-flow assumption is an important first approximation to the linearized Navier-Stokes equations. The stability equations (Orr-Sommerfeld equations) are obtained by superposing small disturbances q' onto the basic state thus giving total flow quantities q of the form

$$q(x,y,z,t) = Q(y) + q'(x,y,z,t)$$

The quantities q and Q separately satisfy the complete Navier-Stokes equations and therefore separately represent real flows, while it is important to remember that the disturbance quantities q' do not. When the basic-state solution is dropped from the equations describing q , the equations in terms of the disturbance quantities q' result.

These equations are further simplified by making the approximation that products of disturbance quantities are neglected, i.e. the disturbance equations are linearized.

The disturbance equations are linear and the coefficients are functions of y only. This suggests a solution for q' in terms of separation of variables using normal modes (i.e. exponential solutions in terms of the independent variables (x,z,t) to reduce the disturbance equations to ordinary differential equations. In a real boundary layer flow, the basic-state quantities vary slowly with the chordwise position. In practice therefore, the normal-mode approach is generalized as:

$$q' = q_0(y) e^{i\Theta} + \text{c.c.}$$

where c.c. stands for complex conjugate and $\Theta(x,z,t)$ is the phase function

$$\partial\Theta/\partial x = \alpha, \partial\Theta/\partial z = \beta, \partial\Theta/\partial t = -\omega$$

Here, α is the chordwise wavenumber, β is the spanwise wavenumber, and ω is the frequency. The amplitude function $q_0(y)$ is complex and q' is real because the Navier-Stokes equations are real. The dimensionless frequency

$$F = \omega/R = 2\pi\nu f/U_\infty^2$$

is used, where f is the frequency in Hertz and is conserved for single-frequency waves. The system constitutes an eigenvalue problem for the eigenvector $q_0(y)$. This step represents a formal variable transformation and produces the correct zeroth-order approximation (quasi-parallel) that can be rigorously justified using a nonparallel analysis (see, for example, Gaster 1974, Saric & Nayfeh 1977).

For a well-posed eigenvalue problem such as plane Poiseuille flow, there are an infinite set of discrete eigenvalues and a corresponding infinite discrete set of eigenfunctions. For boundary layers, there is a finite discrete set of eigenvalues and a continuous spectrum. The eigenfunctions are called modes and form a basis for an arbitrary disturbance profile. For incompressible streamwise instabilities, the least stable mode is called the first mode and there is no more than one unstable mode so that not much attention is paid to higher modes. For some flows (e.g. compressible and centrifugal instabilities), more than one mode can be unstable.

Disturbances can be classified with respect to spatial amplification, temporal amplification, and spatial and temporal amplification. In spatial theory, ω is assumed to be real, while α and β are assumed to be complex. Their real parts, α_r and β_r , represent the physical wavenumbers of the disturbances, while their imaginary parts, α_i and β_i , represent the growth (or decay) rates in the x and z directions, respectively. In temporal theory, α and β are assumed to be real, while ω is assumed to be complex. For both temporal and spatial amplification, ω , α , and β are all assumed to be complex; this concept is applicable to wavepacket disturbances (Gaster 1968, Gaster & Grant 1975).

For spatial stability, the dispersion relation

$$\alpha = f(\beta, \omega, R)$$

yields the unknown pair (α_r, α_i) when β_r, β_i, ω , and R are specified. Whereas β_r can be considered a parameter, β_i is really also an unknown and an additional condition must be specified. For 2-D basic-state flows and 3-D conical basic-state flows (e.g., an infinite-span swept wing, Mack 1988), spanwise-periodic disturbances grow in the chordwise direction and $\beta_i = 0$. This may not be true in the case of localized 3-D disturbances. Arnal (1994) reviews the issue of the determination of β_i .

For temporal stability, the dispersion relation

$$\omega = f(\beta, \alpha, R)$$

yields the unique pair (ω_r, ω_i) when β, α , and R are specified. Because ω appears linearly in the stability equations, much of the early work focused on this case. However, spatial theory corresponds more closely to certain physical situations such as boundary layers.

For the case of a 2-D wave, the approximate temporal growth rate is the product of the spatial growth rate and the real part of the group velocity, i.e.

$$\omega_i = (-\alpha_i) \text{Real}(c_g), \quad c_g = d\omega/d\alpha$$

for small $|\alpha_i|$ (Gaster 1962). Arnal (1994) points out that numerical simulations indicate that this transformation can be applied with confidence for larger amplification rates in 2-D flows. Nayfeh & Padhye (1979) find a relation between 3-D temporal and spatial stabilities and between spatial stabilities using the complex group velocity.

The minimum critical Reynolds number is that Reynolds number below which all disturbances are stable. Squire's theorem states that in determining the minimum critical Reynolds number, 2-D disturbances are most important. Squire's theorem holds only for incompressible, parallel flows with temporally growing disturbances near the minimum critical Reynolds number. Moreover, although the critical Reynolds number may be important from a fundamental point of view, it has nothing to do with the real problem of transition to turbulence. Use Squire's theorem only with extreme caution.

2.1.1 e^N Method

The state-of-the-art transition prediction design tool involves linear stability theory coupled with an e^N transition prediction scheme (Mack 1984, Poll 1984, Arnal 1984, 1992, 1994) and is applied at all speeds (Bushnell et al. 1989). The quantity N is obtained by integrating the linear growth rate from the first neutral-stability point to a location somewhere downstream on the body, but e^N represents nothing more than an amplitude ratio. The role of receptivity, not accounted for in linear stability theory, is key to the overall process as it defines the initial disturbance amplitude (that is, A_0 at the first

neutral-stability point). Transition to turbulence will never be successfully understood or predicted without answering how freestream acoustic signals and turbulence enter the boundary layer and ultimately generate unstable waves. Clearly then, the study of receptivity promises significant advance in practical transition-prediction methods.

The basic design tool is the correlation of N with transition Reynolds number for a variety of observations. The correlation will produce a number for N (say 9) which is then used to predict transition Reynolds number for cases in which experimental data are not available. This is the e^N method of Smith & Gamberoni (1956) and Van Ingen (1956). As a transition prediction tool, it is certainly the most popular technique used today. It works within some error limits only if comparisons are made among experiments with identical disturbance environments. Since no account can be made of the initial disturbance amplitude, this method will always be suspect to large errors and should be used with extreme care. When bypasses occur, this method does not work at all. However, there is no other practical method presently available for industrial applications.

The basic transition control technique endeavors to change the physical parameters and flow conditions in order to keep N within reasonable limits. As long as laminar flow is maintained and the disturbances remain linear, the e^N method contains all of the necessary physics to accurately predict disturbance behavior.

Difficulties in the computation of the N factor increase with the complexity of the basic mean flow. There is practically no problem for 2-D, incompressible flows, because oblique waves do not need to be taken into account, and the only choice is between temporal and spatial theory. When the Mach number increases, the oblique waves become the most unstable ones, so that the wave orientation constitutes a new degree of freedom. The problem is considerably more complex in 3-D flows with the possible coexistence of streamwise and crossflow disturbances.

Mack (1984), Poll (1984), and Arnal (1984, 1992, 1994) give examples of growth-rate and e^N calculations showing the effects of pressure gradients, Mach number, wall temperature, and 3-D for a wide variety of flows. However, before using this method, one should be cautioned by Morkovin & Reshotko (1990).

2.1.2 Numerical Methods

Since the Reynolds number is large, the disturbance equations are stiff and care must be taken in their solution. A good review of finite-difference and spectral methods is given by Malik (1990). Mack (1984) gives a good summary of shooting techniques. An incompressible design code SALLY (Srokowski & Orszag 1977) and a compressible design code COSAL (Malik & Orszag 1981, Malik 1982, Malik et al. 1982) use input swept-wing profiles such as those generated by a Kaups & Cebeci (1977) boundary layer code. The code of Chen & Cebeci (1990) is a direct spatial stability code. COAST, an efficient compressible stability code including curvature effects has been developed at

Deutsche Airbus (Schrauf 1993) and CASTET has been developed at CERT/ONERA (Laburthe 1992).

Dagenhart (1981) considered stationary crossflow vortices and, instead of solving the linear stability equations each time, he used a table lookup of growth rates based on the basic state profile characteristics. He reported that, with his code MARIA, he could adequately reproduce the results of the more complicated stability codes while using less than 2% of the computer time. A similar procedure is used at Deutsche Airbus in a transonic wing-design code (Schrauf et al. 1992).

Before doing any stability calculation, it is required that the basic state be computed. In all cases the numerical accuracy of the basic state must be very high, because the stability results will be very sensitive to small departures of the mean flow from its "exact" shape. The stability of the flow can depend on small variations of the boundary conditions for the basic state, such as freestream velocity or wall temperature. Therefore, basic-state boundary conditions must also be very accurate. See the discussion and examples of Arnal (1994) and Malik (1990).

Recommendation

Although a great deal of faith is placed in the use of the e^N method for transition prediction in design, it must be used with caution. Care must be used in selecting which correlations to use for any given flow, since stability and transition behavior can strongly depend on the details of the flow. Without a clear understanding of the detailed physics and which instabilities are responsible for transition, incorrect results are obtained.

Arnal (1994) indicates that the e^N method works very well in 2-D boundary layers in predicting transition location within acceptable uncertainty for the low disturbance environments of flight. It is the method of choice for 2-D boundary layers.

It is not so successful, however, for absolute transition location prediction in 3-D boundary layers. Linear stability theory accurately predicts which wavelengths are most unstable and which are appropriate for control, and is therefore very useful for airfoil and wing design. However, Arnal (1994) and Schrauf (1994) review the different approaches to the application of the e^N method. When applied to available flight and wind-tunnel experiments, there is large scatter in the values of the e^N factor at the onset of transition among the different methods. There are three reasons for this behavior: 1) Transition location is more difficult to determine accurately in 3-D flow than in 2-D flow. 2) Crossflow disturbances are very sensitive to micron-sized roughness elements which have no effect on streamwise disturbances (Radeztsky et al. 1993). 3) Disturbance development can be dominated by nonlinearities during a large part of the transition process and the use of linear theory up to breakdown is inappropriate and can overestimate wave amplitude (Reibert et al. 1996, Haynes and Reed 2000).

The strength of linear theories is in their use for design by comparing growth rates and N factors from one configuration to another or doing parametric studies. A configuration with a smaller N factor (using the same form of the theory) is likely to remain laminar

longer. If the theory at least qualitatively contains the appropriate relationships, it can be a practical and efficient tool in the evaluation of new airfoil shapes for wings, even in 3-D, in a comparative sense.

In summary, carefully used LST is the method of choice for RATTraP.

2.2 Parabolized Stability Equations

In recent years the PSE have become a popular approach to stability analysis owing to their inclusion of nonparallel and nonlinear effects with relatively small additional resource requirements as compared with DNS (Herbert 1997). For linear PSE (LPSE), a single monochromatic wave is considered as the disturbance, which is decomposed into a rapidly varying “wave function” and a slowly varying “shape function”. Using a multiple-scales approach

$$\phi'(x, y, z, t) = \underbrace{\bar{\phi}(\bar{x}, y)}_{\text{shape function}} \underbrace{\chi(x, z, t)}_{\text{wave function}} + c.c.$$

where

$$\frac{\partial \chi}{\partial x} = i\alpha(\bar{x}), \quad \frac{\partial \chi}{\partial z} = i\beta, \quad \frac{\partial \chi}{\partial t} = -i\omega$$

The “shape function” $\bar{\phi}$ and streamwise wavenumber α depend on the slowly varying scale $\bar{x} = x/R$ while the “wave function” χ depends on the rapidly varying scale x . The frequency is ω and the spanwise wavenumber is β . This gives the following form for the streamwise derivatives of disturbance quantities

$$\begin{aligned} \frac{\partial \phi'}{\partial x} &= \left\{ \frac{1}{R} \frac{\partial \bar{\phi}}{\partial \bar{x}} + i\alpha \bar{\phi} \right\} \chi + c.c. \\ \frac{\partial^2 \phi'}{\partial x^2} &= \left\{ \frac{1}{R^2} \frac{\partial^2 \bar{\phi}}{\partial \bar{x}^2} + \frac{2i\alpha}{R} \frac{\partial \bar{\phi}}{\partial \bar{x}} + \frac{i\bar{\phi}}{R} \frac{d\alpha}{d\bar{x}} - \alpha^2 \bar{\phi} \right\} \chi + c.c. \end{aligned}$$

The explicit streamwise $O\left(\frac{1}{R^2}\right)$ second-derivative term is neglected. This yields the following system of equations

$$(L_0 + L_1)\bar{\phi} + L_2 \frac{\partial \bar{\phi}}{\partial \bar{x}} + \bar{\phi} L_3 \frac{d\alpha}{d\bar{x}} = 0$$

Here L_0 is the Orr-Sommerfeld operator, L_1 contains the nonparallel basic-state terms, and L_2 and L_3 arise due to the nonparallel disturbance terms.

The resulting system of equations is parabolic, so to complete the formulation, upstream (initial) and boundary conditions must be specified. The disturbance quantities are zero at the wall and as $y \rightarrow \infty$. If the analysis begins in a region where the initial disturbance amplitudes are small, linear stability theory can be used to obtain these initial conditions.

There still remains the matter of the ambiguity in streamwise dependence; applying a normalization condition ensures that any rapid changes in the streamwise direction will be “absorbed” by the wave function so that the shape function will vary slowly in this direction. For example, Haynes and Reed (2000) suggest the integral normalization

$$\rho = \int_0^{\infty} \bar{u}^t \frac{\partial \bar{u}}{\partial \bar{x}} dy = 0$$

Assuming the solution is known at streamwise location x^i , Haynes & Reed (2000) suggest the following streamwise marching algorithm:

Guess $\alpha(x^{i+1})$

Solve equation 1 for ϕ^{i+1}

Use ϕ^{i+1} to compute the error ρ

Use Newton’s method with ϕ^{i+1} to update $\alpha(x^{i+1})$

Repeat steps 2-4 until ρ is less than some tolerance

The nonlinear PSE (NPSE) are derived in a fashion similar to LPSE with the exception that each disturbance quantity is transformed spectrally in the spanwise and temporal directions

$$\phi'(x, y, z, t) = \sum_{n=-\infty}^{\infty} \sum_{k=-\infty}^{\infty} \underbrace{\bar{\phi}_{(n,k)}(\bar{x}, y)}_{shapefunction} * \underbrace{A_{(n,k)}(x) e^{i(k\beta_0 z - n\omega_0 t)}}_{wavefunction}$$

where

$$\frac{dA_{(n,k)}}{dx} = A_{(n,k)} i\alpha_{(n,k)}(\bar{x})$$

Here each mode (n,k) is the product of a “shape function” and a “wave function”. The resulting system of equations is

$$\sum_{n=-\infty}^{\infty} \sum_{k=-\infty}^{\infty} \left\{ (L_0 + L_1) \bar{\phi} + L_2 \frac{\partial \bar{\phi}}{\partial \bar{x}} + \frac{d\alpha}{d\bar{x}} L_3 \bar{\phi} \right\}_{(n,k)}^* A_{(n,k)} e^{i(k\beta_0 z - n\omega_0 t)} = N$$

The operators L_i ($i=0,3$) assume the same meaning as in the LPSE form except that they are applied to each particular mode $(\alpha_{(n,k)}, n\omega_0, k\beta_0, \bar{\phi}_{(n,k)})$ where ω_0 and β_0 are the fundamental frequency and spanwise wavenumber, respectively. During the marching procedure, each mode must individually satisfy the normalization condition.

The PSE formulation here utilizes a body-intrinsic coordinate system and the curvature is included in the associated metric coefficients. The marching procedure naturally aligns the disturbance wave propagation in the proper direction. The local radius of curvature of the wing appears in the equations through the following terms:

$$\begin{aligned} k_1 &= 1 + \frac{y}{R_c}, \quad k_2 = \frac{1}{y + R_c}, \\ k_3 &= -\frac{1}{R_c^2} \frac{dR_c}{d\bar{x}} \approx 0, \\ k_4 &= -\frac{y}{R_c^2} \frac{dR_c}{d\bar{x}} \approx 0 \end{aligned}$$

where R_c is the local dimensionless radius of curvature of the airfoil taken as positive or negative for convex or concave regions, respectively. For all the computations presented here, curvature is neglected in the basic-state analysis. This is because the basic-state curvature terms are the same order as the terms neglected according to the boundary layer approximation so it would be inconsistent to retain them. In the limit of infinite curvature (flat plate), $R_c \rightarrow \infty$, so $k_1=1$ and $k_2=0$ are used in the stability equations for cases where curvature is neglected and the above equations are used for cases where curvature is retained.

The code LASTRAC (Chang 2003) has been developed at NASA Langley, validated with numerous convective cases, and is available with limited distribution.

Recommendation

NPSE is more calculation intensive than LST (too much for RATTraP). The good news is that the CFD formulations validated to date demonstrate that if the environment and

operating conditions can be modeled and input correctly, the computations NPSE agree quantitatively with the experiments. What is especially significant and exciting is that the NPSE, which have significantly less resource overhead associated with them compared with DNS, have been shown to accurately model a variety of relevant flows, including 3-D flows. The recommendation is to validate RATTraP LST correlations with NPSE.

2.3 Direct Numerical Simulation

Direct numerical simulations (DNS) are playing an increasingly important role in the investigation of transition; this trend will continue as considerable progress is made in the development of new, extremely powerful computers and numerical algorithms. In such simulations, the full Navier-Stokes equations are solved directly by employing numerical methods, such as finite-difference, finite-element, finite volume, or spectral methods. There are two approaches: 1) simulations in which the disturbances are computed as part of the simulation, and 2) simulations in which transition is estimated based on mean-flow quantities or the location is user specified. Only the first approach is considered here.

For simulations in which the disturbances are computed as part of the simulation, excellent reviews include that of Kleiser & Zang (1991) and two AGARD lectures on spatial simulations (Reed 1994) and temporal simulations (Kleiser 1994). Transition is a spatially evolving process and the spatial DNS approach is widely applicable since it avoids many of the restrictions that usually have to be imposed in other models and is the closest to mimicking experiments. For example, no restrictions with respect to the form or amplitude of the disturbances have to be imposed, because no linearizations or special assumptions concerning the disturbances have to be made. Furthermore, this approach allows the realistic treatment of space-amplifying and -evolving disturbances as observed in laboratory experiments. The temporal simulation, by contrast, uses periodic boundary conditions in the streamwise direction (identical inflow and outflow conditions) and follows the time evolution of a disturbance as it convects through the flow; upstream influence is limited by this assumption. Moreover, in temporal simulations, the basic state is assumed to be strictly parallel, that is, invariant with respect to the streamwise coordinate. All of these restrictions noted are especially suspect when considering complex geometries, 3-D boundary layers, receptivity, and control.

The basic idea of the spatial simulation is to disturb an established basic flow by forced, time-dependent perturbations. Then the reaction of this flow, that is, the temporal and spatial development of the perturbations, is determined by the numerical solution of the complete Navier-Stokes equations.

Problems associated with this method which preclude it from being used routinely for design include:

- (a) A large amount of computer resources (cpu and memory) is usually required for solution (e.g. Herbert (1991) quotes an estimate of cpu $O(10^3)$ hours and double

precision words of memory $O(10^8)$ on a CRAY-YMP for 3-D runs on a flat plate using standard methods and simulating breakdown with limited resolution). Because of the long fetch from the onset of instability to breakdown and the large amplitude ratios associated with this process ($O(e^{10})$ and larger), resolution and bit accuracy limit how far into breakdown that a spatial simulation can go. Because of the large differences in amplitudes throughout the domain and the large growth rates known to exist near breakdown where smaller scales appear, truncation and round-off errors can easily contaminate the solution. Consequently, spatial simulations are currently unable to proceed completely through transition and into turbulence.

(b) There is a need to impose a nonintrusive downstream boundary condition since the periodic assumption (associated with temporal simulations) is no longer used. Several ideas have been developed by various investigators. However, there is typically a region of waste where the Navier-Stokes equations are not valid and the solution is discarded. In light of the discussion in (a), this adds to the resource problem.

(c) The use of either the PSE (Herbert 1993) or DNS simulations, both of which account for nonlinear and nonparallel effects, is hampered by our current lack of knowledge of the connection between the freestream and the boundary layer response. A physically appropriate upstream or inflow condition must be specified. Efforts to bridge this gap are an area of active research.

2.3.1 Numerical Methods

The Navier-Stokes equations are highly nonlinear, time-dependent, and elliptic in space. To simulate the spatial evolution of a disturbance field, a numerical method must account for (a) time-accurate discretization, (b) phase-accurate discretization of the convective terms, (c) sufficient resolution in viscous regions (e.g. close to surfaces and in free shear layers), (d) outflow, nonreflective boundary conditions, and (e) efficiency, speed, and "low" memory.

The most highly studied geometry has been the flat plate. A finite rectangular box, usually placed downstream of the leading edge and extending from X_0 to X_N in the streamwise direction, from 0 to Y_N in the normal direction, and from 0 to Z_N in the spanwise direction, is usually selected as the physical domain. The reaction of this flow to disturbances input along the wall, at the inflow, and/or at the farfield edge of the box is then determined by numerical solution of the complete Navier-Stokes equations for 3-D, time-dependent compressible/incompressible flow. In this formulation a downstream boundary condition must also be specified.

Different formulations of the dependent variables are possible including (in incompressible, Cartesian form): a) primitive variable with three velocity components u, v, w (in the streamwise x , normal y , and spanwise z directions, respectively) and pressure (four unknown physical quantities). b) vorticity/stream function (for 2-D only).

c) vorticity/velocity with three vorticity transport equations. The governing equations can be solved for total flow quantities (basic state plus disturbance) or disturbance quantities (basic state solved separately) and, if written in conservative form, quantities such as vorticity, energy, etc. are "conserved", even for finite step sizes in the discretized equations.

Because of the need for high spatial resolution, higher than in conventional CFD applications, the use of high-order finite differences and spectral methods is particularly attractive. This is particularly important numerically when trying to advance into regions of large growth rates, small scales, and breakdown. High-order finite-difference and compact methods are attractive because of their enhanced accuracy, relative tolerance of inconsistent boundary conditions, usefulness in complex regions, and resulting matrix structure (banded matrix because they are local methods). These techniques are very popular in spatial simulation studies. Spectral and pseudospectral methods are global methods requiring less terms in the approximate solution and attractive numerically because of their high accuracy, good resolution in regions of high gradients, and exponential convergence properties and have become popular in transition simulations in various forms as will be seen in subsequent paragraphs. Another advantageous property of these methods is that the energy can be monitored in the coefficients of the higher terms in the series, thus signaling when resolution is inadequate and the simulation must be terminated. Collocation methods are often used for their ease of application, while Galerkin methods can be used in the development of divergence-free basis functions and tau methods may be used when fast solvers are available. However, the issues of incorporating inconsistent boundary conditions, applying spectral methods to complex geometries and compressible flows, and solving flows with discontinuities away from boundaries (Gibbs phenomenon) need to be further addressed. In general, promising active areas of effort include improved iterative convergence and multigrid techniques and spectral domain decomposition and multidomain methods.

One must determine a workable combination of governing equations, boundary conditions, and numerics for each given problem. What works for one situation may not work for another. The available computer, in particular the architecture, vector length, speed, and memory, also dictates what approach is taken. Thus far, to this author's knowledge, all simulations have assumed periodicity in the spanwise direction and used Fourier series there. (The use of Fourier series allows for the use of Fast Fourier Transforms (FFTs) for the efficient computation of derivatives.)

Investigators are working the prohibitive computer resource issue by developing advanced, highly accurate algorithms and the time and memory savings reported by investigators have thus far been encouraging in allowing the spatial simulation to become a more viable tool for the determination of the basic physics. More work to reduce resource requirements for general geometries must be vigorously pursued, however, if spatial simulations are ever to become routine in design.

2.3.2 Disturbance Input

One advantage of spatial simulations is the freedom and control of what is input as a disturbance; the computation can be made to mimic experiments and provide some guidance. If disturbances are to be introduced directly into the boundary layer along the inflow, typically normal modes from the Orr-Sommerfeld equation and/or random disturbances have been successfully used. As another example, Singer et al. (1989) used a combination of random noise and vortices as upstream conditions in the plane channel and showed that, depending on the amplitude of the vorticity, the route to turbulence can be altered and experimental results matched. Alternatively, a periodic suction/blowing (Fasel et al. 1987, 1990) or heater strip (Kral & Fasel 1989, 1990) on the surface will introduce disturbances; this is incorporated into the wall boundary conditions. Spalart (1989, 1990, 1991, 1993) introduces any of random noise, stationary and traveling waves, packets, etc. by means of a body force added to the right-hand side of the momentum equation.

Providing input upstream of Branch I allows the noise to be washed out of the true disturbance signal in a region of damping before subsequent amplification. All of the above techniques produce linear waves with the appropriate frequency and wavelength, although the introduction of modes at the upstream boundary requires the smallest downstream distance for this adjustment. However, some of the other techniques can be argued to more mimic the experimental setup.

Alternatively, disturbances can be introduced along the boundaries in the freestream along and/or upstream of the body. For receptivity studies, oscillatory sound and vorticity disturbances are prescribed.

2.3.3 Downstream Boundary Conditions

In disturbance propagation problems, it is necessary to impose nonreflecting outflow conditions. The elliptic nature of the Navier-Stokes equations comes from two sources: the pressure term and the viscous terms. Interaction of these two effects produces upstream influence; if local velocity perturbations interact with the condition imposed at the downstream boundary, a pressure pulse can be generated that is immediately felt everywhere in the flowfield including the inflow boundary.

The boundary layer is a parabolic, convectively unstable system, where controlled disturbances applied upstream convect downstream and affect transition. But once these disturbances pass by, the boundary layer reverts to its original state before the forcing. As long as sufficient resolution is used and the boundary layer thickness to streamwise distance is small enough to prevent the transmission of pressure signals over distances of the order of x , advantage can be taken of this property of small upstream influence in formulating the downstream condition.

Several investigators have developed a buffer domain, or region appended to the downstream end of the computational domain. In this region, the governing equations

are modified to support only downstream moving waves or include strong damping. It appears that as long as some sort of reasonable treatment is done downstream ahead of the boundary, the problem of wave reflection back upstream seems to be under control. The major concern is to minimize the wasted region in the computation, in order to keep required resources to a minimum.

Recommendation

DNS is much more calculation intensive than NPSE (way too much for RATTraP). The good news is that the CFD formulations validated to date demonstrate that if the environment and operating conditions can be modeled and input correctly, the DNS computations agree quantitatively with the experiments for complex flows. The recommendation is to validate NPSE and then simpler LST correlations with DNS.

2.3.4 Validation and Verification

Here we distinguish between verification and validation. Per the designations of Roache (1997), we consider verification to mean “confirming the accuracy and correctness of the code” (i.e. is the grid resolved, are there any programming errors in the codes, etc.). Validation requires verification of the code in addition to confirming the adequacy of the equations used to model the physical problem. Strictly speaking, a code can only be validated by comparison with quality experimental data.

There are mainly three sources of error in the abstraction of continuous PDE's to a set of discrete algebraic equations; (1) discretization errors, (2) programming errors (bugs), and (3) computer round-off errors. The objective of code verification is then to completely eliminate programming errors and confirm that the accuracy of the discretization used in solving the continuous problem lies within some acceptable tolerance. Aside from specifying single or double precision, the code developer has little control over the computer round-off errors, but this is usually several orders of magnitude smaller than the discretization error and far less than the desired accuracy of the solution.

In this section we address programming and discretization errors. Many methods are discussed in the literature for code verification using grid refinement, comparison with simplified analytical cases, etc. For recent discussions see Roache (1997) and Oberkampf et al.(1995). Specific suggestions for testing a CFD code for the study of transition include (a) grid-refinement studies, (b) solving test problems for which the solution is known, (c) changing the “far-field” boundary locations systematically and re-solving, (d) comparing linear growth rates, neutral points, and eigenfunctions with linear stability theory, (e) running the unsteady code with time-independent boundary conditions to ensure that the calculations remain steady, and (f) running geometrically unsymmetric codes with symmetric conditions.

In addition to the usual code verification techniques, there is a general method to verify the discretizations and locate programming errors by comparison with “manufactured” analytical solutions (Steinberg & Roache 1985). This method is general in that it can be applied to any system of equations. Although it is an extremely powerful tool, this

method has received relatively little attention in the literature. For clarity the technique is demonstrated on the Poisson equation.

$$Lu \equiv \frac{\partial^2 u}{\partial x^2} + \frac{\partial^2 u}{\partial y^2} = F(x, y)$$

To solve this problem, discretize the operator L using some appropriate approximation (finite differences, spectral, etc.). In general, the exact solution is not available. Therefore, for verification purposes, force the solution to be some combination of analytical functions with nontrivial derivatives. For example, consider the system $g \equiv Lv = 5e^{3y} \sin(2x)$, which has an analytical solution $v = e^{3y} \sin(2x)$. The exact solution can then be compared with the computed solution. Of course, manufactured solutions should be chosen with topological qualities similar to those anticipated for the solution to the “real” problem (e.g. gradients close to the wall). Proper choice for the manufactured solutions also allows the discretization of the boundary conditions to be verified. For large systems of equations a symbol manipulator is recommended for computing g . If a bug occurs, zeroing the coefficients of some terms can help to isolate the bug.

Validation is defined as encompassing verification of the code as well as confirming that the equations used to model the physical situation are appropriate. The basis of validation is assumed to be a successful comparison with the few careful, archival experiments available in the literature. To date the PSE have been applied to a variety of 2- and 3-D flow situations and are generally regarded as appropriate for convectively unstable flows. The reader is encouraged to consult the reviews of Herbert (1997) and Reed et al. (1998) for many more examples, as well as the contrasts with DNS and LST. For leading-edge receptivity problems, DNS has been demonstrated to have been successfully validated.

3 Tollmien-Schlichting Instabilities

3.1 Empirical correlations

When there is some knowledge of transition location, mean laminar and turbulent heat transfer can usually be computed to better than 25% accuracy. However laminar-turbulent transition in the boundary layer is usually estimated from crude algebraic correlations. The scatter in these correlations can be a factor of 2 or more. For example, because transition causes heat transfer to rise by a factor of about 5 in high-speed flows, this uncertainty in transition location dominates overall uncertainty in heat-transfer predictions. Clearly, knowledge of the transition process is crucial for accurate vehicle heating and drag predictions over the whole flight regime (Reed et al. 1997).

Correlations usually try to predict the final onset of fully turbulent flow at Re_x or Re_θ as a function of pressure gradient, freestream turbulence, wall roughness, Mach number, wall suction and blowing, and wall heating and cooling. Most of the approximations deal with only one or two of these parameters. “Viscous Fluid Flow” 2nd edition by Frank M. White pp. 375-392 describes many of these efforts from an engineering standpoint.

Recommendation

Because these correlations usually do not contain physics, they must be used with great caution and only in a comparative conceptual design situation. Use them only within the assumptions of the model (flowfield characteristics and operating conditions). However, because LST contains all the relevant physics, it is suggested that growth rates from families of Falkner-Skan profiles be parameterized with several of these empirical basic-state quantities and placed in a look-up table.

3.2 e^N Methods

Streamwise instabilities are characterized by streamwise traveling waves that appear in 2-D boundary layers and in the mid-chord region of swept wings.

Considering a wide class of instability mechanisms, the general impression is that viscosity can only stabilize a flow. However, a flat-plate boundary layer velocity profile is known to exhibit instability and yet it has no inflection point. Prandtl (1921) first developed the fundamental ideas of a viscous instability mechanism. The instability is called viscous because the boundary layer velocity profile is stable in the inviscid limit and thus, an increase in viscosity (a decrease in Reynolds number) causes the instability. A general energy analysis shows that the Reynolds stress is the production term for instabilities. Viscosity establishes the no-slip boundary condition which in turn creates the Reynolds stress which may destabilize the flow. The actual distribution of Reynolds stress throughout the boundary layer determines whether a particular disturbance is stable or unstable.

Comparisons between the data of the mean-flow and disturbance-flow rms measurements from a single-frequency experiment and the data from the Blasius solution and a solution from linear stability theory show outstanding agreement and demonstrate that the 2-D problem is well understood. Since the Orr-Sommerfeld problem is an eigenvalue problem, amplitude is undetermined. The disturbance shape measured in experiments is characteristic of the first-mode eigenfunction or Tollmien-Schlichting (T-S) wave. The sharp zero and double maximum occur because of a 180 degree phase shift in the region of the critical layer (where the local mean-flow speed equals the disturbance phase speed). This shape is very different from a turbulence distribution or 3-D T-S wave. The higher-mode eigenfunctions are highly damped and disappear within a few boundary layer thicknesses downstream of the disturbance source.

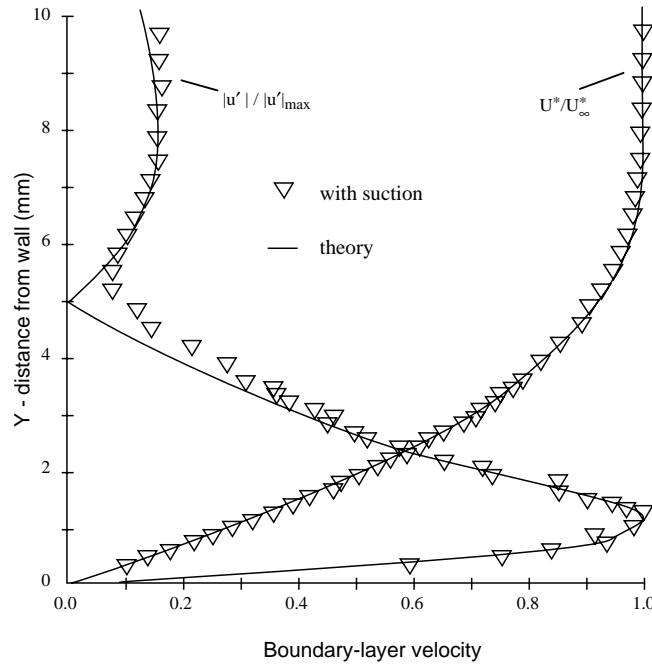


Figure 0: A comparison between linear stability theory (line) and experiment (symbols) for flow over a 2-D flat plate with suction. a) Both the basic state and the rms-amplitude distribution of the streamwise disturbance velocity are shown. The agreement is excellent. (From Reed & Nayfeh 1986, Reynolds & Saric 1986, Saric & Reed 1986).

At constant frequency, the disturbance amplitude initially decays as one marches in the downstream direction until the Reynolds number RI at which the flow first becomes unstable is reached. This point is called the Branch I neutral stability point. The amplitude grows exponentially in the downstream direction until the Branch II neutral stability point RII is reached. The locus of RI and RII points as a function of frequency gives the neutral stability curve.

As mentioned previously, the e^N method was first developed by Smith & Gamberoni (1956) and Van Ingen (1956) who correlated N factors between 7 and 9 with low-speed wind-tunnel experiments. In these situations, the freestream turbulence level Tu influences transition. Mack (1977) proposed relating N factor to Tu by the following relationship:

$$N = -8.43 - 2.4 \ln(Tu)$$

This can be applied with some confidence for $10^{-3} < Tu < 10^{-2}$ for both flat-plate and decelerated flows, as well as transonic Mach numbers (see Arnal 1994). It cannot be used for $Tu < 10^{-3}$, because noise becomes the dominant parameter and the excitation is frequency-dependent. Crouch (2004) points out that data used for this correlation from Schubauer & Skramstad (1947) show a fixed transition Reynolds number for $Tu < 0.07\%$ which is related to wind tunnel acoustics, and that data from a quieter facility would likely follow the N factor relationship to lower values of Tu . The relationship cannot be used for $Tu > 10^{-2}$, because T-S waves are not clearly discernable, and the transition process is dominated by low-frequency, 3-D disturbances which are stable according to linear theory (Klebanoff modes). Wang & Gaster (2004) and Crouch et al. (2004) determine N factor corrections for roughness (discussed in a later section). Arnal discusses the conclusion that the e^N method with $N \gg 10$ can be applied to predict transition in 2-D subsonic and transonic flows if the background turbulence level is low enough (quiet tunnels, free flight conditions) and if the wall is smooth. Since the distance between the end of the linear region of disturbance development and the breakdown to turbulence is very short, the use of linear theory up to the onset of transition can be justified. According to Arnal, for "typical flat-plate conditions, the streamwise extent of linear amplification covers about 75 to 85% of the distance between the leading edge and the beginning of transition. The relative extent of the nonlinear region is even smaller for decelerated flows. This explains why prediction methods based on linear theory can give satisfactory results."

3.2.1 Nonparallel Effects

Mack (1984) and Saric (1990, 1994) are good references for nonparallel effects. Gaster (1974) using asymptotic theory; Herbert & Bertolotti (1987) and Bertolotti et al. (1992) using PSE; and Fasel & Konzelmann (1990) using spatial DNS, all show that the parallel neutral curve is essentially the same as the nonparallel neutral curve. Considering the experiments of Schubauer & Skramstad (1947) and Ross et al. (1970), for $R > 600$, the neutral points from linear stability theory and experiment agree very well for Blasius flow. For $R < 600$, the agreement is not as good; differences between theory and experiment in the linear range are not fully due to nonparallel effects, but rather to some other mechanism at work (Saric 1990, 1994). Klingmann et al. (1993) confirmed Saric's ideas by generating experimental data that fall on the theoretical parallel neutral stability curve all the way forward to the minimum critical Reynolds number ($R \gg 230$).

According to PSE computations for 2-D mean flows, nonparallel effects are negligible for 2-D waves even for strong positive pressure gradients. These effects do become important for oblique waves, however (Arnal 1994).

3.2.2 Envelope methods/Mode tracking methods

The envelope method computes one N factor associated with the maximum growth rate locally (finds the most unstable wave locally) as one marches downstream, whereas mode tracking calculates the N factors for all waves and tells the user the most unstable wave. The envelope method produces a slightly higher N factor and thus is conservative in transition location prediction (farther upstream). Because the region of linear growth is usually long compared with the region over which the growth rates take off in flight situations, the differences in location prediction are within the uncertainty of the LST itself.

Recommendation

Use parallel, envelope LST method. Use DNS or PSE to validate and correlate N factors and develop appropriate characterizing parameters for growth-rate table lookup based on Falkner-Skan basic states. Note that disturbance phase speed is approximately 40% U and unstable wavelengths are on the order of 6-10 boundary layer thicknesses long.

3.3 Other methods

DNS and PSE are overkill for RATTraP. Their role is to correlate N factors and in the development of basic-state parameters to characterize LST results for time-efficient table lookup.

4 Crossflow Instabilities

Transition to turbulence in crossflow-dominated, swept-wing boundary layers has received considerable attention over the past decade or so. The reason is the obvious engineering benefit that would result from enabling laminar flow over most of the wing. The difficulty faced in confronting this problem has been the strongly nonlinear nature of the crossflow instability. Linear methods have been unable to completely predict absolute transition location and therefore tremendous effort has been given to understanding the nonlinear aspects of the phenomenon. The basic review of swept wing stability was given by Reed and Saric (1989) while recent reviews of crossflow efforts have been given by Arnal (1997), Bippes (1997, 1999), Crouch (1997), Haynes and Reed (2000), Herbert (1997a, 1997), Kachanov (1996), Reibert and Saric (1997), Reshotko (1997), and Saric et al. (1998, 2003).

The papers of Reed and Saric (1989), Kohama et al. (1991), Kachanov (1996), Arnal (1997), Bippes (1997), and Saric et al. (2003) provide an extensive list of references for the recent experiments, including the DLR experiments in Germany on a swept flat plate, a Russian swept-flat-plate experiment, the CERT/ONERA experiments on swept wings, the Institute of Fluid Science work in Sendai on cones and spheres, and the Arizona State University (ASU) swept-wing experiments. These papers established the existence of both traveling and stationary crossflow vortices, saturation of the stationary crossflow vortex, the nonlinear secondary instability leading to transition, and the sensitivity to freestream disturbances and surface roughness. Here are some great challenges to the computationalist.

One of the key missing ingredients in all 3-D boundary layer experiments is the understanding of receptivity. Receptivity has many different paths through which to introduce a disturbance into the boundary layer and this “road map” is more complicated because of the amplified stationary vortices. In fact, many aspects of transition in 3-D boundary layers are orthogonal to 2-D boundary layers so such a “road map” is either not unique or too complicated. Aside from the usual mechanisms, such as the interaction of freestream turbulence and acoustical disturbances with model vibrations, leading-edge curvature, attachment-line contamination, discontinuities in surface curvature, etc., the presence of roughness that may enhance a stationary streamwise vortex is very important. In contrast to 2-D boundary layers where small 2-D roughness is important and 3-D roughness is less important unless it is large, the 3-D boundary layer appears to be very sensitive to micron-sized 3-D roughness. In this case, 2-D roughness is only important at its edges.

The net result of the previous efforts is a very complete understanding of the primary crossflow instability, including details of the nonlinear saturation of the dominant stationary mode and the growth of harmonics. An important consequence is that a means of transition suppression has been developed by Saric et al. (1998) that exploits the nature of the nonlinearities.

4.1 Empirical correlations

Owen & Randall (1952) evaluated crossflow stability and transition criteria based on Gray (1952) AW52 flight results and on Anscombe & Illingsworth (1952) wind-tunnel data. They introduced a crossflow Reynolds number $R_{cf} = W_{\max}\delta_{10}/\nu$ (based on the maximum crossflow velocity and the boundary layer height where the crossflow velocity is 10% of the maximum) as the governing parameter and reported a minimum critical crossflow Reynolds number of 96 in the front part of the swept wing. Transition was located at 150. Other more recent experiments demonstrate that this is not the whole story. Michel et al. (1985) correlate transition using three parameters: Reynolds number based on the displacement thickness in the most unstable direction of the flow, the streamwise shape parameter, and the external turbulence level. Poll (1984) also finds he needs an additional parameter in addition to crossflow Reynolds number and shape factor.

With the current interest in high-speed flight, there is also a keen desire to determine correlating parameters, based purely on basic-state profiles, that can be easily incorporated into existing basic-state codes and will predict transition location (or trends) for crossflow-dominated problems. To evaluate parameters quantifying stability characteristics, Reed & Haynes (1994) examined the linear stability of the supersonic flow over a rotating cone at zero incidence. When compressibility and cooling effects are included, a relationship is found between a new crossflow Reynolds number and the maximum crossflow velocity at transition. This result has been verified with the yawed-cone data of King (1991), Stetson (1982), and Holden et al. (1994). The new crossflow Reynolds number is calculated solely from the basic-state profiles and, as such, it can aid in conceptual (only) transition prediction and design for 3-D boundary layers.

Recommendation

These parameters contain crossflow profile features and can be used to parameterize the basic-state profiles generated from Falkner-Skan-Cooke formulation and correlate the LST growth rates for table lookup for RATTraP.

4.2 e^N Methods

Linear stability theory is not so successful in absolute transition location determination for 3-D boundary layers. Arnal (1994) and Schrauf (1994) review the different approaches to the application of the e^N method. When applied to available flight and wind-tunnel experiments, there is large scatter in the values of the N factor at the onset of transition among the different methods. There are three reasons for this behavior: 1) Transition location is more difficult to determine accurately in 3-D flow than in 2-D flow. 2) Crossflow disturbances are very sensitive to micron-sized roughness elements which have no effect on streamwise disturbances (Radeztsky et al., 1993). 3) Disturbance development can be dominated by nonlinearities during a large part of the transition process and the use of linear theory up to breakdown is inappropriate and can overestimate wave amplitude (Reibert et al. 1996, Haynes and Reed 2000).

Whereas linear stability theory predicts that the traveling crossflow waves are more amplified than the stationary crossflow waves, many experiments observe stationary waves. The question of whether one observes stationary or traveling crossflow waves is cast inside the receptivity problem. Deyhle and Bippes (1996) and Bippes (1997) describe a series of comparative experiments in a low-turbulence and a high-turbulence tunnel. They found that for the particular model used in those experiments, turbulence intensities above $Tu = 0.0015$ produced transition behavior dominated by traveling waves, but that for lower turbulence levels, stationary waves dominate. Surprisingly, for increased turbulence levels where traveling waves dominate but the turbulence intensity is not too high, $0.0015 < Tu < 0.0020$, transition was actually delayed relative to low-turbulence cases at the same Reynolds number. The explanation is that the traveling waves excited by the increased freestream turbulence were sufficiently strong to prevent stationary waves from causing transition but were not themselves strong enough to cause transition as quickly as the stationary waves they replaced. This behavior indicates that transition results from many wind tunnels may have no bearing on flight results because quite low levels of turbulence are sufficient to generate traveling-wave-dominated behavior, not what is observed in flight. Since the flight environment is more benign than the wind tunnel, one expects the low-turbulence results to be more important. The implication is that LST and the other CFD techniques be performed assuming stationary crossflow.

One of the important results to come out of the DLR group is the set of data that show early saturation of the disturbance amplitude and the failure of linear theory to predict the growth of the instability. They also report distorted mean profiles similar to those of Kohama et al. (1991) and Malik et al. (1994) due to the presence of the stationary corotating vortices. A similarity between the DLR and ASU experiments is the high N factors and high amplitude of the mean-flow distortion (10%-20%). It is not surprising that linear theory fails.

For low-amplitude crossflow waves, Radeztsky et al. (1994) find that linear stability theory correctly predicts the expected wavelengths and mode shapes for stationary crossflow. For this case, Haynes and Reed (2000) find that linear theory including curvature correctly predicts the growth rates. This is not the case for higher-amplitude crossflow and the results of Reibert et al. (1996) and Haynes & Reed (2000) demonstrate conclusively that a nonlinear calculation is required to obtain complete agreement.

4.2.1 Envelope methods/Mode tracking methods

Difficulties in the computation of the N factor increase with the complexity of the basic mean flow. There is practically no problem for 2-D, incompressible flows, because oblique waves do not need to be taken into account, and the only choice is between temporal and spatial theory. When the Mach number increases, the oblique waves become the most unstable ones, so that the wave orientation constitutes a new degree of freedom. The problem is considerably more complex in 3-D flows with the possible coexistence of streamwise and crossflow disturbances.

There is no unique way to integrate growth rates to achieve N factors because for 3-D disturbances there are more unknowns than equations and extra conditions must be applied for closure. Many groups have published many papers discussing this in the US, Europe, Japan, and Russia. For parallel, 3-D, incompressible stability calculations, a computer code, SALLY, was developed by Srokowski & Orszag (1977) that used the e^N method for correlating the transition location. They calculate the maximum temporal amplification rate for a given dimensional frequency from the parallel incompressible stability equations (the so-called envelope method). Then they use the real part of the group velocity to convert the temporal amplification rate into a spatial one (Gaster 1962) and integrate along the path defined by the real part of the group velocity. Mack (1978, 1980), in his spatial calculations for Falkner-Skan-Cooke yawed wedges, also defines the direction of growth as that of the real part of the group velocity. Cebeci & Stewartson (1980) use the condition that $d\alpha/d\beta$ be real, a condition also found by Nayfeh (1980). Nayfeh & Padhye (1979) find a relation between 3-D temporal and spatial stabilities and between spatial stabilities using the complex group velocity.

Recommendation

Setting the frequency to zero to examine stationary waves only is consistent with experiments and the inescapable presence of roughness. 1) For a conical flow in which the pressure gradient and all derivatives are zero along the generators (conically parallel to the leading edge), setting the growth rate along the generator to be zero is physical. Then fixing the dimensional wavelength in the direction along the generator is physical. That leaves as many unknowns as LST equations. 2) For non-conical situations, we recommend performing the “conical” approximation in strips and marching the disturbances across the wing.

Also, there has been much debate as to whether to include curvature effects. There has been much debate about the effects of curvature. For the swept wing, the inclusion of curvature has a very small effect on the metric coefficients. The maximum values of k_1 and k_2 occur at about 5% chord where they are the order of 1.01 and 10^{-3} , respectively. They both drop off sharply with increasing chordwise distance. These values may compel the researcher to neglect curvature, but the work of Haynes and Reed (2000) demonstrates conclusively that small changes in the metric coefficients can have a significant effect on the development of crossflow vortices. Convex curvature is stabilizing. However, LST neglects nonparallel effects which are destabilizing. These two effects more or less cancel each other in how they affect growth rates. We conclude the following: LST must be performed without curvature.

For stationary crossflow, Crouch (2004) provides N factor approximations taking into account surface roughness. See Section 10.1.

What to do if streamwise and crossflow disturbances coexist? First off, in designing a wing under flight Reynolds numbers, it is injudicious to work at the margins of these instabilities and with more than one possibly present. Having said that, for lack of anything better, for engineering design, several groups (Boeing, Arnal in France) assume a relationship between the N factors for steady crossflow transition and T-S transition, for

example: $NTS = 12 - 1.2 (NCF)$. The present design philosophy for a swept wing should be to eliminate streamwise instabilities and concentrate on mean flow modifications to reduce the growth of crossflow waves.

Note that crossflow wavelength is approximately 4 times the boundary layer thickness.

4.3 Other methods

The NPSE approach has recently been validated for 3-D flows subjected to crossflow disturbances by Haynes & Reed (2000). Here a detailed comparison of NPSE results with the experimental measurements of Reibert et al. (1996) show remarkably good agreement. The configuration is an NLF(2)-0415 45°-swept airfoil at -4° angle-of-attack, so chosen to provide an extensive region of crossflow (at least back to mid-chord) for detailed study of the physics. A spanwise array of roughness elements is used near the airfoil leading edge (at 2% chord) to introduce spanwise-periodic crossflow disturbances into the boundary layer. According to LST, a spanwise spacing of 12 mm corresponds to the most highly amplified stationary crossflow disturbance. The walls of the ASU Unsteady Wind Tunnel were shaped to achieve a spanwise-independent basic-state flow – an “infinite wing” in CFD terms. The freestream turbulence levels are well documented to be $O(10^{-4})$ so that, with any surface roughness, stationary crossflow is expected. Reibert et al. (1996) provide all the details for the experimental facility and set-up.

Haynes and Reed (2000) used a panel-method code to compute the inviscid flow, from which the edge boundary conditions were generated for the boundary layer code. Agreement between the experimental and computational C_p distribution is good.

As a baseline case to study the evolution of crossflow vortices, roughness elements with a spanwise spacing of 12 mm were placed on the experimental model. The initial conditions for the NPSE calculation (with curvature) were obtained by solving the local LST equations at 5% chord location for the fundamental (mode (0,1)) and adjusting its RMS amplitude such that the total disturbance amplitude matched that of the experiment at 10% chord. The NPSE was then marched from 5% chord to 45% chord. Transition occurred on the experimental model at 52% chord.

The primary and higher modes all grow rapidly at first and saturate at about 30% chord. This is due to a strong nonlinear interaction among all the modes over a large chordwise distance. From about 35% chord on, there is still strong nonlinear interaction among the primary and second harmonic, but not the others. The development of crossflow occurs in two stages. The first stage is linear and is characterized by small vertical v and spanwise w disturbance velocities convecting low-momentum fluid away from the wall and high-momentum fluid toward the wall. This exchange of momentum occurs in a region very close to the wall where there are large vertical gradients in the basic-state streamwise velocity. Because of this large gradient, the small displacements caused by the v and w disturbance components quickly lead to large disturbances u superposed on the basic state further downstream. This u component soon becomes too large and nonlinear interactions must be included in any calculations. This is the second stage, evidenced by roll-over seen in the streamwise-velocity contours. Seeing a comparison of the

experimental and computational total streamwise velocity contours at 45% chord, the agreement between the NPSE and the experiments is excellent. Seeing the comparison of the experimental N factor curves with LPSE, NPSE (with curvature), and LST, it is clear that the linear theories fail to accurately describe the transitional flow for this situation.

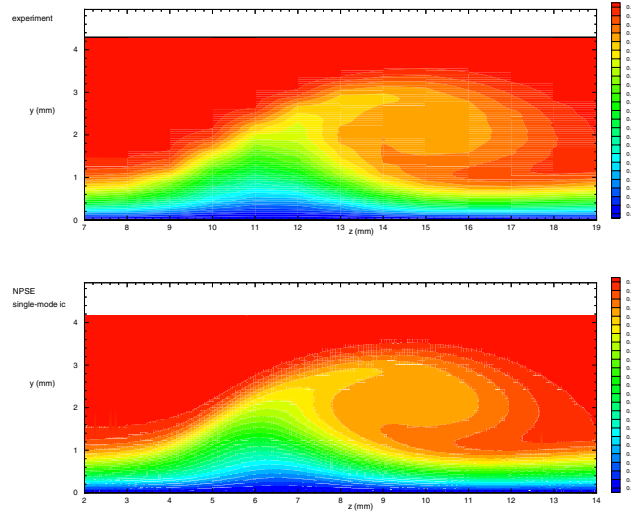


Figure 1: Streamwise-velocity contours for NLF(2)-0415 45° - sweep, $R_c = 2.4\text{million}$, $\lambda_z = 12\text{mm}$, 45% chord. Excellent agreement between NPSE with curvature and experiments.

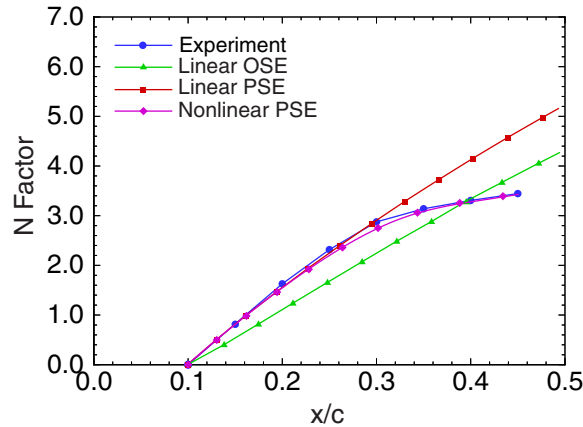


Figure 2: N factors for NLF(2)-0415 45° - swept airfoil, $R_c = 2.4\text{million}$, $\lambda_z = 12\text{mm}$. Shown is the excellent agreement between NPSE with curvature and the experiments.

There has been much debate about the effects of curvature. For this configuration, the inclusion of curvature has a very small effect on the metric coefficients. The maximum values of k_1 and k_2 occur at 5% chord where they are the order of 1.01 and 10^{-3} , respectively. They both drop off sharply with increasing chordwise distance. These

values may compel the researcher to neglect curvature, but the work of Haynes and Reed (2000) demonstrates conclusively that small changes in the metric coefficients can have a significant effect on the development of crossflow vortices.

Radeztsky et al. (1994) studied the effects of angle-of-attack (AOA). Here, in a case of weak favorable pressure gradient, the experiments showed that the crossflow disturbance is decaying in disagreement with various linear theories (LST, LPSE/without curvature, and LST/with curvature) that predicted the disturbance to be growing. Radeztsky et al. (1994) concluded that the disagreement was due to nonlinearity. For this case, Haynes and Reed (2000) found that the LPSE/with curvature and NPSE/with curvature both agreed with the experiment, indicating that in fact the crossflow disturbance decays and there is a strong sensitivity to changes in curvature, nonparallel effects, and pressure gradient (AOA). The disturbance was linear for this case.

Saric et al. (1998) observed that unstable waves occur only at integer multiples of the primary disturbance and no subharmonic disturbances are destabilized. They investigated the effects of distributed roughness whose primary disturbance wavenumber does not contain a harmonic at 12 mm (the most unstable wavelength according to linear theory). In the absence of artificial roughness, transition occurs at 71% chord. Adding roughness with a spanwise spacing equal to the wavelength of the linearly most unstable wave moves transition forward to 52% chord. However, subcritical forcing at 8 mm spanwise spacing actually delays transition beyond the pressure minimum and onto the trailing-edge flap at 80% chord. The NPSE results confirmed this effect.

4.4 Control with Distributed Roughness

Two important observations concerning the distributed roughness results of Reibert et al. (1996) are: (1) unstable waves occur only at integer multiples of the primary disturbance wavenumber; (2) no subharmonic disturbances are destabilized. Spacing the roughness elements with wavenumber $k = 2\pi/\lambda$ apart, excites harmonic disturbances with spanwise wavenumbers of $2k, 3k, \dots, nk$ (corresponding to $\lambda/2, \lambda/3, \dots, \lambda/n$) but does not produce any unstable waves with “intermediate” wavelengths or with wavelengths greater than λ .

Following this lead, Saric et al. (1998) investigate the effects of distributed roughness whose primary disturbance wavenumber does not contain a harmonic at $\lambda_s = 12$ mm (the most unstable wavelength according to linear theory). By changing the fundamental disturbance wavelength (i.e., the roughness spacing) to 18 mm, the velocity contours clearly showed the presence of the 18 mm, 9 mm, and 6 mm wavelengths. However, the linearly most unstable disturbance ($\lambda_s = 12$ mm) has been completely suppressed. Moreover (and consistent with all previous results), no subharmonic disturbances are observed. This shows that an appropriately designed roughness configuration can, in fact, inhibit the growth of the (naturally occurring) most-unstable disturbance. When the disturbance wavelength was forced at 8 mm, the growth of all disturbances of greater wavelength was suppressed. The most remarkable result obtained from the subcritical roughness spacing is the dramatic affect on transition location. In the absence of artificial

roughness, transition occurs at 71% chord. Adding roughness with a spanwise spacing equal to the wavelength of the linearly most unstable wave moves transition forward to 47% chord. However, subcritical forcing at 8 mm spanwise spacing actually delays transition beyond the pressure minimum and well beyond 80% chord (the actual location was beyond view). This promising technique is currently being evaluated for supersonic flight (Saric & Reed 2002).

Subsequent to the experiments, the NPSE results (Haynes & Reed 2000) confirmed this effect. In a DNS solution, Wassermann & Kloker (2002) have shown the same stabilization due to subcritical forcing. Using the same independent approach regarding the calculation of the basic state, they demonstrated the stabilization due to subcritical roughness and coined the name transition delay by “upstream flow deformation.”

4.5 Secondary Instabilities

Once stationary vortices reach saturation amplitude, this state can persist for a very significant streamwise distance. The velocity contours show low-momentum fluid above high-momentum fluid which produces a double inflection point in the wall-normal velocity profile. There is also an inflection point in the spanwise profile. These inflection points are high in the boundary layer and the saturated vortices become unstable to a high-frequency secondary instability that ultimately brings about transition to turbulence. Because of the importance of the secondary instabilities in determining the location of breakdown of the laminar flow, there have been a number of investigations, both experimental and computational, in this area. Bippes (1999) includes details on the German efforts, in particular the work by Lerche (1996) and Lerche & Bippes (1995) that emphasizes secondary instabilities in flows with higher turbulence levels and traveling crossflow waves. Recent efforts involving secondary instabilities in the Russian traveling wave experiments are covered by Boiko et al. (1995, 1999).

The first crossflow experiment for which a high-frequency disturbance was observed prior to transition was by Poll (1985). Traveling crossflow waves were observed with a dominant frequency of 1.1 kHz for $Re_c = 0.9 \times 10^6$. Increasing the chord Reynolds number to 1.2×10^6 increased the traveling crossflow frequency to 1.5 kHz and also included an intermittent signal at 17.5 kHz superposed on the underlying traveling crossflow waves. Poll noted that increasing the Reynolds number beyond 1.2×10^6 resulted in turbulent flow at the measurement location, so the high-frequency signal appeared only in a narrow range just prior to transition. Poll attributed the existence of the high-frequency component to intermittent turbulence.

A high-frequency secondary instability was specifically investigated as a source of breakdown by Kohama et al. (1991). This experiment combined hotwire measurements and flow visualizations and was intended to determine the location and behavior of the secondary instability mode relative to visualized breakdown patterns. It is clear from the Kohama et al. (1991) experiments that there is a growing high-frequency mode in the region upstream of transition that can be associated with an inviscid instability of the distorted mean flow. However, a concern can be raised because the measurements were made without a well-controlled primary disturbance state. Experiments subsequent to this

work used arrays of micron-sized roughness elements near the leading edge that established the spanwise uniformity both of the stationary vortex amplitudes and the transition location. Without the benefit of this technique, the data obtained by Kohama et al. (1991) likely spanned a wide range of stability behavior despite having been obtained at a single chord position. Improvements in experimental techniques mean that more recent secondary instability experiments have replaced the work by Kohama et al. (1991) as the best source for secondary instability data.

Kohama et al. (1996) provide somewhat more detail than Kohama et al. (1991) by including velocity fluctuation maps that are filtered to give either primary instability or secondary instability fluctuation levels. Kohama et al. (1996) conclude that a “turbulent wedge starts from the middle height of the boundary layer” and that this behavior is different from the usual picture of a turbulent wedge that originates in the high-shear regions in naphthalene flow-visualization experiments. A subsequent swept plate experiment by Kawakami et al. (1999) was conducted to further refine these measurements. Kawakami et al.’s experiment featured a small speaker mounted flush with the surface that permitted tracking of particular secondary-instability frequencies. Without acoustic forcing, two separate high-frequency bands of disturbances were observed to be unstable. At a chord Reynolds number of 4.9×10^6 , a band located between 600 Hz and 2.5 kHz destabilized just downstream of $x/c = 0.35$ and a second band located between 2.5 and 4.0 kHz destabilized just upstream of $x/c = 0.50$. Transition was observed around $x/c = 0.70$. With acoustic forcing applied, the secondary instability frequency with the largest growth between $x/c = 0.40$ and $x/c = 0.475$ was observed to be 1.5 kHz.

In an effort to provide a more concrete experimental database on the behavior of the secondary instability, White & Saric (2002) conduct a very detailed experiment that tracks the development of secondary instabilities on a swept wing throughout their development for various Reynolds numbers and roughness configurations. They found a number of unique secondary instability modes that can occur at different frequency bands and at different locations within the stationary vortex structure. In White & Saric’s experiment as many as six distinct modes are observed between 2 and 20 kHz. The lowest-frequency mode is nearly always the highest amplitude of all the secondary instabilities and is always associated with an extremum in the spanwise gradient, $\partial U/\partial z$ which Malik et al. (1996, 1999) refer to as a mode-I or z mode. Higher frequency modes include both harmonics of the lowest-frequency z mode that appear at the same location within the vortex and also distinct mode-II or y modes that form in the $\partial U/\partial y$ shear layer in the portion of the vortex farthest from the wall. The lowest frequency mode is typically detected upstream of any of the higher frequency modes. However, many higher frequency modes appear within a very short distance downstream. All of the secondary instability modes are amplified at a much greater rate than the primary stationary vortices (even prior to their saturation). The rapid growth leads very quickly to the breakdown of laminar flow, within about 5% chord of where the secondary instability is first detected. A consequence of this for transition prediction methodologies is that adequate engineering predictions of transition location could be obtained from simply identifying where the secondary instabilities are destabilized because they lead to turbulence in such

a short distance downstream of their destabilization location. An interesting feature of the breakdown of the stationary vortex structure is that it is highly localized. Spectra obtained by White & Saric at various points within the structure indicate that the first point to feature a broad, flat velocity fluctuation spectrum characteristic of turbulence is a point very close to the wall in the region of highest wall shear. Other points in the structure remain essentially laminar for some distance downstream of the initial breakdown location. This finding supports the notion of a turbulent wedge originating near the wall, not what was concluded by Kohama et al. (1996).

A successful computational approach to the secondary instability was presented by Malik et al. (1994) who used a NPSE code to calculate the primary instability behavior of stationary disturbances of a swept Hiemenz flow. As described previously, the NPSE approach successfully captures the nonlinear effects including amplitude saturation. The distorted mean flow provides a basic state for a local, temporal secondary instability calculation. The most unstable frequency is approximately one order of magnitude greater than the most unstable primary traveling wave similar to Kohama et al. (1991) and the peak mode amplitude is “on top” of the stationary crossflow vortex structure. This location corresponds to what will be referred to below by Malik et al. (1996) as the mode-II secondary instability.

In order to obtain a more direct comparison to experimental data, Malik et al. (1996) used parameters designed to match the conditions found for the swept-cylinder experiment of Poll (1985) and the swept-wing experiment of Kohama et al. (1991). The calculations of Malik et al. (1996) reveal that the energy production for a mode-I instability is dominated by the term $\langle u_2 w_2 \rangle \partial U_2 / \partial z_2$ and the mode-II instability is dominated by $\langle u_2 v_2 \rangle \partial U_2 / \partial y_2$ where the subscript “2” refers to a primary-vortex-oriented coordinate system. This energy production behavior suggests that the mode-I instability is generated primarily by inflection points in the spanwise direction and the mode-II instability is generated by inflection points in the wall-normal direction. This situation is analogous to the secondary instabilities of Görtler vortices (Saric 1994). Malik et al. (1996) claim that the fluctuations observed by Kohama et al. (1991) are mode-II instabilities but the spectral data presented by Kohama et al. (1991) likely includes contributions of both the type-I and type-II modes. Although one or the other production mechanism may dominate for a particular mode, it is too simplistic to assume that only the spanwise or wall-normal inflection points are responsible for the appearance of a particular mode; with such a highly distorted 3-D boundary layer, all possible instabilities must be evaluated.

Malik et al. (1996) also compute the secondary instability behavior observed by Poll (1985) and predict a 17.2-kHz mode compared to Poll's high-frequency signal occurred at 17.5 kHz. Based on the shape of this disturbance, Malik et al. claim that this is a type-II mode. The same approach is applied by Malik et al. (1999) to the swept wing experiments of Reibert et al. (1996). Malik et al. (1999) again apply a local, temporal stability of the stationary crossflow vortices that are established by the primary instability and find that better transition correlation results can be obtained by following the growth of the secondary instability in an N factor calculation than simply basing a prediction on

the location at which the secondary instability destabilizes. A method based on the primary instability alone cannot adequately predict transition location.

An alternative to the approach used by Malik et al. (1994, 1996, 1999) is presented by Koch et al. (2000) who find the nonlinear equilibrium solution of the primary flow. Koch et al. use the nonlinear equilibrium solution as a receptivity-independent basic state for a Floquet analysis of secondary instabilities of the saturated vortices. Yet another approach is by Janke & Balakumar (2000) who use a NPSE for the base flow and a Floquet analysis for the secondary instabilities. Both Koch et al. (2000) and Janke & Balakumar (2000) are in general agreement with the various computations of Malik and coworkers.

A DNS approach to the problem of the stationary-vortex saturation and the ensuing secondary instability was pursued by Högberg & Henningson (1998). These authors impose an artificial random disturbance at a point where the stationary vortices are saturated. These disturbances enhance both the low- and high-frequency disturbances downstream, and each frequency band has a distinct spatial location, with the high-frequency disturbance located in the upper part of the boundary layer and the low-frequency disturbance located in the lower part. Spectral analysis of the resulting disturbance field shows that the most-amplified high frequency is somewhat more than an order of magnitude higher frequency than the most amplified traveling primary disturbance. Another high-frequency peak at approximately twice this frequency is also evident in the spectra. This peak likely corresponds to a type-II mode, although this feature is not described by the authors.

Another very highly resolved DNS study of nonlinear interactions of primary crossflow modes, their secondary instabilities, and eventual breakdown to turbulence is by Wassermann & Kloker (2002). Wassermann & Kloker emphasize disturbance wave packets that may be more realistic than single-mode disturbances. One of the most important findings obtained from the wave-packet approach is that unevenly spaced primary vortices of differing strengths can interact in such a way to bring about an earlier onset of secondary instabilities and breakdown than would be found from a single-mode disturbance. Also, Wassermann & Kloker find that when the forcing that initiates the high-frequency secondary instability in their simulation is removed, the secondary-instability disturbances are convected downstream, out of the computational domain. This indicates that the secondary instability is convective and that the explosiveness of the secondary instability's growth is not associated with an absolute instability. The advantage of Wasserman & Kloker's DNS solution is its ability to reveal the rather intimate details of the breakdown process. As such, the work is one of the foundation contributions.

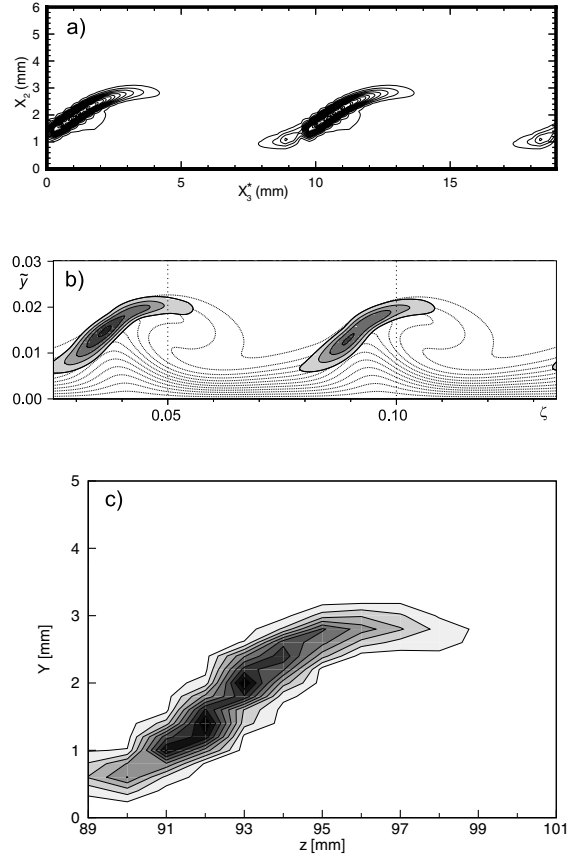


Figure 3: Mode-I velocity fluctuation contours (a) Figure 7 from Malik et al. (1999), (b) Figure 20b from Wassermann & Kloker (2002), and (c) Figure 11 from White & Saric (2002).

At this time, the various approaches to the secondary instability problem, experimental, nonlinear PSE, and DNS, have achieved rather remarkable agreement in terms of identifying the basic mechanisms of the secondary instability, unstable frequencies, mode shapes, and growth rates. This comparison shows agreement on the location of the breakdown and that it is associated with an inflection point in the spanwise direction (an extremum in $\partial U / \partial z$).

Recommendation

A lot of detail was presented above for the experiments and NPSE to illustrate that the crossflow instability is becoming much better understood and NPSE can be used as a validation tool. One interesting result is that different roughness heights (Re_k order 1) produce the same saturation amplitude and transition location in the experiments. This implies the possibility for an amplitude-based transition prediction scheme. It also suggests that LST (assuming stationary crossflow and without curvature) can still be used to estimate the transition location with N determined from available experimental data. Low-amplitude initial crossflow disturbances remain linear for a long distance (as mentioned above). Again LST is best used in a comparative sense.

5 Approximate e^N Methods

The preceding discussion has examined LST (linear stability theory) methods and their application to transition calculations. These methods solve a series of local eigenvalue problems for a specified boundary layer profile and assume eigenmodes are independent and small in amplitude so that the mean flow is unaffected. For these eigenvalue problems several of the free parameters must be specified, and these typically include the disturbance temporal frequency and spanwise wavenumber. The eigenvalue solution yields the associated streamwise wavenumber and spatial growth rate. Alternate eigenvalue formulations can be devised to specify and solve for other combinations of the temporal and spatial parameters. Note that the solution for each unstable mode, frequency or spatial wavenumber requires a new eigenvalue computation. In order to integrate local growth rates to make overall disturbance growth estimates these calculations must be made for each streamwise station (in 2D) where boundary layer profiles are available. In 3D another dimension is added and these sets of streamwise calculations must be repeated for each spanwise station.

While these LST methods are far less computationally intensive than the LPSE or NPSE methods, they require more computational resources than are available in most design environments. As a result approximations to full LST methods are used when boundary layer transition calculations are required in the context of CFD methods. This is the approach selected for the RATRAP work to integrate transition methodologies into Navier-Stokes CFD methods.

These simplified methods take the form of functional approximations such as parametric equations (based on curve fits), table or database lookup and interpolation or more complex response surface methods (such as neural networks) to approximate LST growth rates based on a set of parameters that characterize the boundary layer. The range of applicability of these approximate methods is often limited to specific types of problems (e.g. 2D TS calculations at subsonic to transonic speeds). Within their range of application these methods can be very good substitutes for more comprehensive LST calculations.

5.1 Envelope methods vs mode tracking methods

Two approaches are used for integrating N factors for full LST transition calculations or approximate LST methods for both streamwise and crossflow disturbances. The envelope method is a simplified scheme which computes a single N factor associated with the maximum growth rate locally (finding the most unstable wave on a local basis) as one marches downstream. A mode tracking method calculates N factors for all waves, one of which will be the most unstable wave. The envelope methodology produces a slightly higher N factor and is conservative in transition location prediction (i.e. transition predicted farther upstream than a mode tracking calculation). Envelope methods tend to be based on parametric functions of boundary layer and flow parameters, usually in the form of curve fits to LST results. Mode tracking methods tend to be based

on table driven schemes that interpolate a database of growth rates (from LST results) across the range of modes or frequencies.

5.2 Approximate TS Methods

5.2.1 Drela's Envelope e^N TS Method

The most widely used method for 2D TS stability calculations is the envelope e^N approach developed by Drela (1986) and used in his XFOIL and MSES airfoil analysis and design programs. This method is currently used in the prototype RATRAP code to calculate streamwise TS transition.

The method approximates the spatial amplification envelopes for incompressible Falkner-Skan profiles in H - ω - Re_θ space, as shown in Figure 4. The integrated growth rates for the range of amplified frequencies are shown with solid lines, along with a dashed line through the maximum growth loci for each shape factor (this growth is integrated assuming a similar boundary layer with varying Reynolds number). The key to the simplicity of the method is the remarkable linear character of these maximum growth envelopes.

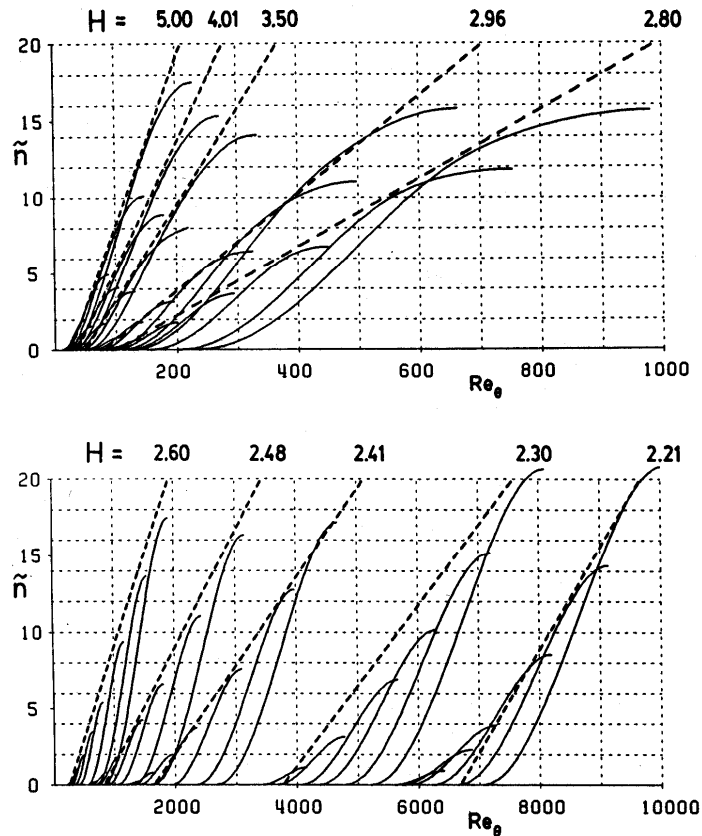


Figure 4: Amplification growth for Falkner-Skan profiles with approximate maximum growth envelopes

The method uses parametric equations for the critical Reynolds number and slope of the envelope line (maximum of integrated growth rates, over all frequencies for a given shape factor).

$$\frac{d\tilde{n}}{dRe_\theta} = 0.01 \left((2.4H - 3.7 + 2.5 \tanh[1.5(H-3.1)])^2 + 0.25 \right)^{\frac{1}{2}}$$

$$\log_{10} Re_{\theta_0} = \left(\frac{1.415}{H-1} - .489 \right) \tanh\left(\frac{20.}{H-1} - 12.9\right) + \frac{3.295}{H-1} + .440$$

This disturbance growth rate can be integrated downstream from the point where $Re_\theta = Re_{\theta_0}$ to arrive at an overall amplification factor. Drela extended the growth rate equation from de Gleyzes et al. (1983) to give the spatial amplification in terms of the streamwise coordinate, ξ .

$$\frac{d\tilde{n}}{d\xi}(H, \theta) = \frac{d\tilde{n}}{dRe_\theta}(H) \frac{m(H) + 1}{2} \ell(H) \frac{1}{\theta}$$

with the definitions

$$\ell(H) = (6.54H - 14.07)/H^2$$

$$m(H) = \left(0.058 \frac{(H-4)^2}{H-1} - 0.068 \right) \frac{1}{\ell(H)}$$

To account for compressibility effects the shape factor H used in these relations is actually H_k , the so-called kinematic shape factor, which ignores density changes on boundary layer thicknesses from compressibility effects. The reasoning is that velocity profiles are more relevant for boundary layer stability than density weighted velocity profiles. The empirical formula below relates the kinematic shape factor to the conventional shape factor and edge Mach number.

$$H_k \equiv \frac{\int_0^\infty \left(1 - \frac{u}{u_e}\right) d\eta}{\int_0^\infty \left(1 - \frac{u}{u_e}\right) \frac{u}{u_e} d\eta} = \frac{H - 0.290 M_e^2}{1 + 0.113 M_e^2}$$

This simple envelope growth relation can be easily applied to calculate transition in a CFD method using an appropriate N_{crit} threshold and this combination provides a remarkably accurate approximation to LST for many applications. The method has been extended for supersonic streamwise TS calculations by Sturdza, who added compressibility corrections for his Mach 1.4-2.2 laminar wing design application.

One limitation of the method is that the correlation is based on integrated growth for similar FS profiles. Users of the method have encountered varying levels of transition errors for nonsimilar flows.

5.2.2 Drela's Full e^N TS Method

Drela's simplified envelope e^N method (Drela, 1986), described above, has been used with good results for many applications. This formulation is strictly correct for only similar boundary layers (boundary layers with constant shape factor over the area of instability and growth). When this method is applied to strongly nonsimilar boundary

layer the transition predictions show errors in terms of integrated growth levels. These errors show up strongly in flows with $H(x)$ increasing, such as on the upper surface of an airfoil with a separation bubble. These problems motivated the recent development of a full e^N method for 2D (streamwise) TS transition (Drela, 2003).

Drela's recent full e^N method is based on a more complete approximation to LST using a functional approach to calculate growth rates for a full range of frequencies (i.e. a mode tracking method that gives growth rates for any frequency). The method uses a table of growth rates for the full range of amplified frequencies, parameterized by three parameters, H , Re_θ , and non-dimensional frequency.

$$\bar{\alpha}(H, Re_\theta, \bar{\omega}) = \bar{\alpha}_r + i \bar{\alpha}_i$$

The growth rates for the table are based on Orr-Sommerfeld calculations for boundary layer profiles from the incompressible Falkner-Skan family with modifications for reduced reverse flow in boundary layers with separation. Note that this is the same boundary layer family that was used to derive the envelope method but this method avoids integrating growth for a single similar profile, instead integrated growth is based on locally varying growth rates (i.e. nonsimilar boundary layer).

$$n(x; \omega) = \int^x -\bar{\alpha}_i(H, Re_\theta, \omega \theta / u_e) \frac{1}{\theta} dx$$

The differences in transition predicted by the full e^N method and the envelope e^N scheme are shown in Figure 5 for a low- Rn E387 airfoil. The upper chart shows the upper and lower surface shape factor while the lower chart shows the corresponding e^N predictions from the envelope method and the full e^N (frequency tracking) method. The two methods agree well in terms of integrated growth factor for the lower surface where the shape factor is roughly constant (near similar) but show large differences on the strongly nonsimilar upper surface boundary layer.

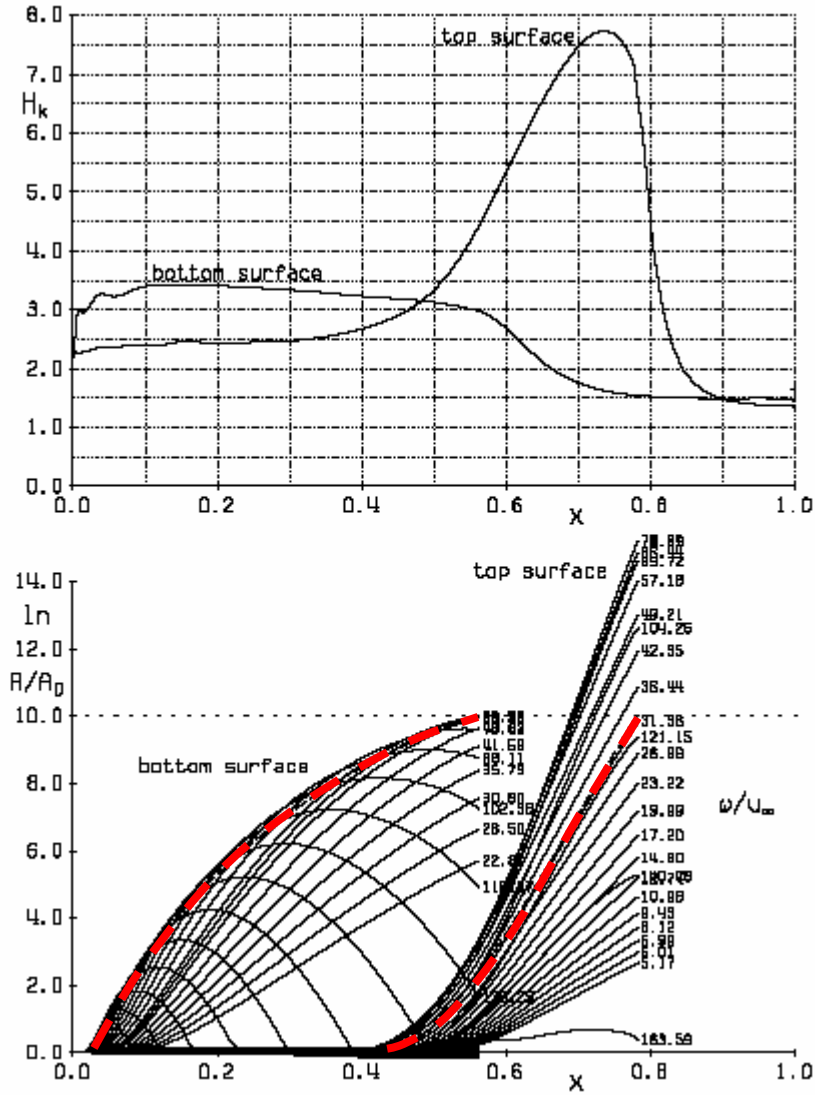


Figure 5: Shape factor and amplification growth for low-Rn E387 airfoil calculated with envelope method (dashed line) and frequency tracking method (solid lines).

This method interpolates tables of complex α (streamwise wavenumber and growth rate) parameterized by the two boundary layer parameters H and Re_θ and by frequency $\omega\theta/u_e$ using tri-cubic splines. The trick in table or database methods is to minimize the size and dimensionality (number of independent parameters) for the table. This reduces both the cost of producing and using the method. In order to produce a compact table for the wide range of parameter values required for H , Re_θ , and ω Drela used the shape factor, H , and two modified parameters (related to Reynolds number and non-dimensional frequency).

$$\mathcal{R} = \log Re_\theta$$

$$\mathcal{W} = \log \bar{\omega} + \frac{1}{2} \log Re_\theta$$

The parameter ranges used to characterize the full range of practical boundary layer conditions were.

$$H = 2.2 \dots 20.0$$

$$\mathcal{R} = 0.5 \dots 6.0$$

$$\mathcal{W} = -3.0 \dots 1.0$$

In order to use this method the growth rates for all frequencies (or a most amplified subset of frequencies of interest) must be tracked and integrated to give N factors at streamwise locations. Transition is assumed for the most amplified mode (frequency) that exceeds the selected N_{crit} threshold. Note that Drela's implementation of this method within the MSES code tracks 20 discrete frequencies. The extra computation associated with tracking a set of discrete modes adds to the computational cost of using this technique although the overall method remains vastly faster than full LST calculations.

Drela's full e^N method appears to be the best candidate for a mode tracking streamwise TS transition code for use with RATTraP. This code could be used alternately to the simpler envelope e^N method and will produce more accurate transition estimates for nonsimilar boundary layer flows.

5.2.3 Sturdza's Compressible Envelope e^N TS Method

Sturdza (2004) developed approximate e^N methods for streamwise TS and crossflow transition in the context of laminar flow design for supersonic wings. His approach was to separately treat streamwise and crossflow transition calculations. His approach for streamwise transition used the computationally simple 2D envelope TS method of Drela (1986) and added compressibility corrections for application to wings at Mach 1.4-2.2. This approach completely ignores oblique TS modes at these Mach numbers which are not modeled in 2D e^N methods.

Sturdza's version of the streamwise envelope e^N method was developed by correlating with LST results from LASTRAC. His method includes new terms involving temperature ratio for compressibility correction to the critical Reynolds number

$$\log_{10}\left(\frac{Re_{\theta_0}}{K_0}\right) = \left(\frac{1.415}{H_k - 1} - 0.489\right) \tanh\left(\frac{20}{H_k - 1} - 12.9\right) + \frac{3.295}{H_k - 1} + 0.44$$

$$K_0 = \frac{2}{\pi} \tan^{-1}\left(10\frac{T_w}{T_e} - 10\right) + 1.$$

And compressible corrections to the amplification rate equation

$$\frac{dn}{dRe_{\theta}} = \frac{0.01}{K_b} (2.4H_k K_a - 3.7 + 2.5K_c \tanh[1.5(H_k - 3.1)] + 0.125 + K_d - K_m)$$

$$K_a = 1 + 0.2(H_k - 2.5918) \left(1 - \frac{T_e}{T_w}\right)$$

$$K_b = 4.7 \left(\frac{T_w}{T_e} - 1\right) + 1, \quad K_c = \frac{T_w}{T_e}, \quad K_d = 1.2 \left(\frac{T_w}{T_e} - 1\right)^{3/2}.$$

The supersonic biconvex wings Sturdza studied had long regions of highly favorable pressure gradient (a core feature of the basic supersonic laminar flow designs he was modeling). Although his envelope e^N method worked very well for adverse gradients, amplification in favorable pressure regions was over-predicted as compared to LASTRAC's LST results. Sturdza attributed this to the same similar boundary layer issue discussed in connection with Drela's envelope e^N scheme and suggested that a mode tracking scheme such as Drela's full e^N method (2003) or the Stock and Dagenhart (1989) mode tracking method would better model this behavior. Sturdza proposed an ad-hoc modification of his basic scheme to match reduced TS instability growth in favorable

pressure gradients by using a “lagged” kinematic shape factor. He proposed further tuning the K_m term in his amplification rate equation using

$$K_m = 115 \sqrt{T_w/T_e} (H_{k_{avg}} - H_k)$$

where the averaged value of H_k is given by an upstream weighted integral of H_k from the instability point.

$$H_{k_{avg}} = \frac{1}{Re_\theta - Re_{\theta_0}} \int_{Re_{\theta_0}}^{Re_\theta} H_k dRe_\theta.$$

Due to the narrow focus for his work Sturdza’s modifications to Drela’s envelope e^N scheme were highly tuned to work for biconvex and near-biconvex supersonic wings where they appear to closely approximate LST results from the LASTERAC code (used to develop the correction scheme). There are indications that these correction terms may not be as well tuned for problems at low or transonic speeds and further work should correlate these for a broader class of flow conditions.

5.2.4 Crouch, Crouch and Ng Neural Net e^N TS Method

Crouch, Crouch and Ng (2001) developed a rapid, approximate e^N method for TS and crossflow transition in the context of use with 3D CFD codes. Their method used a neural network approach to implement a mode (frequency) tracking method for TS transition and an envelope e^N method for stationary crossflow transition.

Crouch et al. calculated a large database of growth rates for Falkner-Skan-Cooke profiles (incompressible, infinite swept wing) using an LST method. The boundary layer profiles for this database span a full range of Falkner-Skan Hartree parameters (corresponding to streamwise shape factors), Reynolds number and boundary layer edge sweep angles. These Orr-Sommerfeld eigenvalue calculations determined maximum growth rates over all spanwise wavenumbers. Rather than devise a compact data table and interpolation scheme for these growth rates (as in Drela’s full e^N method, 2003), neural networks were used to model the complex response surfaces corresponding to these maximized growth rates. These neural networks were trained using the growth rates and corresponding input parameters for the boundary layer profiles, frequencies and flow conditions.

One unique feature of this work was the scheme used to parameterize the boundary layer profiles. Rather than use integral shape parameters for the streamwise and crossflow profiles, Crouch et al. chose to use the first derivatives of the velocities (streamwise and crossflow) at six uniformly spaced locations across the boundary layer, as shown in Figure 6. This is a very general way to use a (relatively) small number of input parameters to characterize any profile. Also, in this way, the neural network has much the same profile information that was used in the LST analysis to generate the growth rates so that the neural net may more fully approximate the eigenvalue solutions.

Nominally, the neural nets are driven with 16 parameters, including the streamwise and crossflow profile derivatives, the streamwise and crossflow Reynolds number, the edge streamline angle and the disturbance frequency. Crouch et al. found the TS neural net

was excessively sensitive to crossflow profile inputs so their implementation for streamwise transition neglects crossflow profile information completely, in effect reducing their TS method to a streamwise e^N approximation.

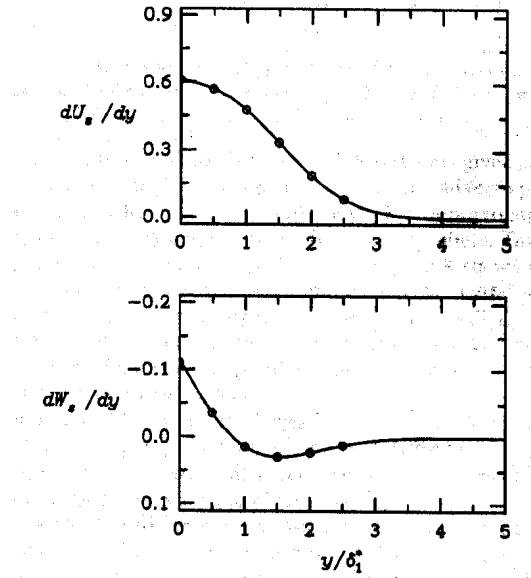


Figure 6: Profile parameters using streamwise and crossflow velocity derivatives at six points across boundary layer

Once the neural network was trained (setting weights for inputs and interconnection levels in the network) it could be used as a black box to process flow and profile inputs into growth rates. This TS neural net implements a mode tracking e^N method which calculates growth rates maximized over all spanwise wavenumbers for a given frequency (mode). The neural net only approximates the training inputs derived from growth rates calculated for incompressible Falkner-Skan-Cooke profiles. Crossflow profile inputs are ignored so this method only responds to streamwise profile inputs. Thus this neural net approach is both less accurate and more complex than the table driven full e^N approach of Drela which was derived from the same profile assumptions.

The TS neural net implemented by Crouch et al. shows significantly greater errors in approximating growth rates than the corresponding neural net trained for stationary crossflow envelope e^N growth rates. That may be an indication that approximations to the crossflow problem are better characterized by this choice of profile and flow inputs.

5.3 Approximate Crossflow Methods

5.3.1 Dagenhart's e^N Crossflow Method (MARIA)

The development of the MARIA code by Dagenhart (1981) was a key work in approximate e^N methods for crossflow transition. This code was a mode tracking e^N stationary crossflow method, generating spatial growth rates as a function of spanwise wavenumber and several basic crossflow boundary layer parameters. The MARIA code could approximate results of more complex linear stability codes (i.e. SALLY, COSAL) using a fraction of the computational effort.

Dagenhart's method was based on a table of stationary crossflow growth rates derived from LST analysis of 10 streamwise boundary layer stations on a transonic swept, infinite wing with a Pfenninger 970 airfoil. The crossflow boundary layer profiles were parameterized in terms of three parameters, the crossflow Reynolds number, shape factor and velocity ratio, as defined in the Figure 7. This choice of crossflow parameters has been validated by subsequent investigators.

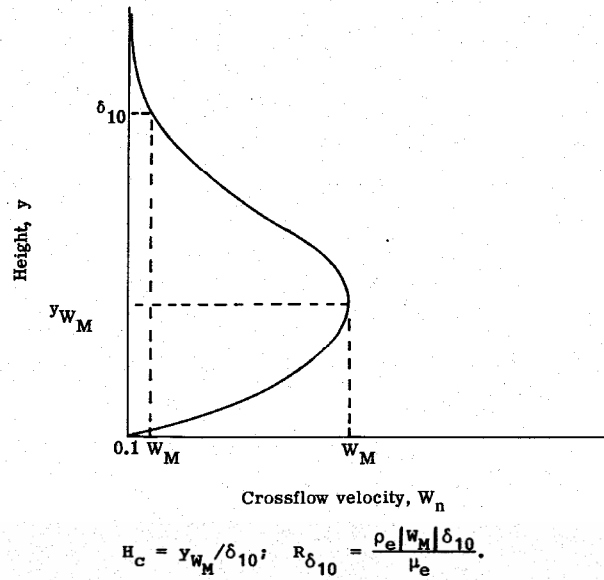


Figure 7: Crossflow velocity profile and crossflow profile parameters

The crossflow shape factor was defined by the thickness, δ_{10} , which corresponds to the height at which the crossflow velocity drops to 10% of the maximum velocity and the height at the velocity maximum. The crossflow Reynolds number was defined by the thickness, δ_{10} and maximum crossflow velocity, W_m .

In his LST calculations for the 10 boundary layer stations Dagenhart found that the curves of constant amplification rate in the crossflow wave direction (i.e. growth rate vs Reynolds number and spanwise wavenumber) had similar shapes for all profiles. He further found that the point of instability for crossflow growth was well characterized by Reynolds number and shape factor, as shown in Figure 8.

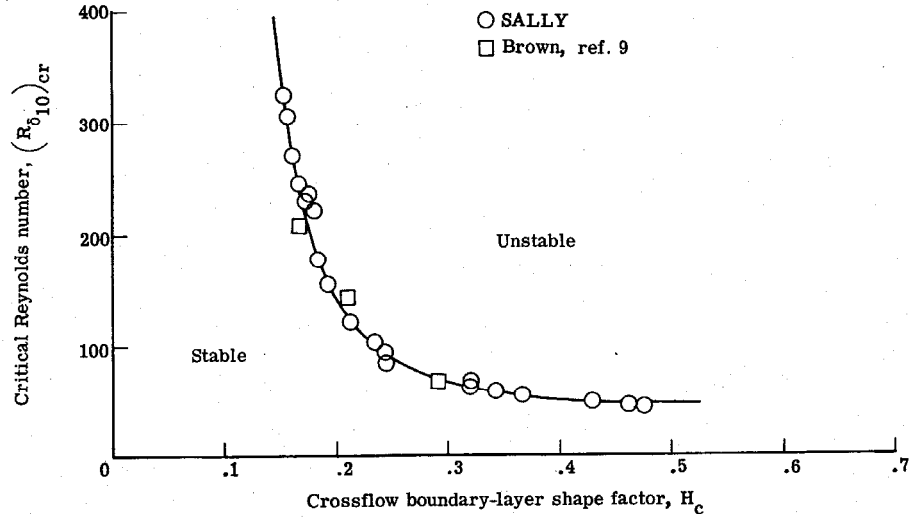


Figure 8: Critical crossflow Reynolds number vs shape factor

Dagenhart's work also led him to find that the spatial amplification rate in the pure crossflow direction (which is very close to the direction for maximum crossflow instability growth for the combined streamwise and crossflow boundary layer) scaled directly with the crossflow velocity ratio W_m/u_e .

The critical Reynolds number correlation and the velocity scaling relationship allowed Dagenhart to apply table data for his airfoil profiles to a more general range of crossflow boundary layers (or at least to boundary layer profiles that fell within the range of crossflow shape factors present on the 970 airfoil). His scheme works on an arbitrary input boundary layer using the shape factor to find the critical Reynolds number from the correlation, then interpolating the table data for growth rates at the input shape factor and Reynolds number. Dagenhart's interpolation scheme used offsets to the table Reynolds numbers by differences in critical Reynolds number for table entries with the nearest shape factor and the input boundary layer.

Dagenhart also uses an approximate method to find the dividing point between upstream and downstream regions of opposite crossflow rotation (rotation direction switches in regions of opposite pressure gradient). The point of reversal is determined by a weighted average of the crossflow velocity across the boundary layer.

For simplicity, Dagenhart integrates growth rates in the direction of the inviscid outer streamline. He observes that angles between the inviscid outer streamline and the group velocity vector are less than 3° . In addition, arc-lengths along the potential flow streamline path or the group velocity path differ by less than 1.8%. The use of the external streamline direction for growth rate integration is within the limits of the accuracy of the approximate method.

The general approach used by Dagenhart will also be used for the mode tracking crossflow methodology for RATTraP. We will replace Dagenhart's limited table of growth rates (parameterized by shape factor, Reynolds number and spanwise

wavenumber) with a more complete table of boundary layer growth rates using the Falkner-Skan-Cooke profile family. The same scaling of growth rate with crossflow velocity ratio will be used to minimize table dimensionality.

5.3.2 Sturdza's Compressible Envelope e^N Crossflow Method

Sturdza (2004) and Kroo and Sturdza (2003) developed approximate e^N methods for streamwise TS and crossflow transition in the context of laminar flow design for supersonic wings. Sturdza split the transition calculation into streamwise TS and crossflow problems. His approach for crossflow transition was an envelope e^N method for stationary crossflow growth maximized across all spanwise wavenumbers. Elements of his approach are derived from the work of Dagenhart (1981) in his MARIA method. Sturdza adopts Dagenhart's parameterization of the crossflow boundary layer in terms of three parameters, the crossflow Reynolds number, shape factor and velocity ratio, as shown in the Figure 9. The crossflow thickness δ_{cf} is defined by the point on the velocity profile where the crossflow velocity is 10% of the maximum w_{max} .

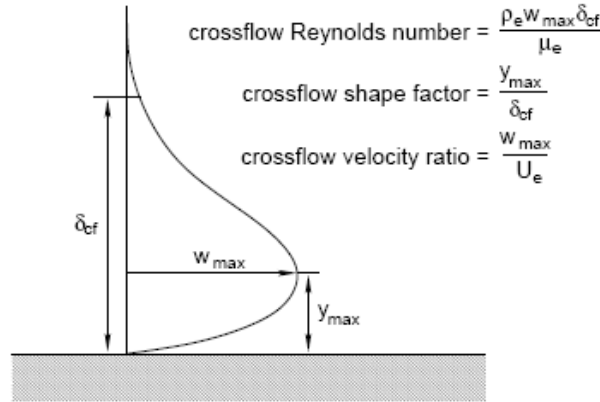


Figure 9: Sturdza's crossflow boundary layer parameters

Using pseudo-similar "similarity sequences" of streamwise profiles combined with scaled and modified crossflow profiles Sturdza used LST results from LASTRAC to construct a parametric model of the envelope of maximum crossflow growth. This model uses a minimal compressibility correction, which validates Dagenhart's original contention that crossflow was largely unaffected by Mach effects. Sturdza's parametric relation for crossflow growth rate as a function of crossflow Reynolds number, shape factor and velocity ratio takes the form

$$\alpha_{\delta_{cf}} = 2.128 \left(\frac{w_{max}}{U_e} \right)^{1.07} H_{ef} \left(\frac{T_e}{T_w} \right)^{0.4} (1 + |H_{ef} - 0.35|^{1.5}) \left[\tanh \left(\frac{R_{cf} - R_{cf0}}{336 - R_{cf0}} \right) \right]^{0.4}$$

$$n_{cf} = \int_{x_0}^x \alpha dx.$$

with the critical crossflow Reynolds number R_{cf0} defined by

$$R_{cf0} = 46 \frac{T_w}{T_e}.$$

This simplistic definition of critical crossflow Reynolds number is troubling because it contradicts the dependence of R_{cf0} on crossflow shape factor that played such a key role

in Dagenhart's MARIA development. This relationship may be specific, or at least most applicable, to Sturdza's supersonic wing boundary layers.

As discussed in the description of Sturdza's compressible modifications to the envelope e^N TS method the focus for his work was biconvex and near-biconvex supersonic wings at Mach 1.4-2.2. The range of application for these parametric relations is unclear. Crossflow growth rates predicted by this approach should be checked at low or transonic speeds to correlate these relations for a broader class of flow conditions.

We will investigate the use of Sturdza's crossflow envelope e^N correlation for use with RATTraP. If this parameterization works at low and transonic Mach numbers we can adopt it as the crossflow envelope method. Sturdza's critical Reynolds number correlation may be replaced with Dagenhart's original correlation if that proves more accurate.

5.3.3 Crouch, Crouch and Ng Neural Net e^N Crossflow Method

The neural net method of Crouch, Crouch, and Ng (2001) was described in the section on TS transition. The method is similar for crossflow transition, except that an envelope method is used for crossflow. The neural net for crossflow was trained with the frequency set to $\omega=0$ so that only stationary crossflow growth was modeled. The crossflow profile is shown in Figure 6.

The crossflow neural net implements an envelope e^N method which calculates stationary mode growth rates maximized over all spanwise wavenumbers. It is important to keep in mind that a neural net only approximates its training inputs. These inputs were derived from growth rates calculated for incompressible Falkner-Skan-Cooke profiles, not from nonsimilar profiles that are present on "real" swept wings. This use of idealized profiles is a common issue in development of approximate e^N methods. The neural net approach, combined with this parameterization of the boundary layer with a set of velocity derivatives, may have advantages in terms of increased accuracy if the training set for the network is extended to include a wider range of nonsimilar boundary layers.

The crossflow neural net implemented by Crouch et al., characterized by this choice of profile and flow inputs, closely models the results from LST calculations and appears to be considerably more accurate than the neural net implemented for TS growth rates. It would be useful to compare the overall accuracy of this envelope crossflow method to the parametric formulation used by Sturdza (2004), though this is unlikely to occur as this neural net crossflow method is proprietary to Boeing.

6 Attachment Line Instabilities

6.1 Empirical correlations

Near the leading edge of a swept wing, there is a line known as the attachment line (corresponding to the stagnation line of an unswept wing) along which the flow is entirely spanwise (see Figure 10). That is, there is no chordwise component to the potential flow outside of the boundary layer. The flow along this attachment line is usually contaminated with turbulent flow at the root from the fuselage, and affects the stability of the flow on the rest of the wing. That is, if the attachment line boundary layer is turbulent, the boundary layer on the entire wing is turbulent. The stability of the attachment line boundary layer is an important problem for swept wing transition prediction, and this will be addressed in the RATTraP transition prediction modules. Leading-edge radius affects attachment-line contamination and instability (Pfenninger 1977; Poll 1985).

For the practical purpose of predicting transition on the attachment line, a criteria using the momentum thickness boundary layer Re_θ has been used almost exclusively. Analytical, computational, and experimental attempts to characterize attachment line transition have historically reduced to this criteria. At this point there seems to be no other available engineering strategy for predicting transition on the attachment line.

The initial flow condition at the root of the wing determines the critical Reynolds number. If the flow is turbulent at the wing root, there exists a Reynolds number below which the turbulent flow disturbances are damped and the flow becomes laminar. If the flow is laminar at the root or if turbulent disturbances have been removed by suction or by some device such as a Gaster bump, then above a certain value of Re_θ small disturbances grow and result in a turbulent attachment line.

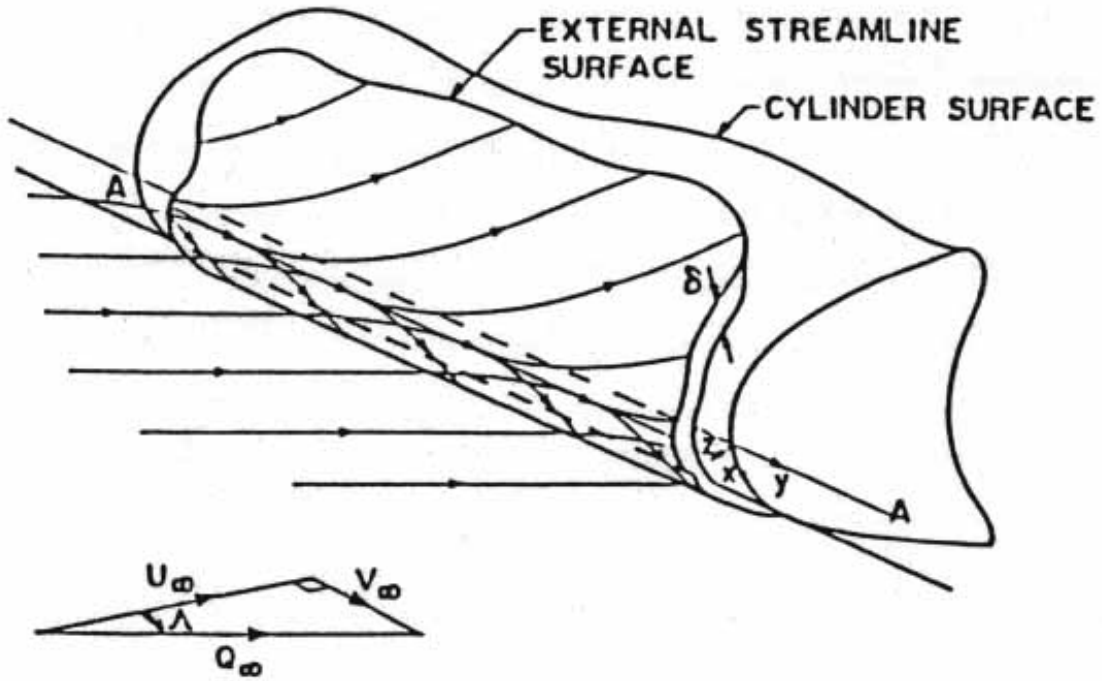


Figure 10: Flow around a swept wing attachment line

Pfenninger(1965) was the first to propose an attachment line transition criteria based on a Reynolds number

$$\bar{R} = V_{\infty} / \sqrt{\nu k},$$

where V_{∞} is the spanwise freestream velocity and k is the chordwise velocity gradient of the potential flow outside of the boundary layer at the attachment line

$$k = \frac{dU_c}{dx}.$$

Cumpsty and Head (1967) introduced the parameter C^* (the square of \bar{R}) and demonstrated using an integral momentum equation that this is the appropriate similarity parameter to analyze attachment line boundary layers. Using a relation for the momentum thickness for laminar boundary layers on an infinite yawed cylinder from Rosenhead (1963) the relation for the momentum thickness Reynolds number becomes

$$Re_{\theta_L} = .4044 * \sqrt{C^*}$$

Poll (1979) used the similarity parameter (also used by Rosenhead)

$$\eta = \sqrt{\nu / k}$$

and an associated definition of the Reynolds number

$$\bar{R} = V_{\infty} \eta / \nu$$

to get the same result as Pfenniger (1965) and Cumpsty and Head (1967). After using the potential flow result for the chordwise velocity gradient, this reduces to

$$Re_{\theta L} = .404 \sqrt{\frac{Q_{\infty} r \sin \Lambda \tan \Lambda}{2\nu}}.$$

This result is only valid for infinite yawed cylinders, but should be reasonably accurate for an infinite swept wing with a cylindrical leading edge. For a leading edge with ellipticity ε , this becomes

$$Re_{\theta L} = .404 \sqrt{\frac{Q_{\infty} r \sin \Lambda \tan \Lambda}{(1 + \varepsilon)\nu}}.$$

but can be controlled by keeping the leading-edge radius below a critical value.

Many experiments have been done to find both critical Reynolds number values. Gaster (1967) performed experiments on a Handley Page laminar flow wing at 43° sweep which indicated that the critical Reynolds number for a laminar boundary layer (small disturbances) was greater than 170 (the highest Re_{θ} used in the experiment). Gaster also designed a bump which bears his name, the purpose of which is to remove the turbulent boundary layer originating at the wing root to help stabilize the flow. Cumpsty and Head (1969) conducted experiments on a swept wing model showing that laminar flow is stable up to $Re_{\theta}=245$. Pfenninger and Bacon (1969) performed experiments on a 45° swept airfoil and found the critical Re_{θ} for laminar flow is 240. The experiments by Poll (1979) indicated that laminar flow was stable to $Re_{\theta}=230$. A good general value for the onset of transition for an uncontaminated root flow is $Re_{\theta}=240$.

If the wing root is contaminated with turbulence from the fuselage or some other structure (pylons, for instance), the disturbances feeding into the boundary layer are relatively large and the critical value of Re_{θ} is much lower. Pfenninger (1965) conducted flight tests to discover that laminar flow was obtained for $Re_{\theta}=100$ for turbulent root. Gregory and Love (1965) performed wind tunnel tests on a swept airfoil and set the critical value at 95. Gaster (1967) first observed turbulent spots at $Re_{\theta}=88$, with the flow fully turbulent at $Re_{\theta}=104$. Cumpsty and Head (1969) and Poll (1985) used the same swept wing model to fix the value at 100. There seems to be wide agreement in the literature that the critical value for damping of turbulent contamination from the root is $Re_{\theta}=100$.

Several investigators have used DNS and linear and nonlinear analysis techniques to look at the nature of the instabilities and to confirm previous experimental results. Hall, Malik, and Poll (1984) used nonparallel linear stability theory on a swept Hiemenz (stagnation point) flow and predicted a critical $Re_{\theta}=245$. Spalart (1989) used a DNS method to confirm this result. Hall and Malik (1986) attempted to bridge the gap between the turbulent and laminar originating flow by using weakly nonlinear theory and DNS, and found that subcritical disturbance growth corresponds to branch II of the neutral curve. Eigenvalue analysis of Lin and Malik (1996, 1997), and DNS work by Joslin (1995, 1996) has confirmed previous results.

Recommendation

Although empirical, this correlation has been demonstrated to be valid over the speed range from incompressible to low supersonic. We will use this in RATTraP.

6.2 Other Methods

DNS has been performed to provide the details of the attachment-line region but in our opinion is not needed as a tool in the present studies. The attachment-line momentum-thickness Reynolds number correlation has been demonstrated to be valid over a wide speed range both here in the United States and in Europe. There seems to be no other transition prediction method analogous to the e^N method for TS and crossflow instabilities for attachment line flows. This approach seems to be the only viable method of this class.

7 Laminar-Turbulent Interaction

7.1 Empirical correlations

Turbulent contamination should propagate outward at an angle of about 10° , consistent with the multitude of experiments and data on the growth of turbulent spots in a laminar boundary layer (e.g. Schubauer & Klebanoff (1955) – see sketch on p. 456 of Schlichting “Boundary-Layer Theory, Seventh Edition”, McGraw-Hill 1979). This could be somewhat less with a strong favorable pressure gradient: the spanwise propagation of turbulence is related to local T-S instabilities and a favorable gradient stabilizes T-S. The opposite would be true for an adverse gradient. There are very few data available, except the work on turbulent spots by various groups. The upcoming stability and transition tests at Texas A&M by William Saric should provide more info on spanwise contamination.

7.2 Other Methods (turbulent diffusion)

The transport equation which is currently used to calculate the N factor for the e^N envelope TS method can be modified to include a diffusion term. It may be possible to tune this diffusion term such that turbulence which is present at some surface can diffuse into the laminar boundary layer as it is convected with the flow. There has been no work on this in the past but this may be investigated as part of this effort.

Recommendation

The 10° rule will be used as the method of choice since it is the only one with empirical data to back it up, but consideration will be given to the turbulent diffusion method as well.

8 Compressibility Effects

8.1 Compressibility corrections

The inclusion of compressibility does not change the fundamental physics for subsonic Mach numbers. Compressibility has a stabilizing influence (Mack 1984, Arnal 1994).

With the current interest in high-speed flight, there is also a keen desire to determine correlating parameters, based purely on basic-state profiles, that can be easily incorporated into existing basic-state codes and will predict transition location (or trends) for crossflow-dominated problems. To evaluate parameters quantifying stability characteristics, Reed & Haynes (1994) examined the linear stability of the supersonic flow over a rotating cone at zero incidence. When compressibility and cooling effects are included (per an Illingworth transformation), a relationship is found between a new crossflow Reynolds number and the maximum crossflow velocity at transition. This result has been verified with the yawed-cone data of King (1991), Stetson (1982), and Holden et al. (1994). The new crossflow Reynolds number is calculated solely from the basic-state profiles and, as such, it can aid in conceptual (only) transition prediction and design for 3-D boundary layers.

8.2 Other methods

Considerable uncertainty exists in both the prediction and control of transition in supersonic flows due to the dearth of reliable experiments. Here we concentrate on the basic fundamental differences between subsonic and supersonic streamwise instabilities in order for the reader to better understand transition control and prediction methods. The paper by Mack (1984) is the most complete description of compressible stability available anywhere.

The linear stability analysis of supersonic boundary layers uncovers three major differences between it and the subsonic analysis.

8.3 Generalized Inflection-Point Criterion

The extension of the Rayleigh inflection-point criterion to compressible boundary layers has an important change. Lees & Lin (1946) studied the temporal growth of 2-D inviscid disturbances in parallel, perfect-gas flows. (Analogous results for 3-D disturbance in a 3-D boundary layer can be found using the "tilde" coordinate system described by Mack. This coordinate system is rotated so that the "x" direction coincides with that of the phase velocity.) They classified the disturbance according to the disturbance phase speed c_r relative to the boundary layer edge velocity U_e :

Subsonic: $U_e - c_r < a_e$
Sonic: $U_e - c_r = a_e$
Supersonic: $U_e - c_r > a_e$

where a_e is the speed of sound at the edge of the boundary layer. One of their most important results was that a neutral subsonic solution will exist if and only if there is a generalized inflection point y_s in the boundary layer

$$D(\rho DU) = 0 \quad \text{at } y = y_s > y_0$$

where y_0 is the point where $U = 1 - 1/Me$ and Me is the local edge Mach number. The proof that the presence of a generalized inflection point implies the existence of a neutral solution requires that the local flow velocity be subsonic throughout the boundary layer relative to the disturbance phase speed. In this case, the disturbance phase speed is equal to the tangential velocity component at the generalized inflection point. Moreover, the neutral solution will have a unique wave number. The presence of a generalized inflection point is also a sufficient condition for the existence of an instability.

The boundary layer on an adiabatic flat plate in a compressible flow always features $D(\rho DU) = 0$ somewhere in the flow. Thus, even zero-pressure-gradient flows are subject to inviscid instabilities that grow with increasing Mach number. As y_s moves away from the wall with increasing Mach number, the range of unstable frequencies is enlarged at high Reynolds numbers. This effect occurs up to a Mach number of approximately 5. In contrast to $M=0$, when viscosity is considered at $M>1$, it may be stabilizing relative to the dynamic instability.

8.4 Multiple Acoustic Modes: Mack Modes

One of the most significant developments in compressible theory comes from Mack, who discovered a new family of solutions to the compressible equations. They can be explained by considering the inviscid stability equation in the form

$$\partial^2 \psi / \partial y^2 + (1 - M^2) \partial^2 \psi / \partial x^2 + f(M, \psi, \partial \psi / \partial y) = 0$$

where

$$\begin{aligned} \psi &= v / (\alpha U + \beta W - \omega) \\ M &= (\alpha U + \beta W - \omega) Me / [(\alpha^2 + \beta^2) T]^{1/2} \end{aligned}$$

$M(y)$ is the relative Mach number between the local basic-state velocity and the propagation speed of a neutral wave. Me is the edge Mach number. Here, we recall that and take advantage of the fact that $\partial^2 \psi / \partial x^2$ was the source of $-(\alpha^2 + \beta^2) \psi$ in the disturbance equation. Obviously, when $M < 1$, this equation is elliptic and the eigenvalue is unique as it is in the case of incompressible inviscid theory. When $M > 1$, this equation is hyperbolic and an infinite discrete set of eigenvalues can satisfy the boundary conditions. $M = 1$ at $y = y_a$ in the boundary layer and y_a is called a turning point. The solution of this equation can be found by using WKB methods. For $y < y_a$, the solutions are oscillatory and for $y > y_a$ they are exponential.

Physically, the disturbances propagate at a speed that is subsonic relative to the edge velocity, but supersonic relative to the region near the wall ($y < y_a$). Thus, for an adiabatic flat plate with $Me = 3.8$, disturbances with phase speeds $cr > 0.5$ are supersonic with respect to the wall region (Morkovin 1991). At the same phase speed cr , a sequence of wavenumbers satisfy the differential equation and boundary conditions. These extra solutions are higher modes and are most unstable as 2-D waves, because it is then that the relative supersonic region is of maximum extent. They have shorter wavelengths than the usual T-S instability waves (first modes) since the wavenumber sequence is approximately

$$2\alpha\nu/\pi = 1, 3, 5, 7, \dots$$

They are not T-S waves by character or behavior and it is fitting that they be called Mack modes. They represent sound waves that reflect inviscidly between the solid wall and the relative sonic line in the boundary layer. See also Mack (1987).

8.5 3-D Viscous Disturbances

In the supersonic case ($1 < Me < 10$), Mack completed extensive computations of 3-D stability maps on a flat plate and found many important results (see Mack 1984 for the details and comparisons with experiment). The earliest results showed that above a Mach number of 1, 3-D waves corresponding to the first viscous mode have a larger amplification factor than the corresponding 2-D disturbance. (The opposite is true for subsonic flows.) As the Mach number is increased above 1, the most unstable wave angle quickly increases to 45° at $Me = 1.3$, 55° at $Me = 1.6$, and 60° at $Me = 2.2$. This phenomenon is due to decreased cross-stream mutual interaction between disturbances and decreased upstream influence both compensated by a lower effective 2-D Mach number. Thus, the assumption of 2-D viscous disturbances cannot be made in supersonic flows.

Mack (1987) gives an example of viscous multiple solutions, along with calculations of higher viscous discrete modes and the compressible counterpart of the Squire mode.

Recommendation

LST has been validated recently for high-speed flow (Lyttle et al. 2005) and is the method of choice. Given the nature of the instabilities, 3-D disturbances must be considered. However, for low supersonic Mach numbers, the growth rates of the 2-D and 3-D disturbances of a flat plate are similar.

9 Intermittency

9.1 Overview

The typical aircraft boundary layer consists of regions of laminar, transitional and fully turbulent flow. Stability theory and the e^N method can provide the location for the beginning of the transitional flow region. This region can extend over a significant portion of an aerodynamic surface. For a flat plate, the full length of the transitional flow region is approximately equal to the distance from the leading edge of the flat plate to the location of transition onset. Once the flow becomes transitional, LST is no longer relevant or valid, and a separate model must be applied to accurately simulate transitional flow. Standard turbulence models are generally applied with modifications to account for the transitional flow using an intermittency factor, γ , derived from an intermittency model.

While algebraic turbulence models do not include any implicit relaxation effects once the turbulence model is “turned on,” transport equation turbulence models such as the $k-\varepsilon$, $k-\omega$ and $k-k_l$ models include an implicit relaxation or history effect because of the turbulence model convection and source terms. However, these implicit relaxation effects are not nearly strong enough to account for the extent of the transitional flow region.

The accurate prediction of the transitional flow region can be critical to accurate aerodynamic predictions. The shape of boundary layer velocity profiles in this region are bounded by laminar and turbulent profiles. In the early part of the transitional flow region they are more laminar-like, while in the later stages they are more turbulent-like. On an airfoil, transition often begins in a region of adverse pressure gradient flow that is susceptible to separation. Accurate prediction of boundary layer velocity profiles in the transitional flow region can affect separation predictions, and thereby aircraft performance predictions.

As will be documented below, the phenomena governing the transitional flow region and turbulent boundary contamination of an adjacent laminar boundary layer are closely related. Thus it should be possible to develop an intermittency model that accounts for both transition and interference effects.

The remainder of this section on intermittency will begin with a review of transitional flow theory and empirical results which have an impact on modeling. This will be followed by a review of transitional flow modeling. The intermittency modeling section will conclude with recommendations for RATTraP transitional flow modeling that leverage existing methods and experimental research.

9.2 Transition region experiments and theory

9.2.1 Turbulent Spots

Water table experiments by Emmons (1951) suggested that the transitional flow region is governed by turbulent spots. These spots are generated over a very narrow streamwise band and grow and merge downstream into a fully turbulent boundary layer. This finding replaced earlier assumptions that turbulence originated over an irregular front that oscillated in time and space, where the flow downstream of this front remained turbulent. With our understanding of turbulent spots, we now understand that at any instant in time along a streamwise trace there can be “intermittent” turbulent zones due to the presence of spots, and laminar zones in front of and in the wakes of spots. This observation has a fundamental effect on our understanding of the characteristics of spot growth and formation, which is essential to accurate transitional flow modeling.

Schubauer and Klebanoff (1956) took detailed measurements of turbulent spots. They found that the boundary layer inside the turbulent spot was fully turbulent. The spots grow in both streamwise and lateral extent as they are convected downstream, with the leading edge of the spot advancing at $0.88 U_\infty$ while the trailing edge advances at $0.5 U_\infty$. The spot is approximately triangular, as shown in Figure 11. It grows laterally with a half angle near $10 \text{ degrees} \pm 1 \text{ degree}$. Outside the spot, the flow remains laminar, but the fuller turbulent profile of the spot influences the laminar flow in its wake causing the laminar profile to be slightly fuller, while approximately maintaining the laminar boundary layer thickness that would be expected if the boundary layer were laminar from the leading edge. This subtle modification of the profiles in the laminar parts of the profiles in the transitional flow region causes the profiles to be more stable to Tollmien-Schlichting instabilities. For this reason, spots are formed over a very narrow streamwise region, not at all points downstream of the location where the n factor reaches a critical value.

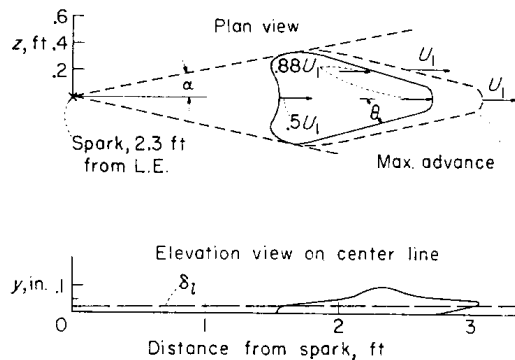


Figure 11: Spot has approximately triangular planform. (From Schubauer, 1956)

9.2.2 Mean Boundary Layer Characteristics in the Transitional Region

The characteristics of the transitional boundary layer for neutral pressure gradient flow were clearly identified by Dhawan and Narasimha (1958). They took detailed

intermittency measurements to determine the character of the intermittency function in the boundary layer. The intermittency function represents the fraction of time that the flow is turbulent at any location in the flow; the intermittency function γ is 1 wherever the flow is fully turbulent, and 0 where the flow is always laminar. Using these intermittency measurements and the probability based intermittency model of Emmons (1951), they were able to prove that turbulent spots were in fact generated over a very short streamwise distance. By their measurements, they were also able to determine some key characteristics of the mean flow in the transitional flow region.

- The mean velocity profile in the transitional flow region is a linear combination of the laminar and turbulent velocity profiles:

$$U = \gamma U_t + (1 - \gamma) U_l$$

where U_t refers to a turbulent velocity profile whose origin is at the transition onset location. The momentum thickness at the origin of the turbulent boundary layer is equal to the laminar boundary layer momentum thickness at the transition onset location, while U_l refers to a laminar boundary layer whose origin is at the leading edge of the flat plate.

- The skin friction near the end of the transition region “overshoots” the skin friction one would obtain for a turbulent boundary layer starting from the leading edge of the plate because of the aft location of the turbulent boundary layer origin.
- The boundary layer displacement thickness can be obtained from the linear combination of laminar and turbulent thicknesses. (Substituting the definition of the transitional velocity profile in the definition of displacement thickness proves that this is the case.)
- The momentum thickness is not a simple linear combination of laminar and turbulent thicknesses.

9.2.3 The Intermittency Function

Dhawan and Narasimha also developed a function for the intermittency that formed the basis for many intermittency models. They found that for a flat plate,

$$\gamma = 1 - \exp \left[-A \left(\frac{x - x_t}{\lambda} \right)^2 \right]$$

Where λ is a measure of the extent of the intermittency region, and A is a constant equal to 0.412, and x_t is the location of transition onset.

$$\lambda = \{x\}_{\gamma=0.75} - \{x\}_{\gamma=0.25}$$

This equation collapses intermittency data for a wide range of Reynolds numbers and flow conditions, including low supersonic Mach numbers and a range of freestream Mach

numbers. However, this relation by itself does not represent a model of the intermittency region because it requires experimental determination of λ .

Mean pitot pressure measured very close to the surface of a flat plate is plotted along with intermittency in Figure 12. The pitot pressure is proportional to the square of the skin friction. Note that the skin friction continues to decrease below the laminar skin friction value for a short distance downstream of the location of transition onset, x_t .

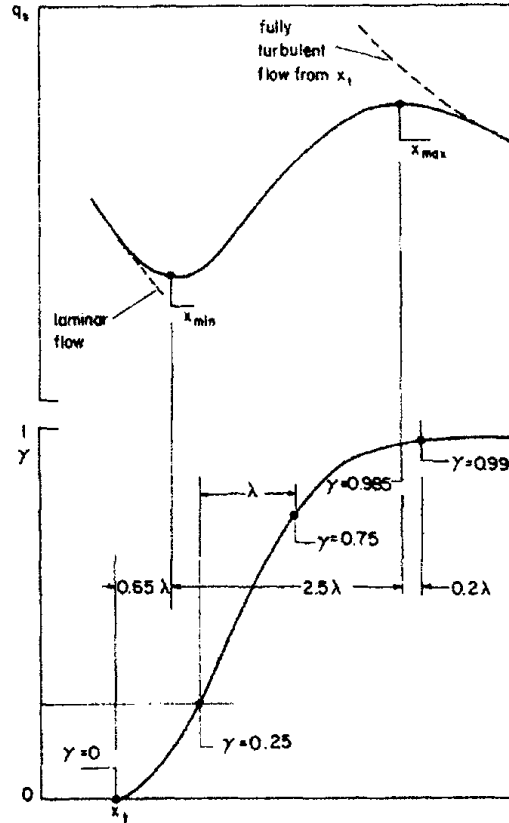


Figure 12: Surface pitot pressure and intermittency measured in the transitional region of a flat plate. (From Narasimha, 1985)

9.2.4 Spot Formation and Propagation

The intermittency region can be better understood by recasting the equation for the intermittency as a function of turbulent spot formation and propagation. We can rewrite the intermittency equation as

$$\gamma = 1 - \exp\left[-\frac{n\sigma}{U}(x - x_t)^2\right]$$

where we have set $A/\lambda^2 = n\sigma/U$. The variable n is the spot formation rate, the number of spots generated per second per unit span length. The variable σ is the nondimensional spot propagation rate. The spot formation and propagation rates are distinct phenomena

and hold out the possibility of developing models that logically account for the effects of freestream turbulence and streamwise pressure gradient.

The spot propagation parameter quantifies the physical growth of turbulent spots. It can be defined as

$$\sigma = \frac{Ut}{x^3} \int b(x,t) dx$$

where b is the width of the spot at some instant in time, t , and x station. This integration is generally performed on a plane parallel to the wall, either at the wall or a short distance off of the wall, since the spot planform is relatively constant until the outer portion of the boundary layer is reached. The velocity U is the freestream velocity. This equation is integrated over one spot at one instant in time. The spot propagation parameter turns out to be approximately constant for zero pressure gradient flows, with values ranging between 0.25 and 0.29 according to Narasimha (1985) and Mayle (1991). The spot propagation parameter represents the speed and size of the turbulent spot downstream of the formation point. The slower the spot moves and the more it grows as a function of x , the more turbulent area will be generated for each spot formed.

Spot formation is more difficult to measure directly than is spot propagation. The spot formation rate is generally determined indirectly by measuring the intermittency as a function of streamwise location, determining λ , and then solving for n .

$$n = \frac{UA}{\sigma \lambda^2}$$

where A is the constant equal to 0.412 for neutral pressure gradient boundary layers.

To this point, none of these results are useful for modeling the transitional flow region because they require measuring λ . However, modeling the formation rate and propagation parameter independently will prove useful.

9.2.5 Pressure Gradient Effects

Most transition problems of interest include streamwise pressure gradients. Initially, Dhawan and Narasimha (1958), Narasimha (1985) and Mayle (1991) assumed, based on very limited data, that intermittency region descriptions based on neutral pressure gradient boundary layers were applicable to flows with pressure gradient. Gostelow (1994) found that adverse pressure gradients had significant effects on the transition region. In a later paper, Gostelow (1996) compiled existing measurements for both favorable and adverse pressure gradients to determine the effects of pressure gradients on spot propagation σ and wedge half angle α . These studies clearly indicate that spot formation and propagation are strong functions of streamwise pressure gradient. Figure 13 shows the spot spreading wedge angle as a function of the non dimensional pressure gradient parameter λ_θ , where $\lambda_\theta = (\theta^2/\nu)(\partial U/\partial x)$. Figure 14 shows the spot propagation

parameter as a function of the pressure gradient parameter. Gostelow's definition of σ used in Figure 1 is slightly different than the standard definition:

$$\sigma = \tan \alpha \left(\frac{1}{b} + \frac{1}{a} \right)$$

where a is the velocity of the front of the spot and b is the velocity of the back of the spot. This definition assumes a triangular spot, whereas the Narisimha (1985) and Emmons (1951) definitions account for the actual size and shape of the spot. The triangular spot of Gostelow is smaller than the actual spot size, so his neutral pressure gradient propagation parameter is 0.14 vs 0.27 for the more exact measurements. Nevertheless, on a relative basis, Figure 14 clearly demonstrates that pressure gradient has a strong effect on spot propagation.

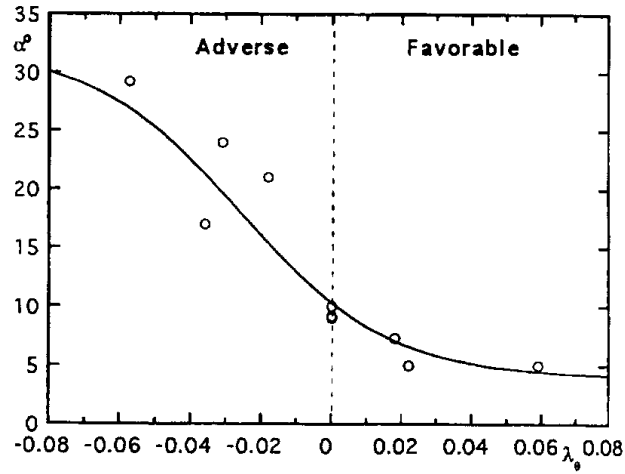


Figure 13: Effect of non dimensional pressure gradient parameter on spot growth wedge angle α . (From Gostelow 1996)

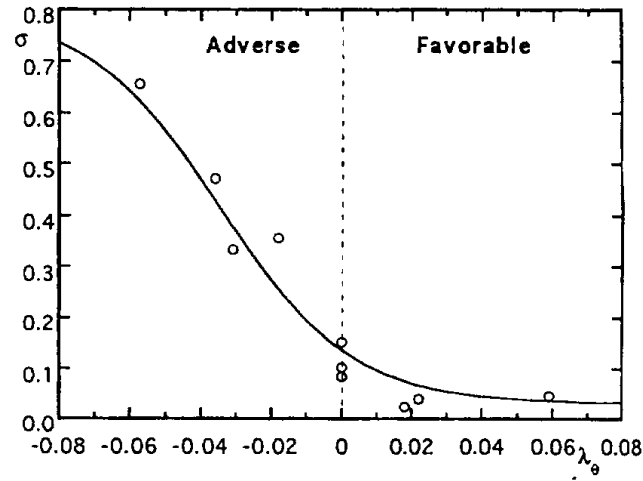


Figure 14: Effect of non dimensional pressure gradient parameter on spot propagation parameter σ . (From Gostelow, 1996)

In addition, Gostelow(1994) investigated the spot formation rate as a function of pressure gradient for adverse pressure gradients. In Figure 15, Gostelow plotted the non-dimensional formation rate parameter, N , as a function of the non-dimensional pressure parameter for a range of freestream turbulent intensities.

$$N = \frac{n\sigma\theta_t^3}{\nu} = 0.412 \frac{\text{Re}_{\theta_t}^3}{\text{Re}_\lambda^2}$$

In this equation, θ_t is the momentum thickness at the transition onset location. Again, pressure gradient has a significant effect on the formation rate parameter. While the non-dimensional formation rate parameter N includes the propagation parameter σ , the very strong dependence of N on pressure gradient indicates that the spot formation rate

increases significantly as adverse pressure gradient strengthens. Fraser (1988) found that favorable pressure gradients continue the trend of Figure 15, with the spot formation rate decreasing as the favorable pressure gradient increases.

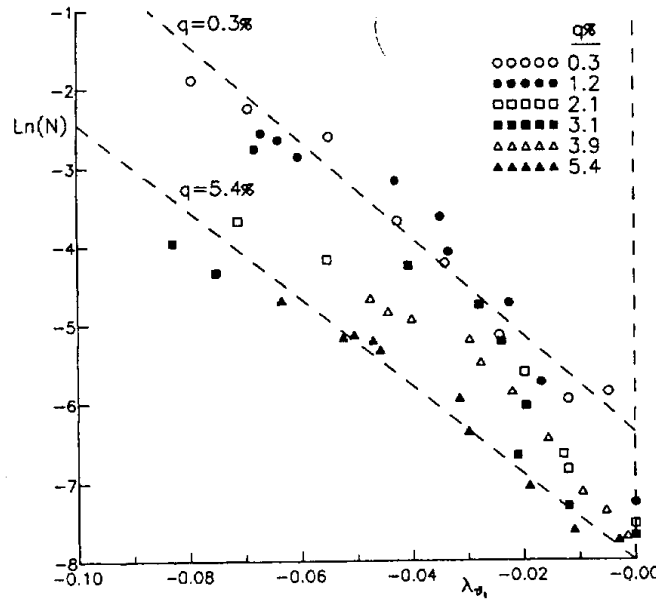


Figure 15: Effect of non-dimensional pressure gradient parameter on spot formation parameter N. (From Gostelow, 1994)

9.2.6 Freestream Turbulent Intensity Effects

A great deal of the work to date on the transition region has been motivated by turbomachinery applications. As a result, significant attention has been paid to the effects of freestream turbulence, since the turbomachinery environment has high freestream turbulence levels due to the wakes of upstream components. For most aircraft applications freestream turbulence levels will be low. However, two cases where freestream turbulence effects will be important are: 1) when analyzing wind tunnel measurements of transition regions where freestream turbulence levels are much higher than flight, and 2) for aircraft components in the turbulent wake of upstream surfaces such as slotted flaps and high-lift devices. While freestream turbulence has a strong effect on the location of transition onset, it does not have a dramatic effect on the transition region. Narasimha (1985), (from Dey and Narasimha, 1984) found the non-dimensional spot formation rate parameter N reaches a constant of 0.7×10^{-3} for turbulent intensities above 0.3%. Gostelow(1994) included new data and reconsidered some of the data used by Dey and Narasimha (1984) and concluded that the value of N continues to decrease at least up to a turbulence intensity value of 1% as shown in Figure 16. Turbulent intensity effects are also included in Figure 15, and the slope of the curves in Figure 15 and Figure 16 should be compared. Gostelow (1994) concludes, “While there is an exponential dependence of transition length...on the levels of both adverse pressure gradient and free-stream turbulence, the dependence on pressure gradient is much the strongest.”

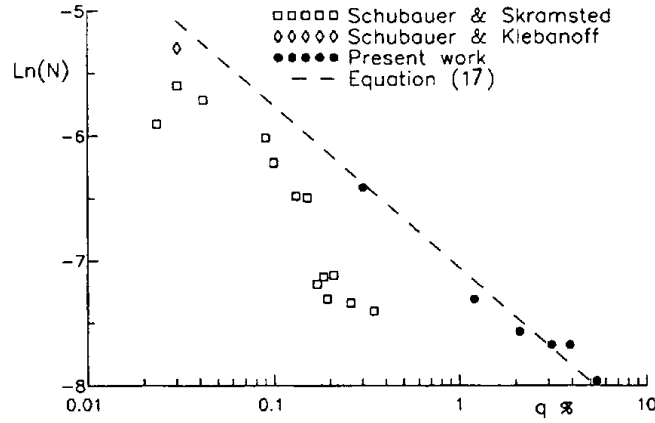


Figure 16: Effect of freestream turbulent intensity on spot formation parameter N . (From Gostelow, 1994)

9.2.7 Reynolds Number Effects

Generally, the effects of Reynolds number are accounted for automatically in the non-dimensional parameters used to characterize the transitional flow region. However, a simple relation between intermittency length scale λ and the transition location was determined by Narasimha (1985) for neutral pressure gradient boundary layers in terms of Reynolds number:

$$Re_\lambda = 9 Re_t^{3/4}$$

Thus given a Reynolds number based on the transition onset location, the transition length λ can be determined and the intermittency function evaluated. This relation is only valid for neutral pressure gradients. It implies that the ratio of the (length of the transitional flow region) to the (distance from the plate leading edge to the point of transition onset) decreases with increasing Reynolds number.

9.2.8 Crossflow Instability Induced Transition Regions

While the development of turbulent spots and the fundamental flow mechanisms in the development of turbulence arising from T-S instabilities are well understood, transitional flow mechanisms for crossflow transition are an area of active research. The breakdown of crossflow instabilities to turbulence can follow multiple paths. Crossflow instabilities can generate inflections in the streamwise profile that cause extremely rapid breakdown to turbulence. This breakdown can occur through either crossflow or T-S instabilities. Joslin (1995) performed a direct numerical simulation and showed that his solutions could be fit in the transitional flow region using an intermittency function for swept wings developed by Arnal (1984). In most cases of interest for swept wings, if transition

is caused by crossflow transition, it will occur relatively near the leading edge of the wing and the transitional flow region will be short.

9.3 Transitional Region Modeling

Transition region models for implementation with Navier-Stokes flow solvers fall into two basic categories, algebraic/integral models and transport models. Algebraic/integral models define the intermittency in the transitional flow region as a function of the location of transition onset and variety of integral boundary layer parameters. Transport models have a transport equation for the intermittency factor that is solved in addition to transport equation turbulence models.

Algebraic/Integral models are better suited to RATTraP requirements because the models can be evaluated along the surface using a surface differential equation similar to the equations used to integrate the stability amplification factor. In addition, the algebraic/integral models can conform easily to the empirical transition region measurements. In contrast, transport equation models require the addition of a transport equation to a flow solver, which would be very difficult to make modular and portable. For these reasons, this section will review some of the algebraic/integral models in detail and give a brief review of transport equation methods.

9.3.1 Zero Pressure Gradient Based Model – Narasimha

Narasimha (1985) derived a basic model from the Dhawan and Narasimha (1958) transition correlations. The intermittency length is calculated from

$$\gamma = 1 - \exp\left[-\frac{n\sigma}{U}(x - x_t)^2\right]$$

and the value of $(n\sigma)$ is determined from the non-dimensional breakdown parameter N ,

$$N = \frac{n\sigma\theta_t^3}{\nu} = 0.7 \times 10^{-3}$$

where θ_t is the momentum thickness at the onset of transition. Narasimha found the constant for this relation from zero pressure gradient boundary layer. By relating spot formation and propagation to the local momentum thickness instead of the x location of transition onset, the model can better take into account variations in the boundary layer thickness leading up to transition due to pressure gradients. However, it does not take into account the effects of the pressure gradient within the transition region.

9.3.2 Pressure Gradient Based Model – Dey and Narasimha

Dey and Narasimha (1988) adjusted the relation for the non-dimensional breakdown parameter to account for favorable pressure gradients:

$$N = \begin{cases} 0.7 \times 10^{-3} & (\lambda_{\theta} \leq 0) \\ 0.7 \times 10^{-3} + 0.24(\lambda_{\theta})^2 & (0 \leq \lambda_{\theta} \leq 0.10) \end{cases}$$

This model does not account for the much stronger effects of adverse pressure gradients later identified by Gostelow (1996) and only consider the effect of the pressure gradient at transition onset.

9.3.3 Solomon – Gostelow model

Gostelow (1994) developed an improved transition region model that accounted for the effects of adverse pressure gradients on the non-dimensional breakdown parameter. The curve fits for the Gostelow (1994) model are included in the Solomon (1996) model which appears to be the most complete algebraic/integral model available, since it includes the effects of pressure gradient and freestream turbulence on both the spot formation rate and the propagation parameter. This model will be presented in some detail.

The non-dimensional breakdown parameter N is obtained from two curve fits, one for adverse pressure gradients, and one for favorable pressure gradients.

For adverse pressure gradients, $\lambda_{\theta} > 0$,

$$N = 0.86 \times 10^{-2} \exp[2.134\lambda_{\theta} \ln(q_t) - 59.23\lambda_{\theta} - \ln(q_t)]$$

where q_t is the freestream turbulent intensity. For favorable pressure gradients, $\lambda_{\theta} < 0$,

$$N = N_0 \exp(-10\lambda_{\theta}^{1/2})$$

where N_0 is the value of N at $\lambda_{\theta} = 0$. The spot propagation parameter σ is evaluated from the curve fit for pressure gradient of Figure 14.

$$\sigma = 0.03 + 0.37 / [0.48 + 3.0 \exp(52.9\lambda_{\theta})]$$

The breakdown parameter N is used to determine the spot formation rate n . Because the spot formation occurs only very near the transition onset location, the pressure gradient at the transition onset location, λ_{θ} is used. The spot formation parameter is evaluated from

$$N = \frac{n\sigma\theta_t^3}{\nu}$$

with the spot propagation parameter evaluated from the curve fit with the pressure gradient parameter evaluated at the transition onset location. Once n and σ are evaluated, the intermittency can be evaluated from the integral

$$\gamma = 1 - \exp \left[-n \int_{x_i}^x \frac{\sigma}{\tan(\alpha)} \left(\frac{dx}{U} \right) \int_{x_i}^x \tan \alpha \, dx \right]$$

In this expression, the spot propagation parameter is evaluated using the local value of the pressure gradient parameter λ_θ based on the laminar component of the boundary layer in the transition region. The propagation wedge angle can be determined from a curve fit of Figure 13.

$$\alpha = 4 + 22.14 / [0.79 + 2.72 \exp(47.63 \lambda_\theta)]$$

This model can be implemented without great difficulty into the RATTraP model. The integrals in the intermittency expression can be integrated using the surface integral routines in the external streamline direction, and then the intermittency can be evaluated from the above equation. Alternatively, the equation for the intermittency could be differentiated with respect to x , and then it could be integrated along streamlines. This approach would allow a diffusion term to be added to the intermittency equation to account for lateral variations in the intermittency so as to account for turbulent contamination and interference effects. The freestream turbulent intensity values can be obtained from the two-equation turbulence model values at the outer edge of the boundary layer in cases where an upstream turbulent wake interacts with the transitional flow region.

The model was tested for a range of pressure gradients and turbulent intensities and gives much better predictions of the transitional flow region than do the Narasimha and Dey and Gostelow models. Figure 17 shows the streamwise velocity and pressure gradients for three flows over flat plates from Solomon (1996). In all three cases the pressure gradient varies significantly in the transition region. The predictions of the intermittency function with the Solomon model are much better than those of the Dey and Narasimha (1988) or Gostelow (1994) models. Figure 18 shows the intermittency function for a case with a favorable pressure gradient. The method labeled “New Method” is the Solomon (1996) model. Figure 19 shows the intermittency function for a case with a favorable pressure gradient followed by a weak adverse pressure gradient. Figure 20 shows the intermittency function for a case with an adverse pressure gradient.

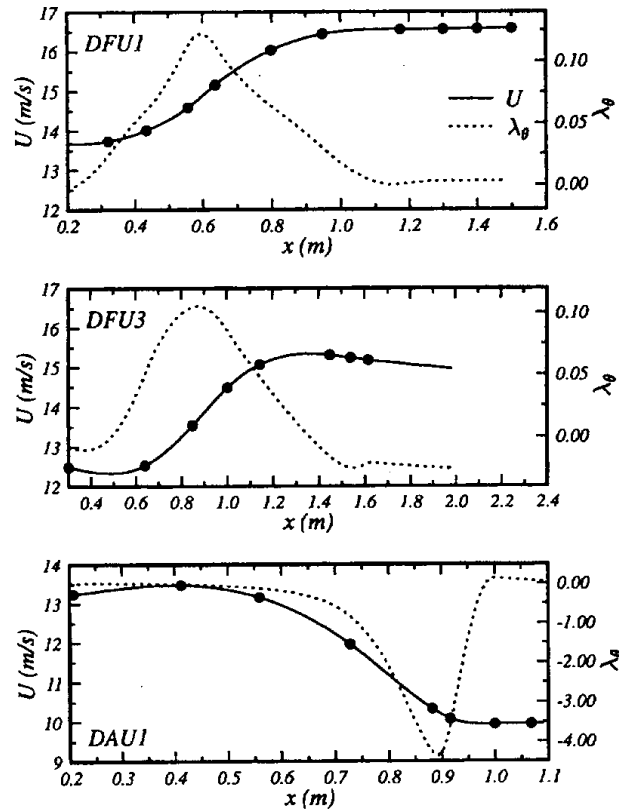


Figure 17: Streamwise velocity and pressure gradient parameter for three test cases from Solomon (1996).

The Narisimha and Dey and Gostelow models do not account for variations in the pressure gradient in the transition region; the input parameters to the transition model are all determined at the transition onset location. As a result, in Case DFU3 where an adverse pressure gradient follows a favorable pressure gradient, (Figure 19), the Gostelow model predicts much too long of a transition region, while the Solomon model predicts the transition region very well because the spot propagation parameter grows as the pressure gradient becomes negative. Also note that both the experimental and Solomon model intermittency functions grow with a steep slope beyond 1.4 meters in Case DFU3 as compared to Case DFU1 where the pressure gradient parameter doesn't go negative. Finally, note that the ratio of the transition region length to distance to transition onset is shortest in the adverse pressure gradient case DUA1, shown in Figure 20, as expected. While the Solomon model does not agree as well with the experimental data in this case as it does for favorable pressure gradients, it agrees with the experimental data far better than do the other two models presented.

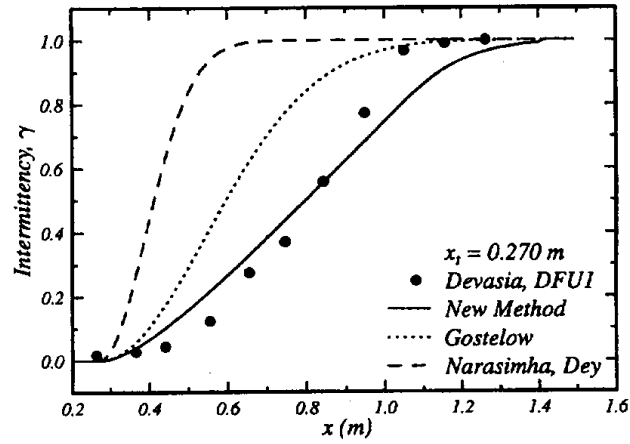


Figure 18: Intermittency prediction with three models for favorable pressure gradient, Case DFU1, from Solomon (1996).

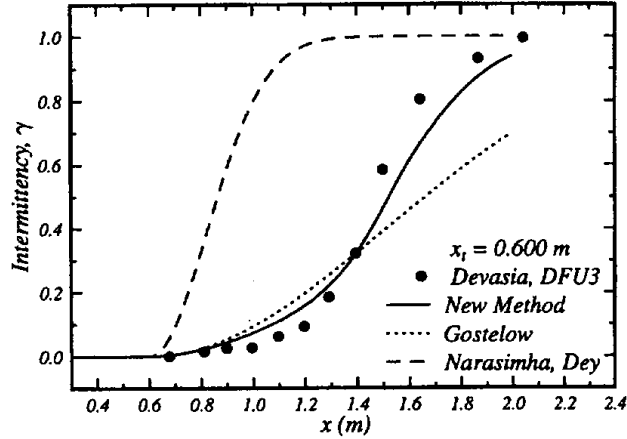


Figure 19: Intermittency prediction for three models for a favorable pressure gradient followed by a weak adverse gradient, Case DFU3, from Solomon (1996).

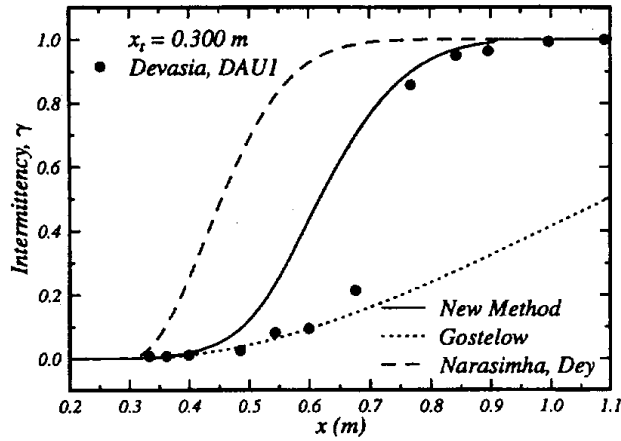


Figure 20: Intermittency prediction for an adverse pressure gradient Case DAU1 from Solomon (1996).

The most difficult aspect of applying the Solomon model directly is the evaluation of the pressure gradient parameter in the transitional flow region using a momentum thickness based on laminar flow. Either an integral equation for the momentum thickness will have to be solved, or a correlation between the laminar and transitional momentum thicknesses will have to be derived.

9.3.4 Transport Equation Intermittency Models

Numerous transport equation intermittency models have been developed and tested. A comprehensive review of these models will not be provided here, but instead a brief overview will be given. These models may eventually be of interest in the RATTraP environment or for use in conjunction with the RATTraP models. These models have the advantage of including history effects automatically, and through diffusion terms can eliminate unrealistic spanwise variations in the intermittency while accounting for

turbulent contamination in laminar regions. On the negative side, the intermittency transport equations developed to date tend to be more complex than the turbulence and length scale transport equations of two equation turbulence models. These intermittency models include a significant degree of empiricism. These models either require input of transition onset locations or they employ transition onset correlations whose accuracy is generally limited to a narrow range of flow problems.

Steelant and Dick (2001) derived a transport equation model for intermittency that includes the effects of both intermittency and freestream turbulence. This model is relatively simple. The transition onset locations are fixed by setting the intermittency variable to zero along all laminar surfaces, which could be determined by any means desired. Their paper presents test cases for a range of pressure gradients and freestream turbulence levels for both flat plates and turbine blades and appears to give good agreement with test data.

Vicedo, Vilmin, Dawes and Savill (1984) developed a transport equation intermittency model for use in separated flow transition. This model includes four source terms for the intermittency equation. This model was tested over a very narrow range of problems – a flat plate with separation downstream of a cylindrical leading edge. While results for this case were promising, more extensive testing of this model is needed.

Langtry, and Menter (2005) developed a transition model that includes transport equations for the intermittency and for the transition momentum thickness Reynolds number. This model was developed primarily for external aerodynamic applications. Again, four source terms are required for the intermittency equation; this is not a simple model. The model has been applied to a range of aerospace and industrial applications including multi-element airfoils and wings with laminar separation bubbles. The model appears to give reasonable results for these complex flows.

Recommendations for RATTraP Modeling

The algebraic/integral models are best suited to the RATTraP method. These models can use surface differential equations for integration of the intermittency functions. The experimental studies of turbulent spots show that the intermittency does not vary significantly normal to the wall (with the exception of turbulent boundary layer edge intermittency which is already accounted for by turbulence models). Thus, there does not appear to be a compelling reason to model an intermittency function which varies across the boundary layer. Determining a single value of the intermittency for use on the entire profile at a given surface location should be sufficient.

Another advantage of the algebraic/integral intermittency modeling is that these models are tied very closely to empirical correlations of spot formation and propagation as functions of pressure gradient and freestream turbulence level. Differential models, while potentially robust computationally, probably will not follow the empirically derived relationships as well as the algebraic/integral methods.

The Solomon (1996) transition model appears to be the most complete model for the transition region available. It has been tested by Sanz and Platzer (1996) on separation bubbles and provided good agreement with test data. Some enhancements of the model may be required to prevent unrealistic lateral variations in the intermittency factor, to account for turbulent contamination, and to allow the model to integrate well with a Navier-Stokes solver. Nevertheless, the basic model formulation and calibrations should provide good predictions for RATTraP.

One area that will require some attention in integrating the Solomon model with RATTraP is the implicit intermittency in transport equation turbulence models. All testing to date has indicated that the implicit intermittency in the LM Aero *k-kl* two transport equation turbulence model is much less than required for accurate modeling of the transitional flow region. However, the implicit intermittency in two equation turbulence models may require some adjustment to the calibration of the Solomon model in order to match experimental data. It should be possible to perform this calibration over a small range pressure gradients on flat plates. It may be necessary to perform this calibration for each turbulence model that is going to be used with the intermittency model to ensure optimal accuracy. The degree of dependence of the transitional model predictions to specific turbulence model will have to be established.

One aspect of intermittency modeling that could be improved is the application of the intermittency function to the turbulence model. In every reference examined, the turbulent viscosity calculated in the turbulence model is multiplied directly by the intermittency to obtain the turbulent viscosity to be applied to the Navier-Stokes equations. Narasimha showed that the transitional velocity profile is a linear combination of fully laminar and fully turbulent profiles. If the turbulent viscosity is multiplied directly by the intermittency factor, and the near wall damping that determines the viscous sublayer thickness is determined from the intermittency region's mean skin friction instead of the skin friction of the fully turbulent spot, the viscous sublayer thickness in the transitional flow region will be in error. It should be relatively easy to modify the near wall damping to use the correct viscous sublayer thickness in the intermittency region.

Intermittency modeling for transition due to crossflow instabilities is not a mature research subject. In some cases, crossflow can generate mean flowfield disturbances that trigger T-S type breakdowns, and the turbulent spot based transitional region flow model may be valid. At the current time, the best that we can do is to apply the algebraic/integral model to crossflow transition and evaluate and calibrate it as required. Continued monitoring of research in this area is warranted.

10 Surface Roughness

The following are rules of thumb used to evaluate roughness and steps and gaps. Much of this information was captured in the DARPA QSP LFC Design Document prepared by Lockheed Palmdale and William Saric & Helen Reed.

10.1 Isolated and Distributed Roughness

Surface roughness can directly trip the boundary layer or unfavorably destabilize the stationary C-F wave. If the roughness Reynolds number exceeds 150, a turbulent wedge is generated directly behind the roughness. Even smaller roughness can cause destabilization (Radeztsky et al. 1999). Appropriate limits on roughness are discussed below.

10.1.1 Tollmien-Schlichting (T-S)

Even though one wants to maintain a favorable C_p as far as possible to eliminate T-S, there can always be problems with steps and gaps:

- 2-D roughness is bad. There may not be an acceptable step height.
- 3-D roughness can be bad if the spanwise wavelength is within the unstable range. For supersonic flow, 3-D T-S is more unstable than 2-D T-S.
- Whole chord sensitive
- Keep $Re_k < 150$ over whole chord to avoid immediately tripping to turbulent. Here Re_k is the roughness Reynolds number based on the roughness height, and the local speed and viscosity at the top of the roughness.
- Steps are bad. Gaps are very bad if not along an isobar.
- Backward-facing steps are worse than forward-facing steps (everything must be done as a forward-facing step).
- Background roughness typical of good aircraft finish (3-4 μm rms) is OK.
- Concave curvature is bad
- Convex curvature is good
- Check that engine-noise frequencies are outside of T-S passband.

10.1.2 Stationary Crossflow

- First 10% chord is most sensitive for roughness (boundary layer thin). After 10% chord, roughness does not affect C-F, provided $Re_k < 150$
- 3-D roughness (isolated and/or distributed) is bad. Isolated roughness at any level can cause problems. Random distributed roughness should be typical of a good aircraft finish (3-4 μm rms)
- 2-D roughness is OK except at the edges
- $Re_k < 150$ over whole chord
- Suggested control roughness $Re_k < 7$
- Waviness or disturbance spacing (steps, gaps) longer than all unstable wavelengths is OK (to avoid harmonics)
- Waviness or disturbance spacing shorter than $\frac{1}{2}$ most unstable wavelength is OK
- Holes as effective as bumps in generating C-F. This is both good (control) and bad (most unstable).

- Backward-facing steps worse than forward-facing steps (everything must be done as a forward-facing step)
- Crouch & Ng (2000) and Crouch (2004) propose a variable N factor expression $N_{CF} = 2.3 - \ln(h_{rms}/\delta^*)$ where h_{rms} is the 3-D rms roughness height and δ^* is the boundary layer thickness at the neutral point for the critical mode.

Numerical criteria for 2-D isolated roughness elements are presented. These criteria use a relevant Reynolds number to scale the roughness element geometry.

10.2 Steps

- o For forward facing steps, the Reynolds number based on step height should be at or below 1800.
- o For rearward facing steps, the allowable height is half that permitted for forward facing steps.

Wang & Gaster (2004) and Crouch et al. (2004) curve fits available data for zero, favorable, and adverse pressure gradients, and propose the following N factor corrections:

Forward facing steps: $N_{TS} = N_{TS0} - 1.6h/\delta^*$

Backward facing steps: $N_{TS} = N_{TS0} - 4.4h/\delta^*$

where N_{TS0} is the smooth-surface N factor for transition, h is the step height, and δ^* is the displacement thickness at the step location.

10.3 Gaps

- o For gaps which run normal to the flow direction over which the flow can easily cross the Reynolds numbers based on gap width should be at or below 15,000.
- o Gaps with flow running along the gap are especially problematic. The allowable gap width for such geometries is 1/7 (14%) of that for gaps with flow across.

10.4 Surface Waves

Allowable amplitude of a single 2D wave, parallel to span

$$\frac{a}{\lambda} = \left(\frac{177000 C \cos^2(\Lambda)}{\lambda(R_c)^{3/2}} \right)^{1/2}$$

where a is the surface wave amplitude, λ is the wavelength of the surface waves, C is the chord of the wing, Λ is the wing sweep angle, and R_c is the chord Reynolds Number

The maximum allowable amplitude of an isolated two-dimensional surface wave that is roughly orientated to the wing span (i.e. running across the flow) is given by the formula.

For chordwise waves wherein the flow runs up and down the surface, the allowable surface wave amplitude is twice that given above.

For multiple waves, the allowable roughness is $1/3$ that for a single wave. This ratio can be applied to either spanwise or stream wise waves.

11 Recommendations

The current report has described in detail the state of the art in transition prediction methods for swept wings in the subsonic/transonic flow regime. For this type of flow there are four major transition mechanisms (T-S, crossflow, laminar-turbulent interaction, and attachment line) (Figure 21) and other factors (compressibility, intermittency, surface roughness) affecting transition. For each of these mechanisms, succinct recommendations were given in the relevant discussion. The purpose of this section is to expand on these recommendations with some broad algorithmic outlines and ideas as to how these methods would be integrated into a general 3D Navier-Stokes solver.

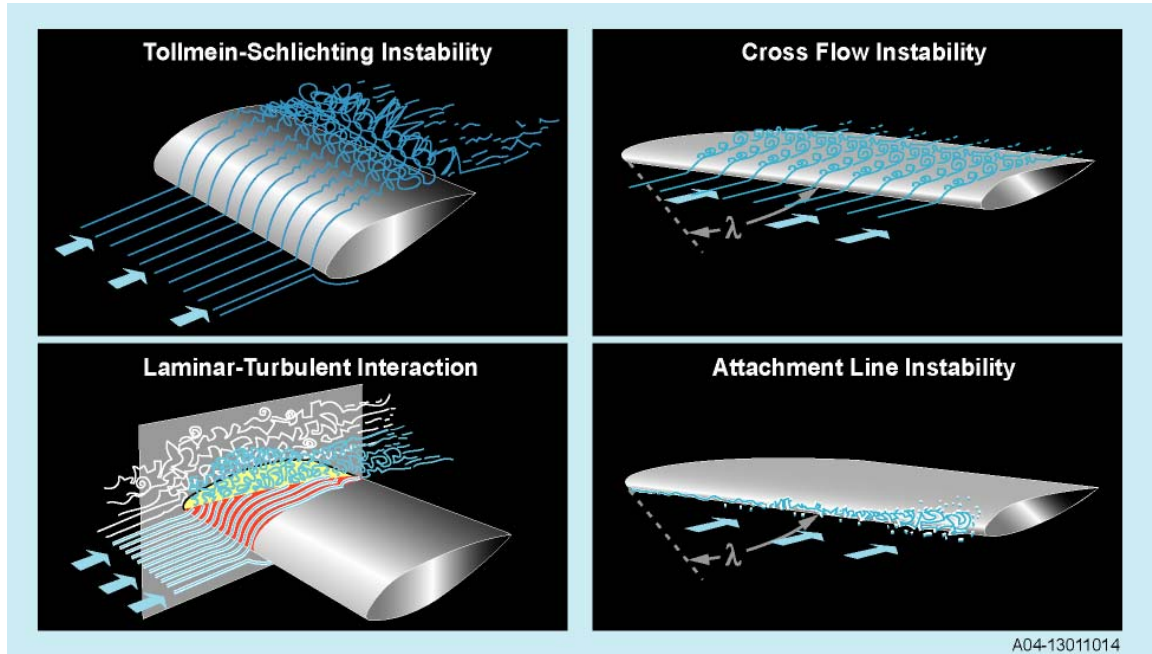


Figure 21: Transition mechanisms for swept wings

Tollmien-Schlichting (T-S) transition will be predicted using both envelope and wave tracking e^N methods. Correlations of the amplification factor N with boundary layer integral parameters H and Re_θ are developed for each important T-S frequency using LST or experimental data and are available a priori. For the envelope method a linear fit of the N factor curves for each shape factor is computed. At each iteration of the Navier-Stokes solver, the computed boundary layer profile is used to calculate the necessary boundary layer integral parameters (in this case H and Re_θ). These are used to calculate the right-hand side(s) for the N factor equation. Then the transport equation for the N factor is solved. If the envelope method is used, only one equation is solved (plus one more for the streamwise distance). For the wave tracking method, a transport equation is solved for each frequency/wave number. Then the computed N factor is compared to N_{crit} to determine transition. For the wave tracking method, the maximum value of N for each frequency is used and compared to N_{crit} . This process is summarized in Figure XX below.

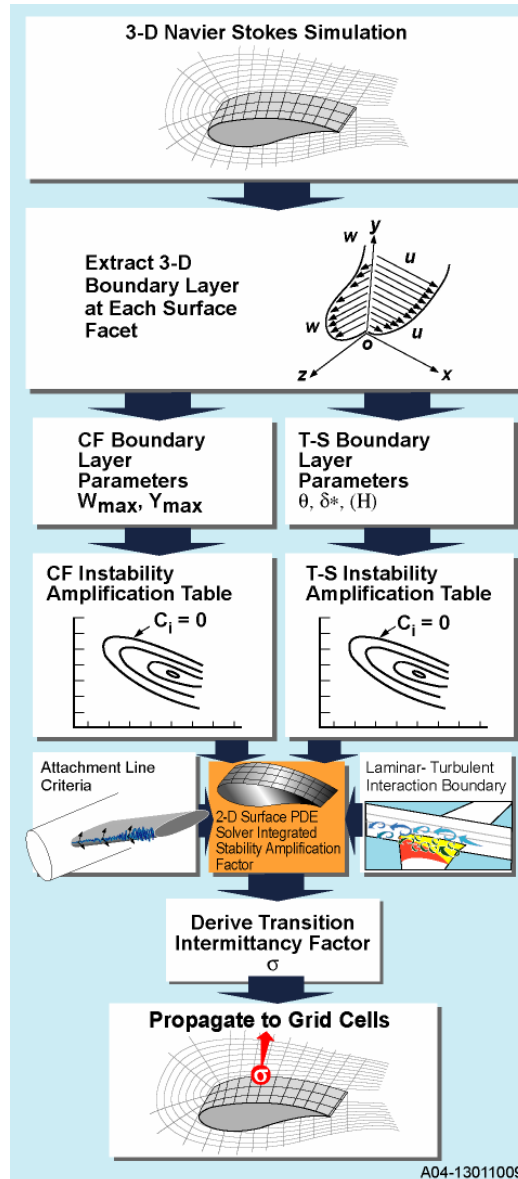


Figure 22: Outline of transition prediction methodology

Transition due to crossflow instabilities is computed in much the same way as for T-S instabilities. The amplification factor is correlated to boundary layer integral parameters, in this case also including W_{max} (maximum crossflow velocity) and Y_{max} (location of maximum crossflow velocity). As in the case of T-S, the correlations in the form of tables are calculated using LST or experiment and are available beforehand. The boundary layer integral parameters are computed from the boundary layer data at each Navier-Stokes iteration and using the correlations an N factor is computed either for the envelope or for individual crossflow modes using a 2D surface transport equation. This is then compared to N_{crit} (in general different for crossflow) to determine transition.

Interactions between T-S and crossflow instabilities which can affect transition will be accounted for using influence parameters to modify the amplification factor. For

example, the T-S N factor can be modified according to $N_{TS} = \alpha - \beta N_{CF}$, where α and β are determined from available data.

The strategy for the prediction of transition of the attachment line boundary layer must start with a determination of whether or not the boundary layer at the root of the wing is laminar or turbulent, because this determines the value of the critical Re_0 for transition. If the surface that wing abuts is a surface on which transition is being calculated, this can (and should) be done automatically by determining the value of the transition function at the intersection point, or as close to it as possible. If transition is not being computed on the intersecting surface, then it must be input or assumed to be turbulent. Geometries which do not have an intersecting surface (flying wings, for example) are of course laminar roots.

The calculation of Re_0 can be done in two ways. The formula in equations (3) or (4) could be used directly although this does not really apply to finite wings. The advantage here is that this is very simple and doesn't need any boundary layer information at all. It also applies to the entire wing. The other alternative is to actually compute the momentum thickness and from this Re_q . Since this approach is more general and the information needed to calculate it is readily available, this is the approach that will be used.

The location of the attachment line must be known in order to extract the necessary boundary layer parameters there. This location can be located automatically as part of the transition solution process by noting when certain velocity components are zero, or (as is currently done) when the upwinding term goes to zero. An alternative would be to locate the attachment line manually but this will not be used as it is not general enough. There are issues with automatic location of the attachment line, as it may also pick up lines in the flow that have similar characteristics (flow over riblets, for example). A scheme will have to be devised to determine which of the detected features is an attachment line, such as proximity to the leading edge.

Once the attachment line is located, the momentum thickness and the velocity at the edge of the boundary layer must be calculated. This information is calculated along with all of the other boundary layer parameters, so it will be available. Re_0 is then calculated at each point on the attachment line and compared to the critical value to determine transition.

If transition has been determined on a part of the attachment line, this needs to be projected back along the inviscid streamline over both the top and bottom surfaces. It may be possible to feed this information into the T-S solution process, or it could be done in a separate routine following the streamlines and setting the transition at each cell along the path.

The strategy for determining transition in a laminar boundary layer due to contamination from an existing turbulent boundary layer is straightforward. First, the surface that has a turbulent boundary layer must be identified, either through definition in an input file or computed as part of its own transition calculation. The forward point of intersection of

the laminar and turbulent boundary layer (for instance at the wing root) then must either be identified or calculated. The contamination of the laminar boundary layer will then be propagated at an angle to the streamlines which will have to be determined from experiment or from LST calculations. This angle will in general be a function of the local Mach number, Reynolds number, surface roughness, and surface curvature.

The length of the transition region will be determined using an algebraic/integral method. This is easily fit into the existing surface based solution scheme. The parameters needed to evaluate and integrate the intermittency model are readily available from the 3-D Navier-Stokes solution and RATTraP boundary layer profile based integral parameter formulation. This intermittency factor will then be used in Navier-Stokes model turbulent stress model to account for the transitional flow region.

The effect of surface roughness on transition is extracted from empirical correlations. For roughness elements, correlations with roughness height are used. For steps, the height of the step is used. For gaps, the width of the gap will determine transition. For surface waviness, the amplitude of the wave and the wavelength determine transition. Transition from roughness will fall into two classes; immediate transition and modifications to N factor.

References

- Anscombe, A., Illingsworth, L.N. 1952. Wind-tunnel observations of boundary layer transition on a wing at various angles of sweep back. ARC R&M 2968.
- Arnal D. 1984. Description and prediction of transition in two-dimensional incompressible flow. AGARD Rep. No. 709 (Special course on stability and transition of laminar flows), Von Karman Inst., Rhode-St.-Genese, Belg.
- Arnal, D. 1992. Boundary-layer transition: Prediction, application to drag reduction. AGARD Rep. No. 786 (Special course on skin friction drag reduction), Von Karman Inst., Rhode-St.-Genese, Belg.
- Arnal, D. 1994. Predictions based on linear theory,” Special Course on Progress in Transition Modelling, AGARD Report No. 793, Von Kármán Institute, Rhode-St.-Genese, Belgium, 1994, pp. 2-1 - 2-63.
- Arnal, D. 1997. Laminar-turbulent transition: Research and applications in France, AIAA 97-1905.
- Arnal, D., Coustols, E., Juillen, J. C. 1984. Experimental and theoretical study of transition phenomena on an infinite swept wing, Laminar-Turbulent Transition, edited by V. V. Kozlov, Springer-Verlag, Berlin, pp. 553-561.
- Bertolotti, F.P., Herbert, Th., Spalart, P.R. 1992. Linear and nonlinear stability of the Blasius boundary layer. J. Fluid Mech. 242: 441-74.
- Bippes, H. 1997. Environmental conditions and transition prediction in 3-D boundary layers, AIAA 97-1906.
- Bippes H. 1999. Basic experiments on transition in three-dimensional boundary layers dominated by crossflow instability. Prog. Aero. Sci. 35(4):363-412.
- Boiko AV, Kozlov VV, Syzrantsev VV, Shcherbakov VA. 1995. Experimental investigation of high-frequency secondary disturbances in a swept-wing boundary layer. J. App. Mech. And Tech. Phys. 36(3):385-93.
- Boiko AV, Kozlov VV, Syzrantsev VV, Shcherbakov VA. 1999. Active control over secondary instability in a three-dimensional boundary layer. Thermophysics and Aeromechanics 6(2):167-78.
- Bushnell, D.M., Malik, M.R., Harvey, W.D. 1989. Transition prediction in external flows via linear stability theory. In IUTAM Symposium Transsonicum III, ed. J. Zierep, H. Oertel. Berlin: Springer.
- Cebeci, T., Stewartson, K. 1980. On stability and transition in three-dimensional flows. AIAA J. 18 (4): 398-405.

Chang, C.-L., et al. 2003. The LAngley Stability and TRansition Analysis Code (LASTRAC): LST, linear & nonlinear PSE for 2D, axisymmetric, and infinite swept wing boundary layers, 2003 Reno AIAA Aerospace Sciences Meeting.

Chen, H.H., Cebeci, T. 1990. An evaluation of stability-based methods for transition of three-dimensional flows. In *Laminar-Turbulent Transition*, ed. D. Arnal, R. Michel, pp. 327-36. Berlin: Springer-Verlag.

Chen, K. K., Thyson, N. A. 1971. Extension of Emmons' spot theory to flows on blunt bodies, *AIAA Journal*, Vol. 9, No. 5, pp. 821-825.

Cousteix, J., Arnal, D., Aupoix, B., Gleyzes, C. 1991. Recent studies on transition and turbulence at ONERA-CERT, AIAA 91-0332.

Cowley, S.J., Wu, X. 1994. Asymptotic approaches to transition modelling, Special Course on Progress in Transition Modelling, AGARD Report No. 793, Von Kármán Institute, Rhode-St.-Genese, Belgium, 1994, 3-1 - 3-38.

Crouch, J. 1997. Transition prediction and control for airplane applications, AIAA 97-1907.

Crouch, J.D. 2004. Instabilities in boundary-layer flows and their role in engineering, IUTAM Symposium "One Hundred Years of Boundary Layer Research", Gottingen, Germany.

Crouch, J.D., Crouch, W.M., Ng, L.L. 2001. Transition prediction for three dimensional boundary layers in computational fluid dynamics applications, AIAA 2001-2989, April.

Crouch, J.D., Kosorygin, V.S., Ng, L.L. 2004. Modeling the effects of steps on boundary-layer transition. IUTAM Symposium on Laminar-Turbulent Transition, 13-17 December, Bangalore, India.

Crouch JD, Ng LL. 2000. Variable N-factor method for transition prediction in three-dimensional boundary layers. *AIAA J*, 38(2), pp. 211-216.

Cumpsty, N.A., Head, M.R. 1967. The calculation of three-dimensional turbulent boundary layers – Part II: attachment line flow on an infinite swept wing, *The Aeronautical Quarterly*, Vol. XVIII, pp. 150-164.

Cumpsty, N.A., Head, M.R. 1969. The calculation of three-dimensional turbulent boundary layers – Part III: Comparison of attachment line calculations with experiment. *The Aeronautical Quarterly*, Vol. XX, pp 99-113.

Dagenhart, J.R. 1981. Amplified crossflow disturbances in the laminar boundary layer on swept wings with suction. NASA TP 1902.

Dey, J. and Narasimha, R. 1988. An integral method for the calculation of 2-D transitional boundary layers, Fluid Mechanics Report 88 FMT Indian Institute of Science, Bangalore.

Deyhle, H., Bippes, H. 1996. Disturbance growth in an unstable 3-D boundary layer and its dependence on environmental conditions, JFM 316, 73-113.

Dhawan, S., Narasimha, R. 1958. Some properties of boundary layer flow during the transition from laminar to turbulent motion, Journal of Fluid Mechanics Vol 3, pp. 418-436.

Drela, M., Giles, M.B. 1986. Viscous-inviscid analysis of transonic and low-Reynolds number airfoils, AIAA 86-1786.

Drela, M. 2003. Implicit implementation of the full e^N transition criterion, AIAA 03-4066, June.

Emmons, H. W. 1951. The laminar-turbulent transition in a boundary layer – Part I, Journal of Aero. Sci., Vol. 8, pp. 490-498.

Fasel, H.F. 1990. Numerical simulation of instability and transition in boundary layer flows, in Laminar-Turbulent Transition, (Arnal, D. and Michel, R., eds.), Springer-Verlag, Berlin.

Fasel, H.F., Konzelmann, U. 1990. Nonparallel stability of a flat-plate boundary layer using the complete Navier-Stokes equations. J. Fluid Mech. 221: 311.

Fasel, H.F., Rist, U., Konzelmann, U. 1987. Numerical investigation of the three-dimensional development in boundary layer transition, AIAA-87-1203.

Fraser, C. J., Milne, J. S., Gardiner, I. D. 1988. Pressure gradient and freeestream turbulence intensity on the length of transitional boundary layers, Proc. Instn. Mech. Engrs., Vol. 202, No. C3, pp. 195-203.

Gaster, M. 1962. A note on a relation between temporally increasing and spatially increasing disturbances in hydrodynamic stability. J. Fluid Mech. 14: 222-24.

Gaster, M. 1967. On the flow along swept leading edges, The Aeronautical Quarterly, Vol. XVIII, pp. 165-184.

Gaster, M. 1968. The development of three-dimensional wave packets in a boundary layer. J. Fluid Mech. 32 (1): 173-84.

Gaster, M. 1974. On the effects of boundary-layer growth on flow stability. J. Fluid Mech. 66:465-80.

- Gaster, M., Grant, I. 1975. An experimental investigation of the formation and development of a wave packet in a laminar boundary layer. *Proc. Roy. Soc. Lond. A* 347: 253.
- Gleyzes, C., Cousteix, J., Bonnet, J.L. 1983. A calculation method of leading edge separation bubbles, Second Symposium on Numerical and Physical Aspects of Aerodynamic Flows, Jan.
- Gostelow, J. P., Blunden, A. R., Walker, G. J. 1994. Effects of free-stream turbulence and adverse pressure gradients on boundary layer transition, *ASME Journal of Turbomachinery*, Vol. 116, July, pp. 392-404.
- Gostelow, J. P., Hong, G., Walker, G. J., Dey. 1994. Modeling of boundary layer transition in turbulent flows by linear combination integral method, *ASME Paper No. 94-GT-358*.
- Gostelow, J. P., Melwani, N., Walker, G. J. 1996. Effects of free-stream turbulence and adverse pressure gradient on turbulent spot development, *ASME Journal. of Turbomachinery*, Vol 118, October, pp. 737-743.
- Gray, W.E. 1952. The effect of wing sweep on laminar flow. *RAE TM Aero 255*.
- Gregory, N., Love, E.M. 1965. Laminar flow on a swept leading edge: Final progress report, *NPL Memo., No. 26, British A.R.C.*
- Hall, P., Malik, M.R., Poll, D.I.A. 1984. On the stability of an infinitely swept attachment line boundary layer, *Proc. R. Soc. Lond. A.*, 395:229-345.
- Hall, P., Malik, M.R. 1986. On the instability of a three-dimensional attachment-line boundary layer: weakly nonlinear theory and a numerical approach, *J. Fluid Mech.*, 163:257-282.
- Haynes, T.S., Reed, H.L. 2000. Simulation of swept-wing vortices using nonlinear parabolized stability equations, *Journal of Fluid Mechanics*, Volume 305, Pages 325-349, February 2000.
- Healy, J.J. 1995. Comparison between the Orr-Sommerfeld and asymptotic theories for the flat-plate boundary layer, *Laminar-Turbulent Transition*, Vol. IV, ed. R. Kobayashi, Springer-Verlag, Berlin, 1995, pp.437-444.
- Heeg, R.S. 1998. Stability and transition of attachment-line flow, *Doctoral Thesis, Universiteit Twente, Enschede*.
- Herbert, Th. 1988. Secondary instability of boundary layers, *Annual Review Fluid Mechanics*, 20, 1988, 487-526.
- Herbert, Th. 1991. Boundary-layer transition - analysis and prediction revisited, *AIAA-91-0737*.

Herbert, Th. 1993. Parabolized stability equations, AGARD FDP/VKI Special Course on "Progress in Transition Modeling," AGARD Report No. 793, Madrid: 22-25 March, Brussels: 29 March-1 April.

Herbert, Th. 1997. Parabolized stability equations, Annual Review of Fluid Mechanics, Vol. 29, 1997, pp.245-283.

Herbert, Th. 1997. Transition analysis of flow over aerodynamic bodies, AIAA 97-1908.

Herbert, Th. 1997. On the stability of 3-D boundary layers, AIAA 97-1961.

Herbert, Th., Bertolotti, F.P. 1987. Stability analysis of nonparallel boundary layers. Bull. Am. Phys. Soc. 32: 2079.

Högberg M, Henningson D. 1998. Secondary instability of crossflow vortices in Falkner–Skan–Cooke boundary layers. J. Fluid Mech. 368:339–57.

Holden, M.S., Bower, D.R., Chadwick, K.M. 1994. Measurements of boundary layer transition on cones at angle of attack for Mach numbers from 11 to 13. Calspan–University of Buffalo Research Center Report to University of Dayton Research Institute, May.

Janke E, Balakumar P. 2000. On the secondary instability of three-dimensional boundary layers. Theoret. Comput. Fluid Dyn. 14:167–94.

Joslin, R. D. 1995. Evolution of stationary crossflow vortices in boundary layers on swept wings, AIAA Journal Vol 33, No. 7, July, pp 1279-1285.

Joslin, R.D. 1995. Direct simulation of evolution and control of three-dimensional instabilities in attachment-line boundary layers, J. Fluid Mech., 291:369-392.

Joslin, R.D. 1996. Simulation of three-dimensional symmetric and asymmetric instabilities in attachment-line boundary layers, AIAA J., 34:2432-2434.

Joslin, R.D. 1997. Direct numerical simulation of evolution and control of linear and nonlinear disturbances in three-dimensional attachment-line boundary layers, NASA Technical Paper 3623.

Kachanov, Y.S. 1996. Experimental studies of three-dimensional instability of boundary layer, AIAA 96-1976.

Kaups, K., Cebeci, T. 1977. Compressible laminar boundary layers with suction on swept and tapered wings. J. Aircraft 14: 661-67.

Kawakami M, Kohama Y, Okutsu M. 1999. Stability characteristics of stationary crossflow vortices in three-dimensional boundary layer. AIAA 99-0811.

King, R.A. 1991. Mach 3.5 boundary layer transition on a cone at angle of attack. AIAA 91-1804.

Kleiser, L. 1994. Direct numerical simulation of transition: the temporal approach, AGARD FDP/VKI Special Course on "Progress in Transition Modeling," AGARD Report No. 793, Madrid: 22-25 March, Brussels: 29 March-1 April.

Kleiser, L., Zang, T.A. 1991. Numerical simulation of transition in wall-bounded shear flows, *Ann. Rev. Fluid Mech.* 23: 495-537.

Klingmann, B.G.B., Boiko, A.V., Westin, K.J.A., Kozlov, V.V., Alfredsson, P.H. 1993. Experiments on the stability of Tollmien-Schlichting waves. *Eur.J.Mech., B/Fluids* 12:493.

Koch W, Bertolotti FP, Stolte A. Hein S. 2000. Nonlinear equilibrium solutions in a three-dimensional boundary layer and their secondary instability. *J. Fluid Mech.* 406:131–74.

Kohama, Y., Saric, W.S., Hoos, J.A. 1991. A high-frequency secondary instability of crossflow vortices that leads to transition, *Proceedings of Boundary Layer Transition and Control Conference*, Peterhouse College, Cambridge, United Kingdom, April 1991.

Kohama Y, Onodera T, Egami Y. 1996. Design and control of crossflow instability field. See Duck & Hall 1996, pp. 147–56.

Kral, L.D., Fasel, H.F. 1989. Numerical investigation of the control of the secondary instability process in boundary layers, AIAA-89-0984.

Kral, L.D., Fasel, H.F. 1990. Numerical simulation of the control of the three-dimensional transition process in boundary layers, in *Laminar-Turbulent Transition*, (Arnal, D. and Michel, R., eds.), Springer-Verlag, Berlin.

Kroo, I., Sturdza, P. 2003. Design-oriented aerodynamic analysis for supersonic laminar flow aircraft, AIAA 2003-0774, January.

Laburthe, F. 1992. Probleme de stabilite lineaire et provision de la transition dans des configurations tridimensionnelles, incompressibles et compressibles. Thesis. ENSAE Toulouse.

Langtry, R. B., Menter, F. R. 2005. Transition modeling for general CFD applications in aeronautics, AIAA 2005-0552.

Lees, L., Lin, C.C. 1946. Investigation of the stability of the laminar boundary layer in a compressible fluid. NACA TN 1115.

Lerche T. 1996. Experimental investigation of nonlinear wave interactions and secondary instability in three-dimensional boundary-layer flow. In *6th European Turbulence Conference*, Lausanne (ed. S. Gavrilakis, L. Machiels, P.A. Monkewitz), pp. 357-60.

- Lin, R.S., Malik, M.R. 1996. On the stability of attachment-line boundary layers. Part 1. The incompressible swept Hiemenz flow. *J. Fluid Mech.*, 311:239-255.
- Lin, R.S., Malik, M.R. 1997. On the stability of attachment-line boundary layers. Part 2. The effect of leading edge curvature. *J. Fluid Mech.*, 333:125-137.
- Lyttle, I.J., Reed, H.L., Shipyluk, Maslov, Buntin, Burov, Schneider, S. 2005. Numerical-experimental comparisons of second-mode behavior for blunted cones, accepted *AIAA Journal*.
- Mack, L.M. 1969. Boundary-Layer Stability Theory. Jet Propulsion Laboratory Doc. 900-277 (Rev. A), JPL, Pasadena.
- Mack, L.M. 1977. Transition prediction and linear stability theory. AGARD C-P No. 224.
- Mack, L.M. 1978. Three-dimensional effects in boundary-layer stability. *Proc. Symp. Nav. Hydrodyn.*, 12th, pp. 63-70. Washington, DC: Natl. Acad. Sci.
- Mack, L.M. 1980. On the stabilization of three-dimensional boundary layers by suction and cooling. In *Laminar-Turbulent Transition*, ed. R. Eppler, H. Fasel, pp. 223-38. Berlin: Springer-Verlag.
- Mack L.M. 1984. Boundary-layer linear stability theory. Special Course on Stability and Transition of Laminar Flows, AGARD Report No. 709.
- Mack, L.M. 1987. Review of linear compressible stability theory. In *Stability of Time Dependent and Spatially Varying Flows*, ed. D.L. Dwyer, M.Y. Hussaini, pp. 164-87. New York: Springer-Verlag.
- Mack, L.M. 1988. Stability of three-dimensional boundary layers on swept wings at transonic speeds. In *IUTAM Symposium Transsonicum III*, ed. J. Zierep, H. Oertel. Berlin: Springer.
- Malik, M.R. 1982. COSAL - A black box compressible stability analysis code for transition prediction in three-dimensional boundary layers. NASA CR-165952.
- Malik, M.R. 1990. Numerical methods for hypersonic boundary layer stability, *Journal of Computational Physics*, Vol. 86, 1990, pp. 376-423.
- Malik, M.R., Chuang, S., Hussaini, M.Y. 1982. Accurate solution of compressible linear stability equations. *ZAMP* 33: 189-201.
- Malik, M.R., Li, F., Chang, C.L. 1994. Crossflow disturbances in three-dimensional boundary layers: Nonlinear development, wave interaction and secondary instability, *Journal of Fluid Mechanics*, 268, 1-36.

- Malik MR, Li F, Chang CL. 1996. Nonlinear crossflow disturbances and secondary instabilities in swept-wing boundary layers See Duck & Hall 1996, pp. 257–66.
- Malik MR, Li F, Choudhari MM, Chang CL. 1999. Secondary instability of crossflow vortices and swept-wing boundary layer transition. *J. Fluid Mech.* 399:85–115.
- Malik, M.R., Orszag, S.A. 1981. Efficient computation of the stability of three-dimensional compressible boundary layers. AIAA Pap. No. 81-1277.
- Mayle, R. E. 1991. The role of laminar-turbulent transition in gas turbine engines, *ASME Journal of Turbomachinery*, October, Vol. 113, pp. 509-537.
- Michel, R., Arnal, D., Coustols, E., Juillen, J.C. 1985. Experimental and theoretical studies of boundary layer transition on a swept infinite wing. In *Laminar-Turbulent Transition*, ed. V.V. Kozlov, pp. 553-61. Berlin: Springer-Verlag.
- Morkovin, M.V. 1991. Panoramic view of changes in vorticity distribution in transition instabilities and turbulence, *Boundary Layer Stability and Transition to Turbulence*, FED-Vol. 114, editors D.C. Reda, H.L. Reed, and R. Kobayashi, ASME, New York, 1991, pp 1-16.
- Morkovin, M.V., Reshotko, E. 1990. Dialogue on progress and issues in stability and transition research. In *Laminar-Turbulent Transition*, ed. D. Arnal, R. Michel, pp. 3-30. Berlin: Springer-Verlag.
- Narasimha, R. 1985. The laminar-turbulent transition zone in the boundary layer,” *Prog. Aerospace Sci.*, vol. 22, pp. 29-80.
- Nayfeh, A.H. 1980. Stability of three-dimensional boundary layers. *AIAA J.* 18 (4): 406-16.
- Nayfeh, A.H. 1980. Three-dimensional stability of growing boundary layers. In *Laminar-Turbulent Transition*, ed. R. Eppler, H. Fasel, pp. 201-17. Berlin: Springer-Verlag.
- Nayfeh, A.H., Padhye, A. 1979. The relation between temporal and spatial stability in three-dimensional flows. *AIAA J.* 17: 1084.
- Oberkampf, W.L., Blottner, F.G., Aeschliman, D.P. 1995. Methodology for computational fluid dynamics code verification/validation, AIAA 95-2226, 1995.
- Owen, P.R., Randall, D.J. 1952. Boundary layer transition on the swept wing. *RAE TM Aero 277*.
- Pfenninger, W. 1965. Flow phenomena at the leading edge of swept wings, *Recent Developments in Boundary Layer Research*, Part IV, AGARDograph 97.
- Pfenninger, W., Bacon, J.W. 1969. Amplified laminar boundary layer oscillations and transition at the front attachment line of a 45° swept flat-nosed wing with and without

boundary layer suction, Viscous Drag Reduction, C Sinclair Wells, ed., Plenum Press, pp 85-105.

Pfenninger, W. 1977. Laminar flow control - Laminarization, Special Course on Drag Reduction, AGARD Rep.654, VonKármánInstitute, Rhode-St. Genese, Belgium, 1977.

Poll, D.I.A. 1978. Some aspects of the flow near a swept attachment line with particular reference to boundary layer transition, Cranfield Inst. Of Tech., CoA Report No. 7805.

Poll, D.I.A. 1979. Transition in the infinite swept attachment line boundary layer, The Aeronautical Quarterly, 30:607-629.

Poll, D.I.A. 1984. Transition description and prediction in three-dimensional flows. AGARD Rep. No. 709 (Special course on stability and transition of laminar flows), Von Karman Inst., Rhode-St.-Genese, Belg.

Poll DIA. 1985. Some observations of the transition process on the windward face of a long yawed cylinder. J. Fluid Mech. 150:329-56.

Prandtl, L. 1921. Bemerkungen Über die entstehung der turbulenz. Z.Angew. Math. Mech. 1:431-36.

Radeztsky, R.H. Jr., Reibert, M.S., Saric, W.S., Takagi, S. 1993. Effect of micron-sized roughness on transition in swept-wing flows, AIAA 93-0076, 1993.

Radeztsky, R.H. Jr., Reibert, M.S., Saric, W.S. 1994. Development of stationary crossflow vortices on a swept wing, AIAA 94-2373, 1994.

Radeztsky RH Jr, Reibert MS, Saric WS. 1999. Effect of isolated micron-sized roughness on transition in swept-wing flows. AIAA J. 37(11):1371-7.

Reed, H.L. 1994. Direct numerical simulation of transition: The spatial approach, AGARD Rep. No. 793 (Special course on progress in transition modelling), Von Kármán Inst., Rhode-St.-Genese, Belg.

Reed, H.L., Haynes, T.S. 1994. Transition correlations in 3-D boundary layers. AIAA J. 32: 923-29.

Reed, H.L., Haynes, T.S., Saric, W.S. 1998. CFD validation issues in transition modelling, AIAA Journal, Volume 36, Number 5, Pages 742-752, May 1998.

Reed, H.L., Kimmel, R., Schneider, S., Arnal, D. 1997. Drag prediction and transition in hypersonic flow, Invited Paper, AGARD Interpanel (FDP&PEP) Symposium on "Future Aerospace Technology in Service to the Alliance", Paris, France, April 14-18, 1997. Also, Invited Paper, AIAA-97-1818, Snowmass, June 1997.

Reed, H.L., Nayfeh, A.H. 1986. Numerical-perturbation technique for stability of flat-plate boundary layers with suction. AIAA J. 24 (2): 208-14

Reed, H.L., Saric, W.S. 1989. Stability of three-dimensional boundary layer, *Annual Review of Fluid Mechanics*, Vol. 21, 1989, pp. 235-284.

Reed, H.L., Saric, W.S., Arnal, D. 1996. Linear stability theory applied to boundary layers, *Annual Review of Fluid Mechanics*, Vol. 28, 1996, pp. 389-428.

Reibert, M.S., Saric, W.S. 1997. Review of swept-wing transition, AIAA 97-1816.

Reibert, M.S., Saric, W.S., Carrillo, R.B., Chapman, K.L. 1996. Experiments in nonlinear saturation of stationary crossflow vortices, AIAA 96-0184, 1996.

Reshotko, E. 1994. Boundary layer instability, transition, and control, AIAA 94-0001, 1994.

Reshotko, E. 1997. Progress, accomplishments and issues in transition research, AIAA 97-1815.

Roache, P. 1997. Quantification of uncertainty in computational fluid dynamics, *Annual Review of Fluid Mechanics*, Vol. 29, 1997, pp. 123-160.

Rosenhead, L. (ed.), 1963. *Laminar Boundary Layers*, Oxford University Press.

Ross, J.A., Barnes, F.H., Burns, J.G., Ross, M.A.S. 1970. The flat plate boundary layer, Part 3. Comparison of theory with experiment. *J. Fluid Mech.* 43 (4): 819.

Sanz, W., Platzer, M. F. 1996. On the Navier-Stokes calculation of separation bubbles with a new transition model, *Transactions of the ASME*, 96-GT-487.

Saric, W.S. 1990. Low-speed experiments: Requirements for stability measurements. In *Instability and Transition*, Vol I, ed. M.Y. Hussaini, p. 162-74. New York: Springer-Verlag.

Saric, W.S. 1994. Physical description of boundary-layer transition: Experimental evidence. AGARD Rep. No. 793 (Special course on progress in transition modelling), Von Karman Inst., Rhode-St.-Genese, Belg.

Saric, W.S. 1994. Görtler vortices, *Annual Review of Fluid Mechanics*, Vol. 26, 1994, pp. 379-409.

Saric, W.S., Nayfeh, A.H. 1977. Nonparallel stability of boundary layers with pressure gradients and suction. AGARD C-P No. 224: 6.

Saric, W.S., Reed, H.L. 2002. Supersonic laminar flow control via distributed roughness, Invited Paper, AIAA Aerospace Sciences Meeting, AIAA 2002-0147, January.

Saric, W.S., Carrillo, R.B., Reibert, M.S. 1998. Leading-edge roughness as a transition control mechanism, AIAA 98-0781.

Saric, W.S., Reed, H.L., Kerschen, E.J. 2002. Boundary-layer receptivity, *Annual*

Review of Fluid Mechanics, Volume 34, 2002.

Saric, W.S., Reed, H.L., White, E.B. 2003. Stability of three-dimensional boundary layers, Annual Review of Fluid Mechanics, Volume 35, 2003.

Saric WS, White EB. 1998. Influence of high-amplitude noise on boundary-layer transition to turbulence. AIAA Pap. No. 98-2645.

Schrauf, G. 1993. COAST2 - A compressible stability code, user's guide and tutorial. Deutsche Airbus DA-Report EF11-1973.

Schrauf, G. 1994. Transition prediction using different linear stability analysis strategies, AIAA 94-1848, 1994.

Schrauf, G., Bieler, H., Thiede, P. 1992. Transition prediction - the Deutsche Airbus View. Proceedings of the First European Forum on Laminar Flow Technology, Hamburg, DGLR-Bericht 92-06: 73-82.

Schrauf, G., Herbert, Th., Stuckert, G.K. 1995. Evaluation of transition in flight tests using nonlinear PSE analysis. AIAA 95-1801, 1995.

Schubauer, G.B., Klebanoff, P.S. 1955/1956. Contributions on the mechanics of boundary layer transition. NACA TN 3489 (1955) and NACA Rep. 1289 (1956).

Schubauer, G.B., Skramstad, H.K. 1947. Laminar boundary-layer oscillations and transition on a flat plate. J. Res. Nat'l. Bur. Stand. 38: 251.

Singer, B. A. 1994. Modeling the transition region, AGARD Report 793, Special Course on Progress in Transition Modelling, April. (Also NASA CR-4492).

Singer, B.A., Reed, H.L., Ferziger, J.H. 1989. Effect of streamwise vortices on transition in plane channel flow, Physics of Fluids A , Vol. 1, 1989, pp. 1960-1971.

Smith, A.M.O., Gamberoni, N. 1956. Transition, pressure gradient, and stability theory. Rep. No. ES 26388, Douglas Aircraft Company, Inc.

Solomon, W. J., Walker, G. J., Gostelow, J. P. 1996. Transition length prediction for flows with rapidly changing pressure gradients, ASME Journal of Turbomachinery, Vol. 118, October.

Spalart, P.R. 1989. Direct numerical study of leading-edge contamination. AGARD-CP No.438.

Spalart, P.R. 1990. Direct numerical study of crossflow instability. In Laminar-Turbulent Transition, ed. D. Arnal, R. Michel, pp. 621-30. Berlin: Springer-Verlag.

- Spalart, P.R. 1991. On the crossflow instability near a rotating disk. Proceedings of Boundary Layer Transition and Control Conference, Peterhouse College, Cambridge, UK.
- Spalart, P.R. 1993. Numerical study of transition induced by suction devices, Proceedings of the International Conference on Near Wall Turbulent Flows (So, R.M.C., ed.), March 15-17, Elsevier.
- Spalart, P.R. 19XX, Direct numerical study of leading-edge contamination, Fluid Dynamics of Three-Dimensional Turbulent Shear Flows and Transition, AGARD-CP-438, pp. 5-1-5-13.
- Srokowski, A.J., Orszag, S.A. 1977. Mass flow requirements for LFC wing design. AIAA 77-1222.
- Steelant, J., Dick, E. 2001. Modeling of laminar-turbulent transition for high freestream turbulence, ASME Journal of Fluids Engineering, Vol 123, March, pp.22-30.
- Steinberg, S., Roache, P. 1985. Symbolic manipulation and computational fluid dynamics, Journal of Computational Physics, Vol. 57, 1985, pp. 251-284.
- Stetson, K.F. 1982. Mach 6 experiments of transition on a cone at angle of attack. J. Spacecraft Rockets 19 (5): 397-403.
- Stock, H.W., Degenhart, E. 1989. A simplified e^N method for transition prediction in two-dimensional incompressible boundary layers, Z. Flugwiss. Weltraumforschung, Vol. 12.
- Sturdza, P. 2004. An aerodynamic design method for supersonic laminar flow aircraft, Phd Thesis, Stanford University, December.
- Suzen, Y. B., Huang, P. G. 1999. Modeling of flow transition using an intermittency transport equation, NASA CR 1999-209313.
- Theofilis, V. 1995. Spatial stability of incompressible attachment-line flow, Theoret. Comp. Fluid Dyn, 7:159-171.
- Theofilis, V. 1998. On the linear and nonlinear instability of the incompressible swept attachment-line boundary layer., J. Fluid Mech., 355:193-227.
- Van Ingen, J.L. 1956. A suggested semi-empirical method for the calculation of the boundary-layer transition region. Rep. Nos. VTH 71 and 74, Dept. Aeronaut. Eng., Univ. Technol., Delft, Neth.
- Vicedo, J., Vilmin, S., Dawes, W. N., Savill, A. M. 2004. Intermittency transport modeling of separated flow transition, ASME Journal of Turbomachinery, Vol. 126, July, pp. 424-431.

Wang, Y.X, Gaster, M. 2004. Effect of surface steps on boundary layer transition. Exp. in Fluids, to appear.

Wasserman P, Kloker, M. 2002. Mechanisms and control of crossflow-vortex induced transition in a 3-D boundary layer. J. Fluid Mech. 456:49-84.

Wassermann, P., Kloker, M. 2005. Transition mechanisms in a three-dimensional boundary-layer flow with pressure-gradient changeover, J. of Fluid Mech., vol. 530, pp.265-293.

White EB, Saric WS. 2002. Secondary instability of crossflow vortices. Submitted to J. Fluid Mech.